# Collagen-inspired self-assembling materials

**Paulina Janina Skrzeszewska**

**Thesis committee**

**Thesis supervisor**

Prof. Dr. M.A. Cohen Stuart
Professor of Physical Chemistry and
Colloid Science,
Wageningen University

**Thesis co-supervisors:**

Dr.ir. J. van der Gucht
Assistant professor, Laboratory of
Physical Chemistry and Colloid Science,
Wageningen University

Dr. F.A. de Wolf
Senior scientist at Food and Biobased
Research,
Wageningen University

**Other members:**

| | |
|---|---|
| Prof. Dr. G. Eggink | Wageningen University, The Netherlands |
| Dr. R.D. Groot | Unilever Research, Vlaardingen, The Netherlands |
| Prof. Dr. T. Nicolai | Université du Maine, Le Mans, France |
| Prof. Dr. J.C. M. van Hest | Radboud University, Nijmegen, The Netherlands |

This research was conducted under the auspices of the Graduate School VLAG

# Collagen-inspired self-assembling materials

Paulina Janina Skrzeszewska

**Thesis**

submitted in fulfillment of the requirements for the degree of doctor
at Wageningen University
by the authority of the Rector Magnificus
Prof. dr. M.J. Kropff,
in the presence of the
Thesis Committee appointed by the Academic Board
to be defended in public
on Friday 20 May 2011
at 4 p.m. in the Aula

Paulina Janina Skrzeszewska

Collagen-inspired self-assembling materials

PhD thesis, Wageningen University, Wageningen, The Netherlands (2011)

ISBN: 978-90-8585-869-0

*Rodzicom*

This research forms part of the research program of the Dutch Polymer institute (DPI), Technology area Bio-inspired Polymers, DPI project #602

# CONTENTS


| | | |
|---|---|---|
| **Chapter 1** | Introduction | 1 |
| **Chapter 2** | Production of collagen-inspired telechelic protein polymers | 15 |
| **Chapter 3** | Physical gels of telechelic triblock copolymers with precisely defined junction multiplicity | 27 |
| **Chapter 4** | Influence of middle block design on gel properties, formed by telechelic polypeptides | 43 |
| **Chapter 5** | Kinetics of network formation by telechelic polypeptides with trimeric nodes | 61 |
| **Chapter 6** | Fracture and self-healing in a well-defined self-assembled polymer network | 79 |
| **Chapter 7** | Shape-memory effects in biopolymer networks with collagen-like transient nodes | 97 |
| **Chapter 8** | Summary and General Discussion | 115 |
| **Samenvatting** | | 133 |
| **Podsumowanie** | | 139 |
| **Acknowledgements** | | 145 |
| **About the author** | | 147 |
| **List of publications** | | 149 |

# Chapter 1

## Introduction

## 1.1 Material science throughout the centuries

Just after *Homo sapiens* discovered his brain, he realized that, besides food, he was surrounded by loads of natural materials such as wood, stones or leather, which could be put into use in the daily life practice. With time, humans learnt about metals and natural fibres to make weapons, jewellery or clothes. For centuries, people were relying mostly on these natural materials. That was until the breakthrough in 1907, when Belgian chemist Leo Baekeland created the first synthetic polymer, Bakelite [1]. Thanks to his invention, the twentieth century, with no doubts, was the century of polymeric materials. Nowadays we cannot imagine life without *e.g.* nylon, Teflon or silicone. Synthetic polymers are widely used in daily life, aerospace, civil engineering and military. Also in medicine, synthetic polymers replaced many traditional materials, because of their better performance and functionality. Millions of lives were improved by implementing polymers as vascular stents, implants or dental restoratives. However, as life expectations increase, the need for newer, better controlled and tuneable systems with desired properties, architectures and behaviours increases as well. This is of course a big challenge for scientists. Especially a great interest is focused on soft polymeric materials such as hydrogels, which can be used as drug delivery systems [2], intravenous infusions, matrix implants, wound treatment materials [3] or scaffolds for tissue engineering [4]. Many synthetic polymers have been successfully used for such medical applications [5]. However, even though since 1907 great progress has been made in the field of synthetic chemistry, the level of controllability and complexity, characteristic for biological polymers such as nucleic acids or proteins, is still far away.

After the molecular biology revolution in the 1970s and the advances in genomics and proteomics in the 1990s and 2000s the perspective on the design and synthesis of new materials has significantly changed. The biotechnological progress has provided not only new synthesis tools but also many ideas for new architectures and functions. Accordingly, a lot of effort has been made to mimic natural polymers and their structures, with the aim to create a new generation of precise, stimuli-responsive nanomaterials.

## 1.2 Proteins

The most sophisticated and complex natural polymers are proteins. They have many important roles in nature, including catalysis, transportation or signalling. Nature has developed reliable and precise protein production machinery, which allows synthesising monodisperse polymers with specific molecular weight, composition and sequence, tailored

for their specific function. These polymers can fold into well-defined three dimensional structures through multiple levels of organization, stabilized by non-covalent interactions such as hydrogen bonds, electrostatic and hydrophobic interactions.

On the level of their primary structure proteins are linear macromolecules, long chains of amino acids. Twenty different amino acids are encoded by DNA. Every amino acid has a common structural feature, namely the α-carbon to which a variety of side groups are bonded. The side groups can vary in size, polarity and charge; they can be linear, branched or cyclic, *e.g.* aromatic. Some of them can undergo posttranslational modification (either *in vivo* or *in vitro*). Although nature has provided only twenty of these building blocks, they can be combined into a huge variety of spatial arrangements, producing proteins with widely varying properties. Depending on their primary amino acid sequence, proteins can organize first into a secondary structure (α-helix, β-sheet, β-turn *etc.*) and then into more complex three-dimensional (3D) (tertiary) and multimolecular (quaternary) structures.

***Collagen***

One protein that has received significant attention from material scientists, due to its interesting and unique quaternary structure, is collagen [6-8]. Collagen is the main component of connective tissues (cartilage, ligaments), tendons bones and teeth. It constitutes up to 25 % of the total protein content in mammalians. Together with keratin and elastin it is responsible for skin strength and elasticity. It is present in the cornea and lens of the eye in crystalline form. The typical tropocollagen subunit is a rod of approximately 300 nm long and 1.5 nm in diameter, made up of three polypeptide strands, each of which is a left handed helix (note that the α-helix is right handed). In collagen, three left handed helices [8] are twisted together into a right handed rigid super helix (triple helix). This quaternary structure is stabilized by hydrogen bonds among adjacent molecules.

The most characteristic feature of collagen, which allows formation of the above mentioned quaternary structure, is its distinctive regular amino acid sequence. The repeated motif is Gly-Xxx-Yyy. Glycine (Gly) is present every third position and always goes to the interior (axis) of the triple helix. That is because there is not enough space for any larger side groups than hydrogen. In position Xxx and Yyy different amino acids can be found, with a relatively high incidence of proline (*ca.* 20 % in many collagens). Proline residues in position Yyy are posttranscriptionally (enzymatically) modified to hydroxyproline (Hyp). The hydrogen bonds that stabilize the helix are formed between the NH group of glycine and the CO group of an amino acid residue in the Xxx position of adjacent strands. The presence of a

4-hydroxygroup in hydroxyproline provides an additional hydrogen bond [7]. Proline and hydroxyproline stabilize the left-handed structure of single collagen strands by steric repulsion. There are no hydrogen bonds within the same molecule and a triple helix is formed directly by folding three single strands in a zipper-like manner [9, 10].

Biosynthesis of fibril-forming collagens is a multifaceted process that includes several intracellular (in fibroblasts) and extracellular steps. Collagen is first synthesised as procollagen with globular propeptides on the N and C terminus. The C-terminal propeptides form a nucleation site for triple helix formation that propagates towards the N-terminus. After folding, the procollagen molecules are secreted into the extracellular space where the N and C proteins are cleaved off. Then, the tropocollagen subunits spontaneously assemble into larger structures (microfibrils and fibrils (Figure 1.1)), which are stabilized by the formation of covalent crosslinks, for example due to enzymatic activation of specific amino acids (lysine) [6, 8].

The melting temperature of collagen is determined by its amino acid sequence. For coldblooded organisms it is lower, due to lower content of proline and hydroxyproline.

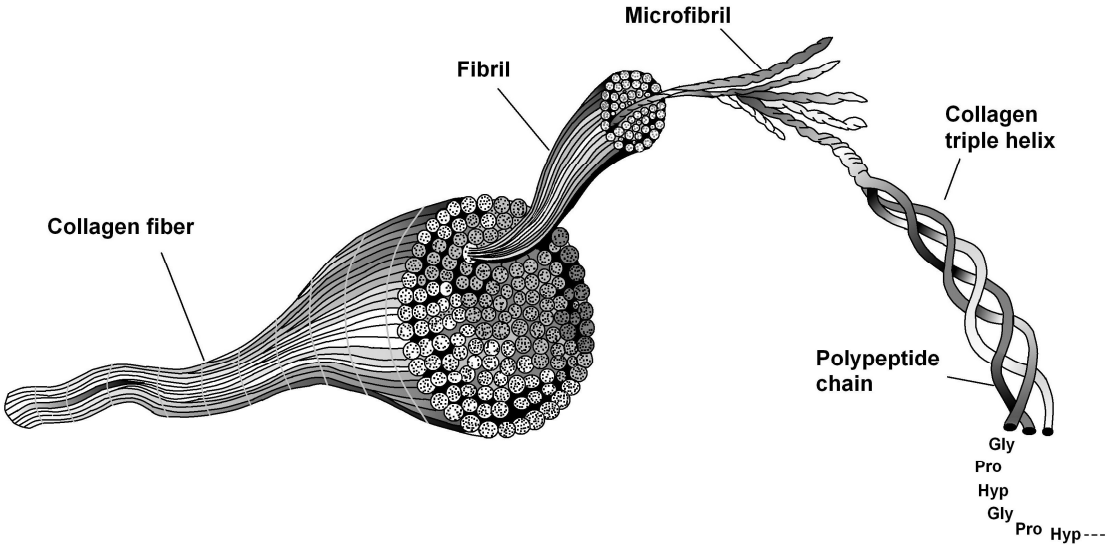


Figure 1.1 Organization of fibril-forming collagen.

Collagen can be denatured, usually after partial hydrolysis, to form a more soluble derivative, called gelatin. In solution at high temperatures, all gelatin molecules are in a random coil state but when cooled down, triple helical structures can partially reform. However, in the absence of propeptides present in mature collagen and due to the deficiency of chaperones, the three strands do not align properly and consequently a random network is

formed composed of rigid collagen rods connected via flexible coils [11] (Figure 1.2). Gelatin has a lot of medical, pharmaceutical, food and cosmetic applications. Unfortunately it suffers from batch to batch variations in molecular composition and material quality, and thus exhibits a limited range of controllability, which is very disadvantageous from an application point of view [12]. Subsequently, a lot of effort is done to produce hydrogels that circumvent these obstructions and have well-defined and reproducible properties.

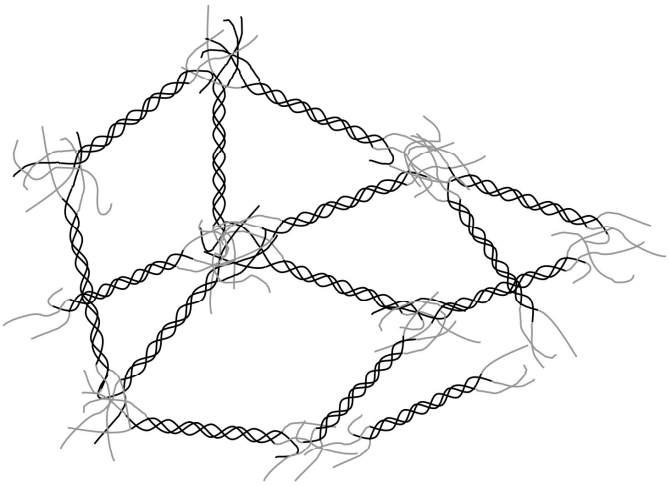

Figure 1.2 Three-dimensional structure of gelatin.

## 1.3 Hydrogels

Hydrogels are crosslinked polymer networks filled with water. Due to their specific properties they have a lot of applications in food, medicine or bulk chemistry [2, 13, and 14]. In general, they can be divided into two categories, based on the chemical or physical nature of the crosslinks. In the case of chemical (permanent) gels, the junctions are formed by strong covalent bonds, which can be formed by exposure to heat or radiation [15-17], or by adding reactive crosslinking agents [18]. These gels cannot restructure or flow. In the case of physical networks, the nodes are created in a reversible (transient) manner, due to weak, non-covalent interactions such as hydrogen bonds, van der Waals forces, hydrophobic or electrostatic interactions. These gels can restructure and flow. The node relaxation time strongly depends on the nature of the crosslinks but also on environmental conditions. They can respond to changes in pH, ionic strength [19] or temperature [20]. Furthermore, physical gels, due to their finite relaxation time, often show self-healing behaviour. Upon shearing they

break or become inhomogeneous but after taking the load away they can recover to their initial state.

## 1.4 Block copolymers

An interesting class of physical hydrogels, with precisely-controlled relaxation behaviour, is formed by associative triblock copolymers. These copolymers have groups at their ends that can reversibly assemble into supramolecular knots. The middle block has a hydrophilic character and serves as a spacer. A lot of research has been dedicated to water-soluble polymers (such as PEO) terminated with hydrophobic groups at both ends [21, 22]. These molecules form reversible networks in which the junction points consist of micelles formed by association of the hydrophobic ends. Very similar networks, but with complex coacervate nodes, are formed by telechelics with charged ends. Gelation occurs after they are mixed with oppositely charged polymers [23].

***Protein block copolymers***

Synthetic triblock polymers have been investigated already for several decades. Although many interesting molecules have been synthesised and characterized, they have some disadvantages, such as poorly-controlled chain length and sequence, limited number of possible assemblies, lack of degradability, poor interactions with cells and tissues, or toxic properties, precluding applications in medicine and food. These problems can be overcome by designer protein copolymers consisting of blocks inspired by natural motifs [19, 24-26]. The production of such polypeptides, with programmed three dimensional structures, has become possible due to the rapid developments in genetic engineering. By changing the underlying DNA template, molecules with precisely-controlled sequence, composition, molecular weight and length can be synthesised.

DNA is a double-stranded polymer consisting of regions (genes) that encode proteins. In front of the actual gene, a so-called promoter region is located that regulates the activity of the gene. The gene can be switched on or off by transcription factors binding or unblocking the promoter region. Whenever a given protein is needed, the promoter is unblocked, which allows RNA polymerase to begin transcription of DNA into many identical copies of mRNA. Messenger RNA is then transported to the ribosomes (“protein factories”) and translated to many identical copies of protein molecules. By such DNA-based synthesis, monodisperse and identical molecules can be produced with high yields.

In order to produce designer block polymers, an artificial gene, inserted into a so-called vector (usually a plasmid or a circular self-replicating piece of DNA that can be multiplied in bacterial cultures), has to be introduced into the host organism. First of all, however, the gene has to be designed and constructed. Construction of a new gene can be done either by using DNA codes copied from existing natural DNA (genes) or by using entirely new sequences, synthesised chemically. The main tools to combine DNA fragments in the desired manner are restriction and ligation enzymes, which cut and connect DNA in specific sites. When the vector with its desired gene is complete, it is transfected into a host organism that can produce the desired molecule in a fermentation process.

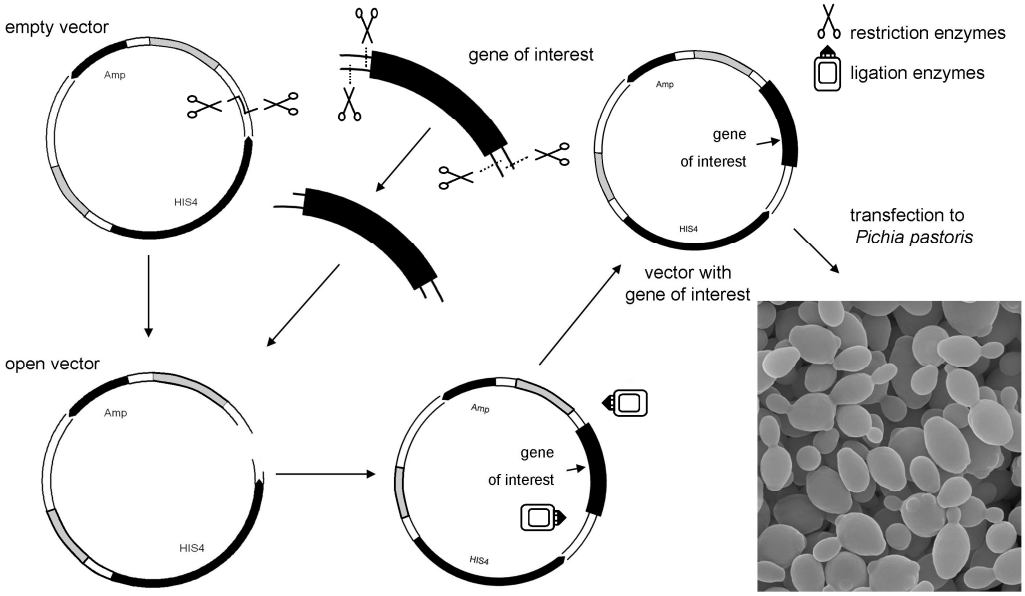


Figure 1.3 Schematic representation of the cloning procedure, in which *Pichia pastoris* with the gene of interest is obtained.

The first protein block copolymers, produced biotechnologically were reported by Capello [27]. They consisted of a silk-like and an elastin-like block. The silk-like fragment assembled into organized crystalline structures, similar to β-sheet assemblies found in natural silk, while the flexible elastin-like motif was used to influence the degree of crystallinity. After that, many protein block copolymers have been reported. The triblock protein copolymers reported by Petka [28] consisted of relatively short "leucine zipper" end blocks flanking a $(Ala\text{-}Gly\text{-}Ala\text{-}Gly\text{-}Ala\text{-}Gly\text{-}Pro\text{-}Glu\text{-}Gly)_{10}$ water soluble domain. Leucine zippers represent a subcategory of coiled-coil domains, which are widely found in nature. Coiled-coils consist of heptad repeats designated as *abcdefg*, where positions *a* and *d* are occupied by hydrophobic residues and *e* and *g* by charged residues [29]. Each coiled-coil motif folds in

such a way that the *a* and *d* residues are placed on a hydrophobic face of the helix, and *e* and *g* face opposite charges in the neighbouring helix. Electrostatic and hydrophobic interactions drive α-helices to associate into oligomeric bundles. In nature two, three, four and five stranded coiled-coils occur. However, in case of Petka's polymers the end blocks assemble mostly into tetrameric bundles [30]. Fluorescence measurements showed that the system tends to form elastically inactive loops. The ratio between loops and active bridges depends on the orientation of the leucine domains in a node, the network multiplicity (2-4), the charge density on the middle domain and the length of the middle block [19].

Another group of biotechnological triblock copolymers was described by Wright [24]. They were composed of an elastin-like polypeptide sequence in which identical hydrophobic end blocks (Val-Pro-Ala-Xxx-Gly) were separated by a more hydrophilic middle block (Val-Pro-Gly-Xxx-Gly). These materials aggregate in aqueous solution due to the selective phase separation of the hydrophobic end blocks above a lower critical solution temperature (LSCT). The transition temperature can be tuned by introducing more or less polar amino acid residues in position Xxx of the hydrophobic block. The middle block is derived from a pentapeptide sequence that has a much higher transition temperature than the side blocks. Thus, just above the transition temperature of the side blocks, the middle block maintains its random coil-like state. By varying the length and amino acid composition of the middle block, materials were obtained with a variety of different physicochemical properties (such as storage modulus, relaxation time) [25].

As shown by Martens [31], triblock polymers with silk-like octapeptide (abbreviated as S) and random coil-like motifs (abbreviated as C) can form pH responsive gels with very high storage modulus. Two variants of the molecule were tested, SCCS and CSSC. For both of these, network formation was triggered by silk-like block assembly: first it folded into secondary β-roll structures and then these β-rolls assembled into supramolecular semi flexible ribbons. The random coil-like C motifs prevented isotropic segregation of the silk repeats, and thereby stabilized the entire structure.

All above-mentioned molecules form physical gels, *i.e.,* polymer networks filled with water. Their rheological, structural, physical or biological properties can be modified by varying the length or composition of the different blocks in the molecule. This is essential when designing new materials, especially for biomedical applications such as drug delivery, cell based therapeutics, or in soft tissues engineering [32].

In this thesis we present a new class of triblock protein polymers, which form very well-defined hydrogel networks with triple helical nodes.

## 1.5 The aim and organization of the thesis

The aim of this thesis is to study a new class of hydrogel networks formed by collagen-inspired telechelic polypeptides with a hydrophilic random coil-like middle block and collagen-like end blocks that assemble upon cooling into well-defined triple helical nodes. The study addresses, in particular, the effects of temperature, concentration and molecular design on the macro- and nano-scopic properties of the network.

These new class of collagen-inspired triblock copolymers, developed in our group, consist of identical end blocks, abbreviated as T (trimer-forming) and a random coil-like middle block abbreviated as R*n* or P*n* (Figure 1.4A). The T domains consist of nine amino acids triplets Pro-Gly-Pro, and fold upon cooling into collagen-like triple helices (Figure 1.4B). The middle block consists of a tandem repeat of *n* highly hydrophilic, *ca.* 100 amino acids long, P or R motif; these blocks are identical with respect to molecular weight and amino acid composition, but have a different sequence. In P, glycine occurs in every third position (as in collagen). Nevertheless, a polymer consisting of only P does not form any supramolecular structures and maintains its random coil-like conformation at any temperature [33]. Block R is a shuffled version of P, in which glycine never occurs in the third position after a previous glycine. This ensures that R will not ever be capable of forming triple helices together with T blocks (hybrid T-R helices). This cannot be excluded for P.

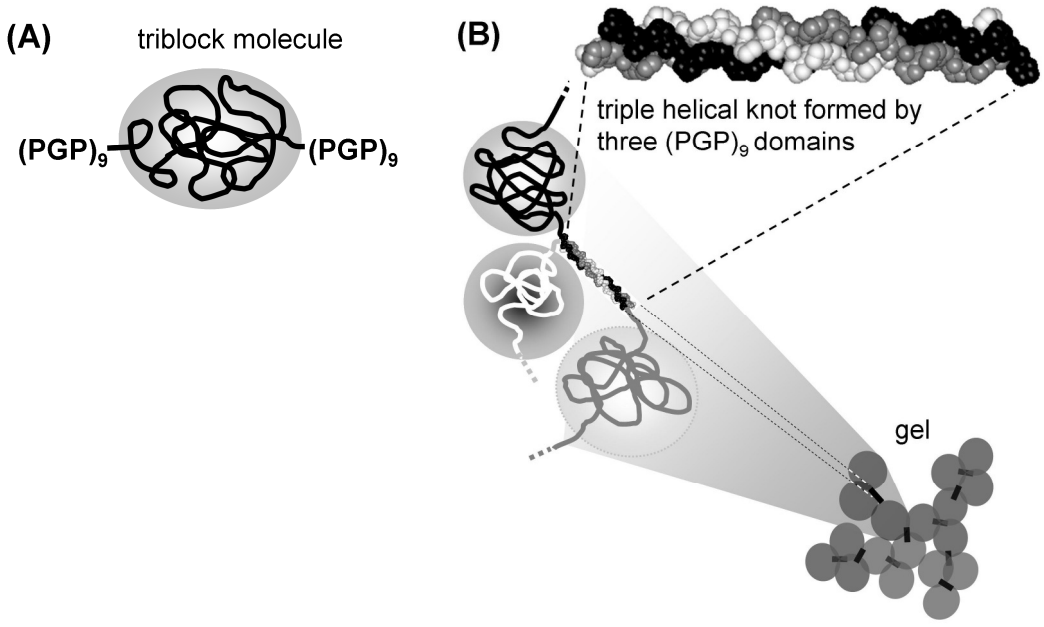


Figure 1.4 (A) Schematic representation of telechelic collagen-inspired molecule. (B) Scheme of the gel with triple helical nodes.

The investigated molecules form very well-defined gel networks with a precisely-known multiplicity of three. Because of that we could develop an analytical model that links the nanoscopic structure of the gel with its macroscopic properties. Consequently, we can control the physicochemical properties of the system by influencing the internal gel structure through the protein concentration, the temperature, or the molecular design of the polypeptides and their tendency to form intramolecular loops.

In **Chapter 2** we describe in more detail the molecular design of the investigated proteins, as well as the production route, which consists of cloning, fermentation and a separation process. In **Chapter 3** we investigate the viscoelastic properties of networks formed by collagen-inspired polypeptides as a function of polymer concentration and temperature. We explain the experimental data with the help of an analytical model that takes into account the multiplicity of the network and the transient character of the triple helical junctions. The model is based on classical gel theory and does not require any adjustable parameters. It accounts for the molecular structure of the gel, and the presence of loops and dangling ends. In **Chapter 4** we extend our study to the influence of length and amino acid sequence of the middle block on melting behaviour and on the viscoelastic properties of the networks. To describe the experimental results we use the analytical model developed in **Chapter 3**. By taking into account that the overlap concentrations are different for molecules with different middle block lengths, we can fit all experimental data with the theory. In **Chapter 5** we study the kinetics of the gel formation. We experimentally characterize the amount of triple helix (by calorimetry) and the mechanical properties of the gel (by rheology) as a function of time. To describe these experimental data, we extend the model presented in **Chapter 3** to include the kinetics of nucleation and propagation of triple helices. In **Chapter 6** we investigate the non-linear behaviour of our networks, such as fracturing and self-healing. By means of shear start-up experiments we find the critical stress for gel failure and the steady-state stress after fracture, both as a function of shear rate. We also investigate delayed network rupture under a fixed applied stress. To get more insight into the mechanism and nature of network disintegration, we carried out particle image velocimetry (PIV). The two-dimensional velocity maps determined from these experiments confirm shear-induced fracture, which we elaborate in more detail using the stress-activated bond rupture theory proposed by Chaudhury and Evans [34, 35]. Finally, we investigate self-healing of the system after rupture by following the recovery of the storage modulus in time. The experiments show that the system can fully heal after different fracture histories. In **Chapter 7** we test shape-memory effects for our materials, by employing collagen-like end blocks to “pin” the

temporary shape. The permanent shape is achieved by adding the crosslinking agent (glutaraldehyde) that binds lysine residues present in the middle block. When cooled down, while deformed, the formation of the triple helices fixes the material in its temporary shape. Once the system is exposed to temperature, above which the triple helices melt (45 ºC), it slowly returns to its original, programmed, shape.

## References


[1] www.wikipedia.org.

[2] M. Sutter, J. Siepmann, W.E. Hennink, W. Jiskoot, Recombinant gelatin hydrogels for the sustained release of proteins. Journal of Controlled Release 119(3) (2007) 301-312.

[3] B. Balakrishnan, M. Mohanty, P.R. Umashankar, A. Jayakrishnan, Evaluation of an in situ forming hydrogel wound dressing based on oxidized alginate and gelatin. Biomaterials 26(32) (2005) 6335-6342.

[4] S.G. Zhang, F. Gelain, X.J. Zhao, Designer self-assembling peptide nanofibre scaffolds for 3D tissue cell cultures. Seminars in Cancer Biology 15(5) (2005) 413-420.

[5] G. Chan, D.J. Mooney, New materials for tissue engineering: towards greater control over the biological response. Trends in Biotechnology 26(7) (2008) 382-392.

[6] G.N. Ramachandram, Biochemistry of Collagen, Plenum Press, New York, 1976.

[7] J. Engel, H.T. Chen, D.J. Prockop, H. Klump, Triple helix reversible coil conversion of collagen-like polypeptides in aqueous and non aqueous solvents - comparison of thermodynamic parameters and binding of water to (L-Pro-L-Pro-Gly)n and (L-Pro-L-Hyp-Gly)n. Biopolymers 16(3) (1977) 601-622.

[8] J.M. Berg, J.L. Tymoczko, L. Stryer, Biochemistry, W.H Freeman & Company 3rd edition, New York, 1988.

[9] J. Engel, D.J. Prockop, The zipper-like folding of collagen triple helices and the effects of mutations that disrupt the zipper. Annual Review of Biophysics and Biophysical Chemistry 20 (1991) 137-152.

[10] A. Bachmann, T. Kiefhaber, S. Boudko, J. Engel, H.P. Bachinger, Collagen triple-helix formation in all-trans chains proceeds by a nucleation/growth mechanism with a purely entropic barrier. Proceedings of the National Academy of Sciences of the United States of America 102(39) (2005) 13897-13902.

[11] W.Y. Aalbersberg, R.J. Hamer, P. Jasperse, H.H.J. de Jongh, C.G. de Kruif, P. Walstra, F.A. de Wolf, Progress in Biotechnology; Industrial Proteins in Perspective, Elsevier, New York, 2003.

[12] R. Langer, D.A. Tirrell, Designing materials for biology and medicine. Nature 428(6982) (2004) 487-492.

[13] J.P. Jung, J.Z. Gąsiorowski, J.H. Collier, Fibrillar Peptide Gels in Biotechnology and Biomedicine. Biopolymers 94(1) (2009) 49-59.

[14] B. Kickhofen, H. Wokalek, D. Scheel, H. Ruh, Chemical and physical properties of a hydrogel wound dressing. Biomaterials 7(1) (1986) 67-72.

[15] M. Wang, L. Xu, X.C. Ju, J. Peng, M.L. Zhai, J.Q. Li, G.S. Wei, Enhanced radiation crosslinking of carboxymethylated chitosan in the presence of acids or polyfunctional monomers. Polymer Degradation and Stability 93(10) (2008) 1807-1813.

[16] B. Singh, S. Kumar, Synthesis and characterization of psyllium-NVP based drug delivery system through radiation crosslinking polymerization. Nuclear Instruments & Methods in Physics Research Section B-Beam Interactions with Materials and Atoms 266(15) (2008) 3417-3430.

[17] F. Cataldo, O. Ursini, E. Lilla, G. Angelini, Radiation-induced crosslinking of collagen gelatin into a stable hydrogel. Journal of Radioanalytical and Nuclear Chemistry 275(1) (2008) 125-131.

[18] T.H. Chen, H.D. Embree, L.Q. Wu, G.F. Payne, In vitro protein-polysaccharide conjugation: Tyrosinase-catalyzed conjugation of gelatin and chitosan. Biopolymers 64(6) (2002) 292-302.

[19] W. Shen, J.A. Kornfield, D.A. Tirrell, Structure and mechanical properties of artificial protein hydrogels assembled through aggregation of leucine zipper peptide domains. Soft Matter 3(1) (2007) 99-107.

[20] K.T. Nijenhuis, On the nature of crosslinks in thermoreversible gels. Polymer Bulletin 58(1) (2007) 27-42.

[21] T. Annable, R. Buscall, R. Ettelaie, D. Whittlestone, The rheology of solutions of associating polymers-comparison of experimental behaviour with transient network theory. Journal of Rheology 37(4) (1993) 695-726.

[22] J. Sprakel, E. Spruijt, M.A.C. Stuart, N.A.M. Besseling, M.P. Lettinga, J. van der Gucht, Shear banding and rheochaos in associative polymer networks. Soft Matter 4(8) (2008) 1696-1705.

[23] M. Lemmers, J. Sprakel, I.K. Voets, J. van der Gucht, M.A.C. Stuart, Multiresponsive Reversible Gels Based on Charge-Driven Assembly. Angewandte Chemie-International Edition 49(4) (2010) 708-711.

[24] E.R. Wright, V.P. Conticello, Self-assembly of block copolymers derived from elastin-mimetic polypeptide sequences. Advanced Drug Delivery Reviews 54(8) (2002) 1057-1073.

[25] K. Nagapudi, W.T. Brinkman, B.S. Thomas, J.O. Park, M. Srinivasarao, E. Wright, V.P. Conticello, E.L. Chaikof, Viscoelastic and mechanical behaviour of recombinant protein elastomers. Biomaterials 26(23) (2005) 4695-4706.

[26] P.J. Skrzeszewska, F.A. de Wolf, M.W.T. Werten, A.P.H.A. Moers, M.A. Cohen Stuart, J. van der Gucht, Physical gels of telechelic triblock copolymers with precisely-defined junction multiplicity. Soft Matter 5(10) (2009) 2057-2062.

[27] J. Cappello, J. Crissman, M. Dorman, M. Mikolajczak, G. Textor, M. Marquet, F. Ferrari, Genetic-engineering of structural protein polymers. Biotechnology Progress 6(3) (1990) 198-202.

[28] W.A. Petka, J.L. Harden, K.P. McGrath, D. Wirtz, D.A. Tirrell, Reversible hydrogels from self-assembling artificial proteins. Science 281(5375) (1998) 389-392.

[29] W.H. Landschulz, P.F. Johnson, S.L. McKnight, The leucine zipper-a hypothetical structure common to a new class of DNA-binding proteins. Science 240(4860) (1988) 1759-1764.

[30] S.B. Kennedy, K. Littrell, P. Thiyagarajan, D.A. Tirrell, T.P. Russell, Controlled structure in artificial protein hydrogels. Macromolecules 38(17) (2005) 7470-7475.

[31] A.A. Martens, G. Portale, M.W.T. Werten, R.J. de Vries, G. Eggink, M.A.Cohen Stuart, F.A. de Wolf, Triblock Protein Copolymers Forming Supramolecular Nanotapes and pH-Responsive Gels. Macromolecules 42(4) (2009) 1002-1009.

[32] A.J. Engler, S. Sen, H.L. Sweeney, D.E. Discher, Matrix elasticity directs stem cell lineage specification. Cell 126(4) (2006) 677-689.

[33] M.W.T. Werten, W.H. Wisselink, T.J.J. Jansen-van den Bosch, E.C. de Bruin, F.A. de Wolf, Secreted production of a custom-designed, highly hydrophilic gelatin in Pichia pastoris. Protein Engineering 14(6) (2001) 447-454.

[34] M.K. Chaudhury, Rate-dependent fracture at adhesive interface. Journal of Physical Chemistry B 103(31) (1999) 6562-6566.

[35] E. Evans, K. Ritchie, Dynamic strength of molecular adhesion bonds. Biophysical Journal 72(4) (1997) 1541-1555.

# Chapter 2

# Production of collagen-inspired telechelic protein polymers

*Abstract*

In this chapter we focus on the design, synthesis and purification of collagen-inspired triblock polymers, which form very well-defined hydrogel networks upon cooling. We describe the cloning procedure, fermentation and purification. We also show some results concerning production yields, purity and quality of the produced proteins.

## 2.1 Introduction

For many applications, such as controlled drug delivery, tissue engineering, self-healing coatings *etc*., precisely-controlled, stimuli-responsive, self assembling polymers are desired. Most of the available macromolecules, however, suffer either from lack of controllability or biocompability, biodegradability and biofunctionality. For example, conventional gelatin, which is often used in biomedicine, and which is partially hydrolyzed and chemically modified animal collagen, is composed of a variety of molecules and structures with different thermal stabilities. Furthermore, as an animal derivative, it is a subject to a risk of contamination with prions or viruses and a risk of bringing about allergic reactions [1]. On the other hand, synthetic polymers that have a rather well-controlled size distribution, often lack biocompatibility, biofunctionality or biodegradability. All the downsides of the currently used materials, with simultaneous progress in genomics and proteomics, have brought scientists towards new approaches in material science, *viz.* molecular biology. Rapid progress in recombinant techniques allows producing molecules of defined composition and structure, and offering full control over the length and sequence of the biopolymer and its component blocks by changing the underlying DNA template. As a result, these materials combine the advantages of natural and synthetic polymers.

The collagen-inspired telechelic polypeptides, presented in this thesis are representative for such biotechnologically produced polymers. They are composed of three blocks. The side, blocks, abbreviated as T; consist of nine Pro-Gly-Pro (PGP) repeats. The resulting triple helices have a melting temperature of around 42 °C. The T blocks are spaced by a middle block, which is a concatemer of four or eight repeats of highly hydrophilic R or P designer sequences (Figure 2.1). R and P have an identical molecular weight and composition but a different sequence. The P sequence, although with glycine in every third position (as in collagen), does not form any supramolecular structures and maintains a random coil-like conformation at any temperature. Block R is a shuffled version of the P sequence [2] and behaves as a random coil, just like P. Every R/P motif consists of 99 amino acids where 33 residues are occupied by glycine (G), 22 by proline (P), 16 by glutamine (Q), 12 by asparagine (N), 8 by serine (S), 4 by glutamic acid (E), 3 by lysine (K) and 1 by alanine (A) (Figure 2.1). Due to the small number of charged amino acids (glutamic acid and lysine) in the polymer chain, the R and P blocks are pH and salt-independent. Four collagen-inspired polypeptides (TR4T, TP4T, TR8T, TP8T) (Figure 2.1) were designed and produced. The desired genes were constructed from synthetic DNA oligomers by overlap-extension PCR

according to Werten *et al.* [2] and restriction-mediated combination of various concatemeric segments and (polymer) blocks, cloned in *E. coli* and then transfected into the genome of the production host, the methylotrophic yeast *Pichia pastoris*. Even though several microbial production systems are known for the successful production of structural proteins [3-5] we chose *Pichia pastoris* because of its track record of high-level of heterologous gene expression and low-level endogenous protein secretion [6-8], which considerably facilitates the downstream processing. Furthermore, *Pichia pastoris* is an attractive production strain for scale-up to industrial levels as it can grow on cheap carbon sources (glycerol and methanol) and offers good genetic stability.

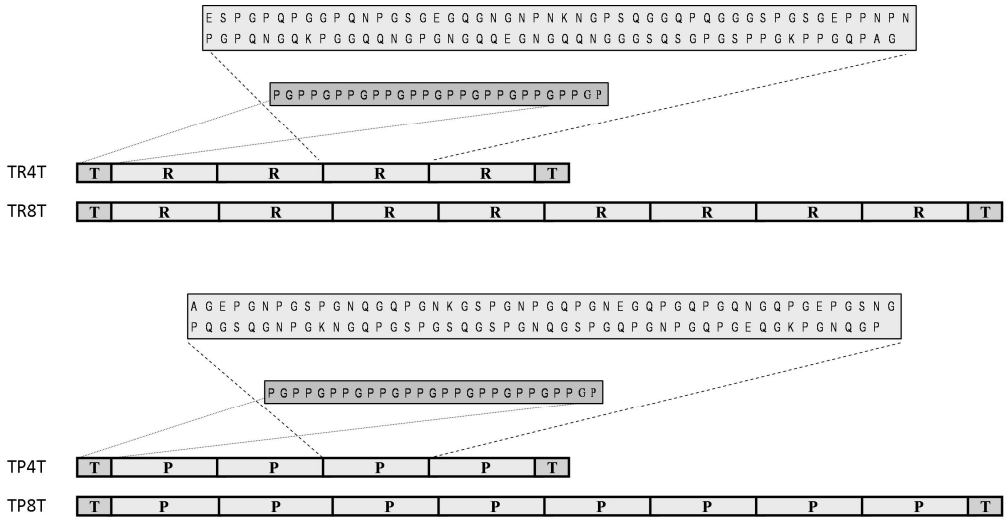


Figure 2.1 Schematic representation of collagen-inspired telechelic polypeptides: TR4T, TR8T, TP4T and TP8T.

## 2.2 Materials and methods

***TR4T- encoding vector preparation***

Here we give a short example of the standard cloning procedure used in our lab. More details can be found in reference [9].

The T block encoding vector was prepared by cloning 0.1 kb T- DNA fragments (prepared by PCR) into vector pCR4-TOPO (Invitrogen). The resulting vector pCR4-TOPO-T was digested with *Dra*III/*Van*91I. Then the released T block was ligated into the linearized and dephosphorylated previously described vector pMTL23-R4 (with *Dra*III), to yield vector pMTL23-TR4. This vector was then digested with *Van*91I, dephosphorylated, and the second T fragment was added, to yield vector pMTL23-TR4T. The TR4T encoding fragment was

released by digestion with *Xho*I/*Eco*RI and ligated into the *Pichia pastoris* expression vector pPIC9, to yield vector pPIC9-TR4T. The plasmid used for transformation was linearized with *Sal*I to promote normal growth on methanol by integration at the *his4* locus [10]. *Pichia pastoris* was transformed by electroporation as described previously [4].

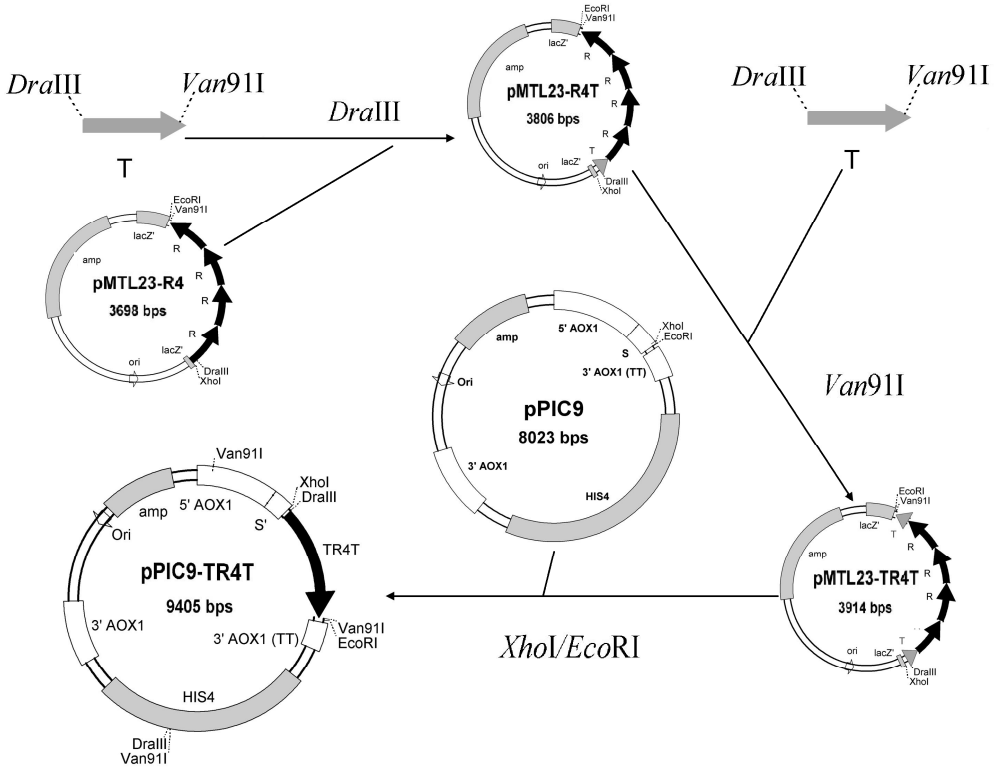


Figure 2.2 Construction of a vector with the gene encoding TR4T block polymer.

***Fermentation***

The fed-batch fermentation of transgenic *Pichia pastoris* was carried out either in a 3-l Bioflo 3000 (New Brunswick Scientific) or a 20-l Applikon fermenter at 30 °C and pH 3. Ammonium hydroxide was added to maintain the right pH. To assure aerobic conditions, air was continuously supplied to the reactor. The desired level of dissolved oxygen (DO) was maintained by changing the agitation speed, the air flow or in the case of the 20-l reactor the reactor overpressure. The batch medium, containing glycerol, basic salts and trace elements [11], was carbon-depleted within ~20-25 hours after inoculation. Subsequently, the feeding phase started: first with 50 % glycerol (4 hours), then with 99 % methanol (45 hours). In order to have a smooth transition from glycerol to methanol uptake, both feeds overlapped for two or three hours, during which the glycerol feed was slowly decreased. The methanol level in the fermentation broth was kept constant at ~0.2 % (w/v) by using a home-made semiconductor gas sensor-controller, similar to the one described by Katakura *et al.* [12]. At

the end of the process, the biomass was separated from the supernatant by centrifugation for 30 minutes at 20,000 xg in an SLA-3000 rotor (Sorval). After that, the collected supernatant was microfiltered in order to completely remove the remaining yeast cells.

***Purification***

All separation steps were carried out in a Sorval centrifuge with an SLA-3000 or SLA-1500 rotor for 30 minutes at 20,000 xg. Resuspension of protein pellets was done in MQ water for 30 minutes at 65 °C. Prior to the purification process, the supernatant was preheated for 30 minutes at 65 °C in order to melt possible gel structures formed by the recombinant protein. By raising the pH to 8 by slow addition of sodium hydroxide (1-2 M), medium salts, especially bi- and/or tri- valent cations, were precipitated and then separated by centrifugation. From the collected supernatant, the protein product was salted out by adding stepwise ammonium sulphate to a concentration of 40 % (w/w), followed by overnight incubation at 4 °C. The collected protein pellets were resuspended in three-fold smaller volume of MQ water and the precipitation procedure was repeated one more time. After the second salting out cycle, sodium chloride (50 mM) and acetone (40 % (v/v)) were added to precipitate the remaining *Pichia* proteins. After centrifugation at 4 °C the pellets were discarded and extra acetone (up to 80 % (v/v)) was added to the supernatant, to precipitate the recombinant gelatin. The obtained pellets were air-dried overnight, resuspended and lyophilized. Some batches were dialyzed prior to freeze drying. The batches that were not dialyzed contained roughly 15-20 % ammonium sulphate.

***SDS-PAGE***

The fractions obtained after every purification step, and the pure products were analyzed by SDS-PAGE using the NuPAGE Novex system (Invitrogen), with 10 % Bis-Tris gels, MES SDS running buffer and SeeBlue Plus2 prestained molecular mass markers. Gels were stained in Coomassie SimplyBlue SafeStain (Invitrogen) and destained in MQ water.

***Matrix Assisted Laser Desorption/Ionization (MALDI) Mass Spectrometry (MS)***

MALDI MS was performed using an Ultraflex mass spectrometer (Bruker). Samples were prepared by the dried droplet method on a 600 μm AnchorChip target (Bruker), using 5 mg/ml 2,5-dihydroxyacetophenone, 1.5 mg/ml diammonium hydrogen citrate, 25 % (v/v) ethanol and 1 % (v/v) trifluoroacetic acid as matrix. Measurements (20 Hz) were made in the positive, linear mode, with the following parameters: ion source 1, 20000 V; ion source 2,

18450 V; lens, 5000 V; pulsed ion extraction, 550 ns. Protein Calibration Standard II (Bruker) was used for external calibration.

## 2.3 Results and discussion

***Fermentation***

*Pichia pastoris* strains, transfected with the genes encoding collagen-like triblock polypeptides (TR4T, TP4T, TR8T and TP8T) were fermented in a 3-l or 20-l reactor. The whole fermentation process took ~70 hours. The batch phase lasted 20-25 hours and was followed by a feeding phase: 3-4 hours with glycerol and ~45 hours with methanol. In order to have a smooth transition from glycerol to methanol uptake, both feeds overlapped for two or three hours, during which the glycerol feed was slowly decreased. In Figure 2.3 we plot: the wet biomass concentration ($C_{X\_wet}$), the specific growth rate ($\mu$), the specific methanol uptake ($q_M$) and the biomass yield on methanol ($Y_{XM}$) as a function of fermentation time for two typical TR4T fermentations. The specific growth rate ($\mu$) and specific methanol uptake ($q_M$) were calculated for each time interval ($t_i$-$t_{i-1}$) as: $\mu=[M_x(t_i)-M_x(t_{i-1})]/[(t_i-t_{i-1})\cdot M_{x\_avr}(t_i,t_{i-1})]$ and $q_M=[M_M(t_i)-M_M(t_{i-1})]/[(t_i-t_{i-1})\cdot M_{x\_avr}(t_i,t_{i-1})]$, respectively, where $M_x(t_i)$ is biomass amount in the whole reactor at given time $t_i$, $M_M$ ($t_i$) is the amount of methanol consumed at a given time $t_i$, and $M_{x\_avr}(t_i,t_{i-1})$ is the average amount of biomass in the reactor between $t_{i-1}$ and $t_i$. Biomass yield on methanol was calculated as: $Y_{XM}= \mu/q_M\ [g_X/g_M]$.

From the data plotted in Figures 2.3A and B we can see that the increase of the biomass in the 3-l fermenter develops in a slightly different way than in the 20-l fermenter. These variations are possibly caused by differences in oxygen transfer in the 3-l and 20-l reactor. It is known that oxygen transfer is more efficient in smaller vessels [13]. Since *Pichia pastoris* fermentation is an oxygen-limited process, differences in oxygen transfer influence the specific oxygen uptake and hence $\mu$. Contrary to $\mu$, we do not notice important differences in specific methanol uptake $q_M$ (Figure 2.3C). Both in the 3-l or in the 20-l vessel $q_M$ is roughly the same and varies between 0.01 and 0.04 $g_M/g_X$. The methanol, which is not used for biomass production probably is used for maintenance ($m_s$ in the Herber-Pirt equation [13]). However, as we do not know the complete process kinetics we can not make clear conclusions.

The dissimilarities in specific growth rate between different reactors obviously lead to different yields of biomass on methanol (Figure 2.3D). The big reactor showed a lower biomass yield calculated at each time interval but also calculated cumulatively at the end of the fermentation *i.e.* ~1.4 $g_X/g_M$ for the 3-l fermenter and ~1 $g_X/g_M$ for the 20-l reactor.

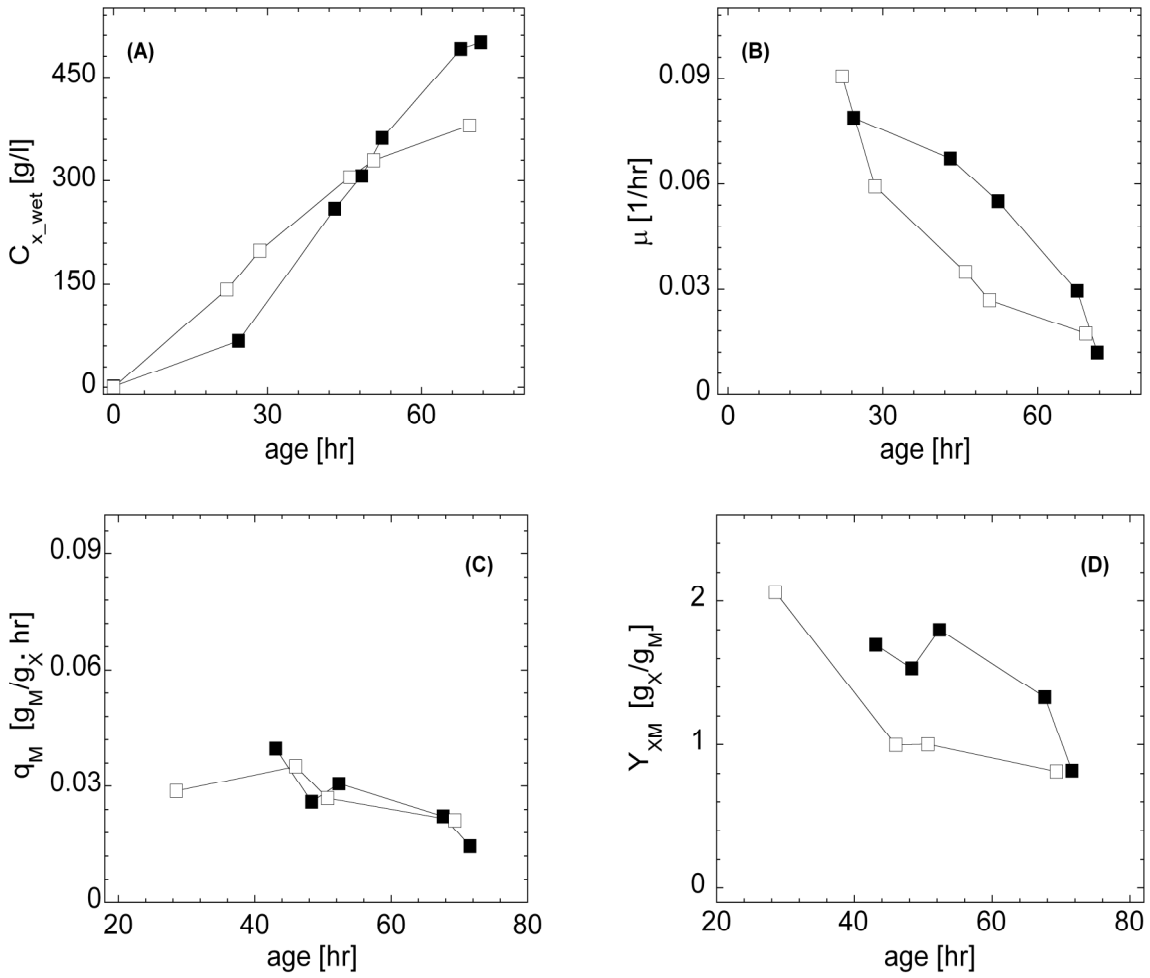


Figure 2.3 (A) The wet biomass concentration, (B) the specific growth rate, (C) the specific methanol uptake, and (D) the wet biomass yield on methanol during TR4T fermentation in a 3-l (■) and a 20-l (□) fermenter.

### *Purification*

The purification process for collagen-inspired proteins was relatively simple since the expression system secretes the heterologous product into the fermentation medium, while it secretes only modest amounts of endogenous proteins [6]. Cell-free supernatant was obtained by consecutive centrifugation and microfiltration of fermentation broth. The protein was then purified from the supernatant by a two step ammonium sulphate precipitation, followed by acetone precipitation. The protein flocks obtained, were separated by centrifugation and then dissolved in MQ water. Some protein samples were dialysed prior to lyophilisation. Figure 2.4 shows SDS-PAGE analysis of TR4T protein after different purification steps.

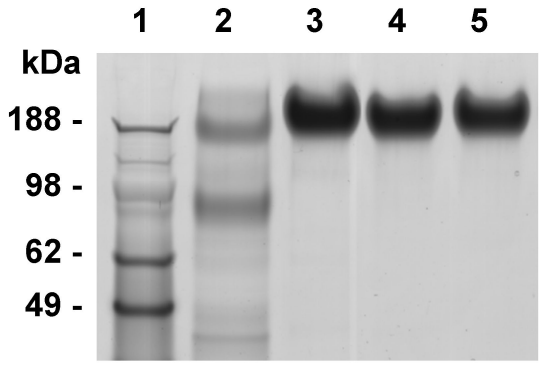


Figure 2.4 SDS-PAGE analysis of TR4T protein after different purification steps: lane 1- molecular weight marker; line 2 cell-free supernatant; lane 3-resuspended pellets after first ammonium sulphate precipitation; lane 4-resuspended pellets after second ammonium sulphate precipitation; lane 5-final product after lyophilisation.

***Protein quality***

The purified proteins were analyzed with SDS-PAGE (Figure 2.5). All of them migrated as single bands demonstrating a high purity and intactness. However, they showed abnormal migration in SDS-PAGE gels. This has been observed before for collagenous proteins, which on SDS-PAGE usually migrate to an apparent $M_w$ that is 1.4 times lower [14]. P and T containing constructs migrate even slower than normal collagen [2]. That is because they are very hydrophilic and therefore bind little SDS. SDS binds its hydrophobic chain to hydrophobic patches on protein and confers those proteins a negative charge.

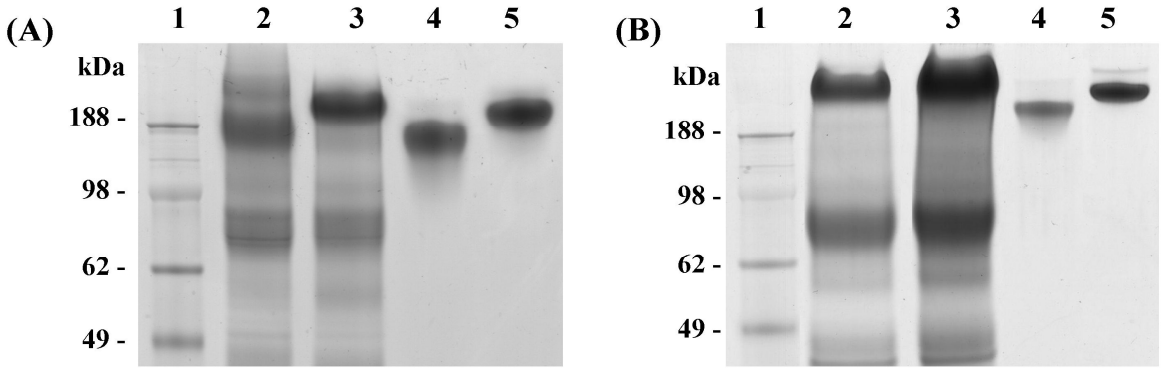


Figure 2.5 Protein polymers: (A) SDS-PAGE: lane 1-molecular weight marker; lane 2 cell-free TR4T fermentation broth; lane 3 cell-free TP4T fermentation broth; lane 4 purified TR4T; lane 5 purified TP4T. (B) SDS-PAGE: lane 1-molecular weight marker; lane 2 cell-free TR8T fermentation broth; lane 3 cell-free TP8T fermentation broth; lane 4 purified TR8T; lane 5 purified TP8T. 15µl of cell-free fermentation broth and ~20 µg of purified protein were applied. Figure A has been taken (in a modified form), from reference 9 with a permission of authors.

The molecular weight and product purity for all molecules were verified with MALDI-TOF MS. Figure 2.6 shows that pure monodisperse products were obtained with the molecular weights within experimental error equal to the theoretical values of 41.741 kDa for TR4T and TP4T and 78.176 kDa for TR8T and TP8T.

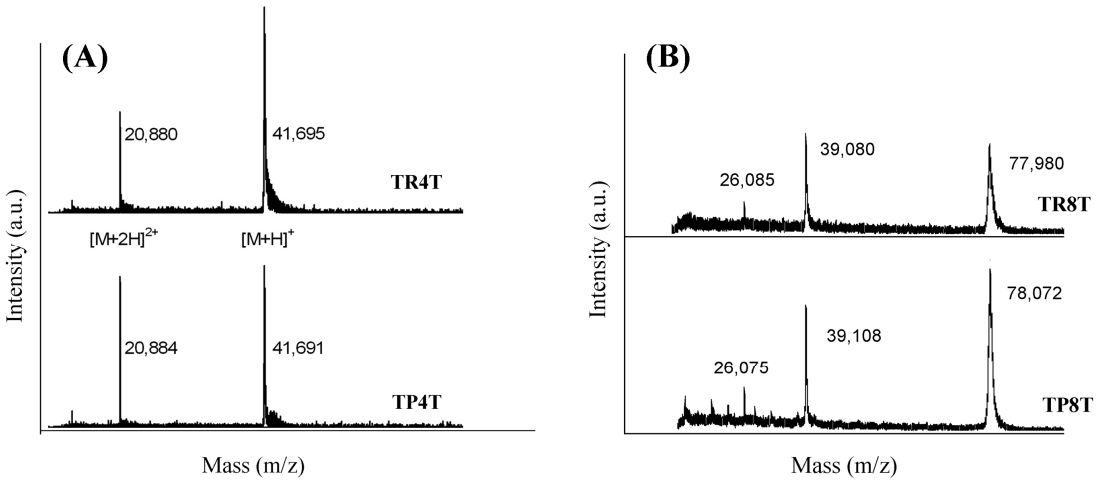


Figure 2.6 MALDI-TOF MS of purified: (A) TR4T and TP4T, and (B) TR8T and TP8T. Single and doubly charged molecular ions are indicated. Figure A has been taken (in a modified form), from reference 9 with a permission of authors.

## 2.4 Concluding remarks

In this chapter we presented the production route of collagen-inspired telechelic block polymers. By employing the methylotrophic expression host *Pichia pastoris*, we could produce, in high yields heterologous, monodisperse gel-forming proteins, utilizing a cheap carbon source (methanol 200-270 $/tonne [15] ). As the objective proteins are directly targeted to the fermentation broth and secretion of endogenous proteins is low, the downstream processing is simple and requires essentially only an ammonium sulphate precipitation. This, in case of biotechnological processes, is highly advantageous, as often 50-70 % of the operating costs have to be devoted to protein separation [16].

All the economical concerns, together with advantages such as monodispersity, biocompability, biodegradability and controllability (see next chapters), which are characteristic for biotechnologically produced polymers make collagen-inspired polypeptides very promising molecules for the demanding application market.

## Acknowledgements

We thank Marc Werten for the construction, cloning and transformation to *Pichia pastoris* of TR4T, TP4T, TR8T and TP8T genes and Antoine Moers for developing the purification procedure. We also thank Werten *et al.* [9] for allowing us to use some of their data to plot Figures 2.5A and 2.6A.

## References


[1] European Commission, Updated opinion on the safety with regards to TSE risks of gelatine derived from ruminant bones or hides. (2003).

[2] M.W.T. Werten, W.H. Wisselink, T.J.J. Jansen-van den Bosch, E.C. de Bruin, F.A. de Wolf, Secreted production of a custom-designed, highly hydrophilic gelatin in Pichia pastoris. Protein Engineering 14(6) (2001) 447-454.

[3] E.C. de Bruin, F.A. de Wolf, N.C.M. Laane, Expression and secretion of human alpha 1(I) procollagen fragment by Hansenula polymorpha as compared to Pichia pastoris. Enzyme and Microbial Technology 26(9-10) (2000) 640-644.

[4] M.W.T. Werten, T.J. Van den Bosch, R.D. Wind, H. Mooibroek, F.A. De Wolf, High-yield secretion of recombinant gelatins by Pichia pastoris. Yeast 15(11) (1999) 1087-1096.

[5] G. Gellissen, C.P. Hollenberg, Application of yeasts in gene expression studies: A comparison of Saccharomyces cerevisiae, Hansenula polymorpha and Kluyveromyces lactis - a review. Gene 190(1) (1997) 87-97.

[6] P.Z. Li, A. Anumanthan, X.G. Gao, K. Ilangovan, V.V. Suzara, N. Duzgunes, V. Renugopalakrishnan, Expression of recombinant proteins in Pichia pastoris. Applied Biochemistry and Biotechnology 142(2) (2007) 105-124.

[7] R. Schipperus, R.L.M. Teeuwen, M.W.T. Werten, G. Eggink, F.A. de Wolf, Secreted production of an elastin-like polypeptide by Pichia pastoris. Applied Microbiology and Biotechnology 85(2) (2009) 293-301.

[8] A. Moers, E.J.H. Wolbert, F.A. de Wolf, M.W.T. Werten, Secreted production of self-assembling peptides in Pichia pastoris by fusion to an artificial highly hydrophilic protein. Journal of Biotechnology 146(1-2) (2010) 66-73.

[9] M.W.T. Werten, H. Teles, A. Moers, E.J.H. Wolbert, J. Sprakel, G. Eggink, F.A. de Wolf, Precision Gels from Collagen-Inspired Triblock Copolymers. Biomacromolecules 10(5) (2009) 1106-1113.

[10] J.M. Cregg, K.J. Barringer, A.Y. Hessler, K.R. Madden, Pichia Pastoris as a host system for transformations. Molecular and Cellular Biology 5(12) (1985) 3376-3385.

[11] W.H. Zhang, M.A. Bevins, B.A. Plantz, L.A. Smith, M.M. Meagher, Modeling Pichia pastoris growth on methanol and optimizing the production of a recombinant protein, the heavy-chain fragment C of botulinum neurotoxin, serotype A. Biotechnology and Bioengineering 70(1) (2000) 1-8.

[12] Y. Katakura, W.H. Zhang, G.Q. Zhuang, T. Omasa, M. Kishimoto, W. Goto, K.I. Suga, Effect of methanol concentration on the production of human beta(2)-glycoprotein I domain V by a recombinant Pichia pastoris: A simple system for the control of methanol concentration using a semiconductor Gas Sensor. Journal of Fermentation and Bioengineering 86(5) (1998) 482-487.

[13] J.J. Heijnen, Fermentaion Technology. Delft, 2002.

[14] R.J. Butkowski, M.E. Noelken, B.G. Hudson, Estimation of the size of collagenous proteins by electrophoresis and gel chromatography. Methods in Enzymology 82 (1982) 410-423.

[15] http://www.icis.com/v2/chemicals/9076034/methanol/pricing.html.

[16] L. van der Wielen, Downstream Processing Advanced Course. Delft, 2005.

# Chapter 3

# Physical gels of telechelic triblock copolymers with precisely-defined junction multiplicity

*Abstract*

In this chapter we study transient networks formed by monodisperse telechelic polypeptides with collagen-like end blocks and a random coil-like middle block. These artificial proteins are created using recombinant DNA techniques. Upon cooling, the end blocks associate reversibly into triple helices, leading to gels with a well-defined junction multiplicity of three. Both, the storage modulus and the relaxation time of the gel increase very strongly as a function of concentration, and decrease with increasing temperature. All the experimental results are described quantitatively by an analytical model, based on classical gel theory that requires no adjustable parameters, and accounts for the molecular structure of the gel, and the presence of loops and dangling ends.

Published as: P.J. Skrzeszewska, F.A. de Wolf, M.W.T. Werten, A.P.H.A. Moers, M.A.Cohen Stuart, J. van der Gucht, Physical gels of telechelic triblock copolymers with precisely defined junction multiplicity. Soft Matter 5(10) (2009) 2057-2062.

## 3.1 Introduction

Polymer gels, due to their properties, have many applications, for example as drug delivery systems [1], wound dressing materials [2], and rheological regulators in polymer blends [3]. In general, two classes of gels can be distinguished. Permanent gels are formed by strong covalent crosslinks. They do not restructure or flow. By contrast, physical or reversible gels are formed by weak interactions such as hydrogen bonds, van der Waals forces, hydrophobic or electrostatic interactions. These gels have the possibility to restructure. Moreover, the crosslinks can respond to changes in conditions, such as temperature, concentration, or pH. Examples of thermoreversible physical gels are gelatin and agarose [4] (formed upon cooling) or polymethacrylic acid [4] and methyl cellulose [5] (formed upon heating).

An interesting class of physical gels is formed by associative telechelic polymers. These are triblock copolymers with groups at their ends that can reversibly assemble into supramolecular knots. The middle block has hydrophilic character and serves as a spacer. A lot of research has been devoted to water-soluble polymers (such as PEO) terminated with hydrophobic groups at both ends [6, 7]. These molecules form reversible networks in which the junction points consist of micelles formed by association of the hydrophobic end groups. Other examples of associating telechelic polymers are biosynthetic protein polymers with end groups inspired by the natural protein elastin, which associate by hydrophobic interactions [8, 9], and protein polymers with leucine zipper domains at the ends, which aggregate by coiled-coil interactions [10, 11].

Associative telechelic polymers serve as model molecules for studying the structure and rheological behaviour of physical gels. Qualitatively, the network formation in these systems and its dynamics can be understood from theoretical models that take into account intra- and inter-molecular associations, as well as the transient character of the crosslinks [12, 13]. However, quantitative modelling is very difficult for the systems that have been studied so far, because the multiplicity of the nodes is not controlled and invariably polydisperse.

In this chapter we study a new class of thermoreversible gels [14], in which the node multiplicity is precisely known. The gel network is formed by a telechelic polypeptides [14] with $(Pro\text{-}Gly\text{-}Pro)_9$ end blocks inspired by, and behaving like natural collagen [14, 15], while the middle block (399 amino acids long) is rich in hydrophilic amino acids and assumes a random coil structure in water in a wide range of temperatures (Figure 3.1A). The polypeptide, produced by genetically modified yeast (*Pichia pastoris*), is monodisperse and

has well-defined length and amino acid sequence. Below the melting temperature, the side blocks assemble and form triple helices in a reversible manner (Figure 3.1B), while the middle block maintains a random coil structure. Stable junction points can only be formed when three collagen-like side blocks form a triple helix, as double helices are not stable (Chapter 5). As a consequence, a physical gel is formed in which the node multiplicity is exactly three (Figure 3.1C). As we will show this well-defined multiplicity allows us to model the network properties quantitatively.

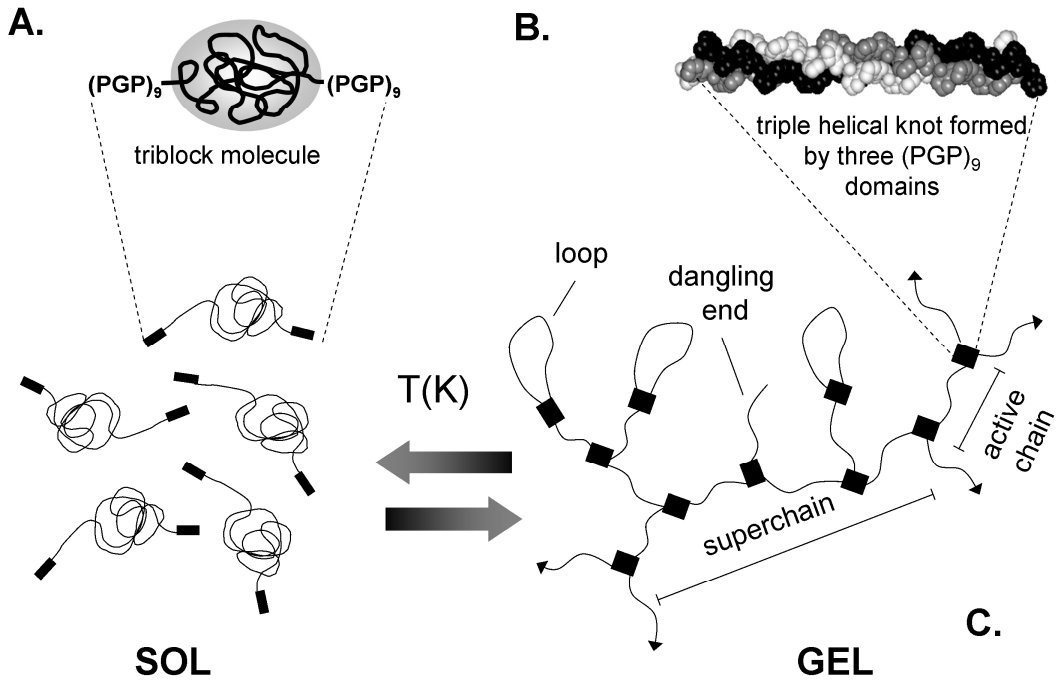


Figure 3.1 Gel network formations by telechelic polypeptides. (A) Single polypeptide consisting of a random coil-like middle block flanked by collagen-like end blocks (G-glycine, P-proline). (B) Triple helical knot formed by three collagen-like end blocks. (C) Gel network formed reversibly by telechelic molecules upon cooling. Chains terminated with an arrow are connected to the percolated gel network.

In addition to being an ideal model system for studying the relation between structure and rheology of physical gels, the investigated system could also provide an improved alternative for gelatin, in for example, medical, pharmaceutical, food, or cosmetic applications. Conventional gelatin, derived from partially hydrolyzed and chemically modified animal collagen, is susceptible to a risk of contamination with prions or viruses and a risk of eliciting allergic reactions, particularly against the non helix-forming domains of collagen. The molecules studied here, produced in microbial cells, eliminate those risks.

In this chapter we investigate the viscoelastic properties of these collagen-inspired telechelic polypeptides as a function of polymer concentration and temperature. To explain

the experimental data, an analytical model is developed that takes into account the multiplicity of the network and the transient character of the triple helical junctions.

## 3.2 Material and methods

***Recombinant protein***

The recombinant protein (TR4T) was prepared by inserting an artificial gene into the genome of *Pichia pastoris* and then produced in a fed-batch fermentation process [14]. Purification consists of several precipitation steps. More details can be found in Chapter 2. The protein has a molecular weight of ~42 kDa and comprises three blocks (Figure 3.1A). The end blocks, abbreviated as T (trimer-forming), consist of nine consecutive Pro-Gly-Pro triplets [14]. Such $(Pro\text{-}Gly\text{-}Pro)_n$ stretches are know to form collagen-like triple helices [16]. The middle block R4 (399 amino acids) has a sequence that does not lead to any secondary or tertiary structure; it assumes a random coil configuration [14]. The amino acid sequence of the middle block corresponds to a randomized version of the sequence of the P4 block (Chapter 2), in such a way that glycine is not every third residue, thus preventing triple helix formation. Accordingly, it was shown by circular dichroism spectroscopy [14] and differential scanning calorimetry (Chapter 5) that the end blocks exclusively (near-quantitatively) participate in triple helix formation. The amino acid sequences of the TR4T triblock protein and of a separately produced protein corresponding to the R4 middle block have been deposited in GenBank under accession numbers ACF33479 and ACF33477, respectively.

***Rheology***

Four different concentrations of protein were tested (0.96, 1.1, 1.3 and 1.4 mM). All samples were prepared in the same way. A given amount of protein was dissolved in phosphate buffer (pH 7, I=10 mM) and then heated at 50 °C for half an hour, allowing the protein to dissolve completely under conditions where no triple helices form. The rheological measurements were made using an Anton Paar, Physica MCR 301 rheometer equipped with a cone and plate geometry of 50 mm diameter. The temperature was controlled by a Peltier system, which allowed fast heating and cooling. A solvent trap was used to minimize evaporation. Before adding the warm protein solution, the plate was preheated to 50 °C. After lowering the cone, the system was quenched to 20 °C. Gel formation was monitored by applying a sinusoidal deformation to the system (f=1 Hz and $\gamma$=1 %) and determining the storage (G') and loss (G") moduli. It was checked that this deformation does not significantly influence the kinetics of gel formation (Chapter 5). Viscoelastic dynamic characterization of

the steady state gel was performed in a frequency range 0.001-20 Hz (0.00628-125 rad/s) and with deformation amplitude of 1 %, well within the linear response regime. Creep experiments were carried out at different applied stresses between 5 and 20 Pa, depending on protein concentration. The stress values were chosen not to go beyond the linear regime. The duration of the deformation phase was 1800 s, which was followed by 1800 s of recovery. Creep experiments were done at different temperatures. After the gel was formed at 20 °C, the temperature was decreased in steps to 15, 10 and 5 °C. At each temperature, the system was equilibrated for 5 hours, before doing measurements.

## 3.3 Experimental results

At temperatures above 50 °C, solutions of TR4T were viscous without detectable elastic response. When the sol was cooled down to 20 °C a physical gel was formed as a result of triple helix formation by the collagen-like end blocks.

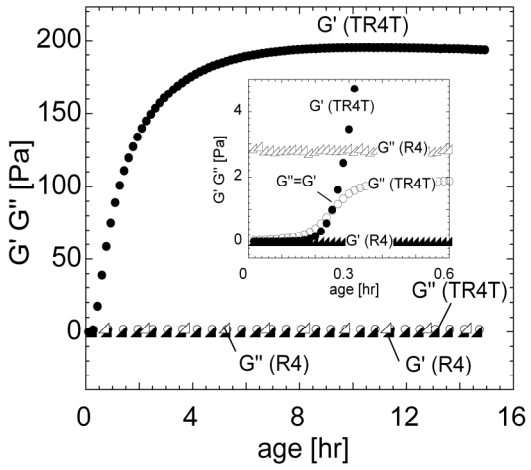


Figure 3.2 Storage (●) and loss (○) moduli for 1.4 mM TR4T; storage (◢) and loss (◿) moduli for 1.4 mM R4 as a function of age (f=1 Hz, γ=1 %). Inset presents a zoom of the initial stages of gelation.

Figure 3.2 displays the development of the storage (G') and loss (G") moduli for a 1.4 mM solution. In the beginning, viscous properties are dominant and the system does not show any gel-like behaviour. With time, as the gel forms, the elastic properties start to play a more important role. After some time (~12 minutes) G' and G" cross. The steady-state is reached after approximately 6 hours. The same type of experiment with the R4 block only (hence without helix-forming ends) showed no development of the storage modulus with time (Figure 3.2). From this, we concluded that the network formation is a consequence of triple helix formation by the end blocks, and not caused by entanglements.

The dynamic, viscoelastic behaviour of the stable gel was investigated by means of frequency sweeps. Storage and loss moduli as a function of frequency for different protein concentrations are presented in Figure 3.3A.

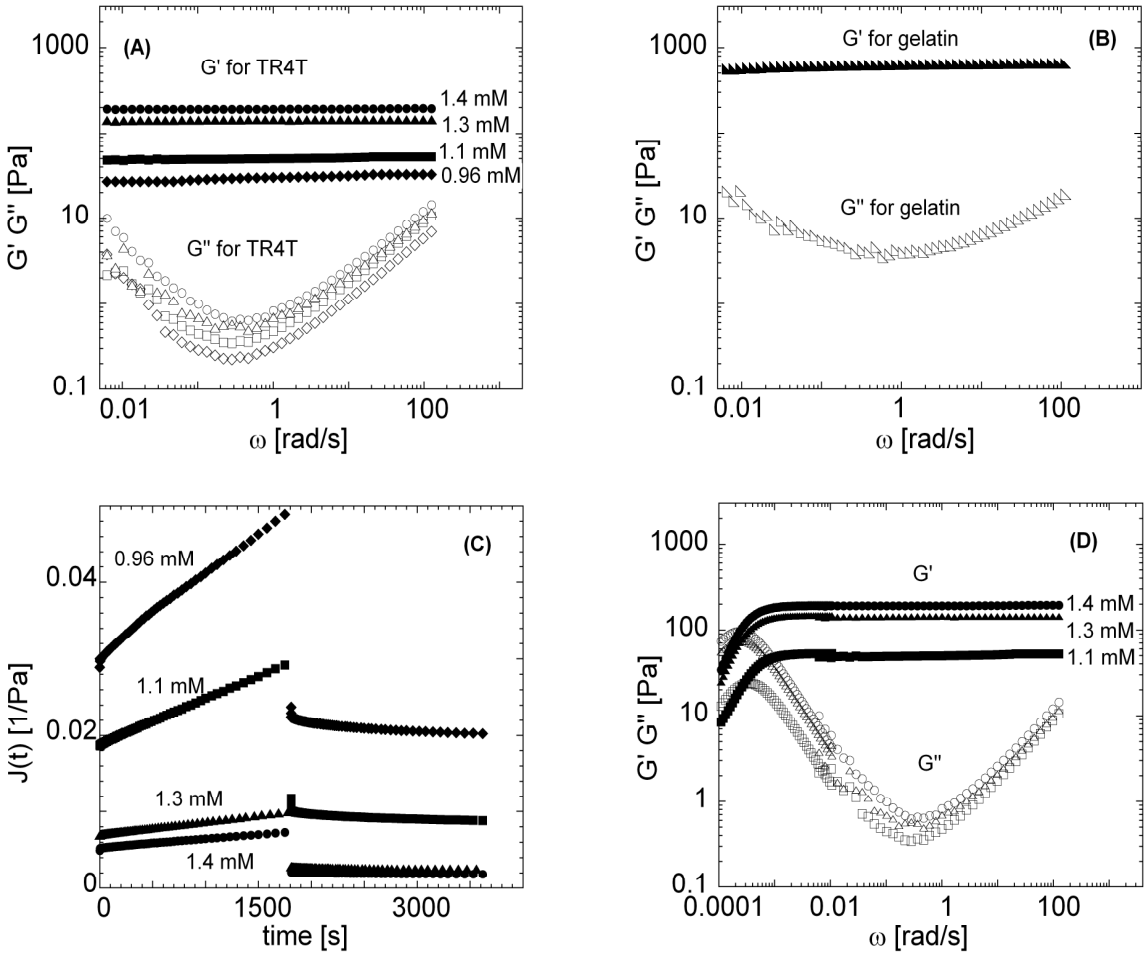


Figure 3.3 (A) Frequency sweeps at T=293 K for different protein concentrations (as indicated). (B) Frequency sweep for 50 g/l of gelatin at T=293 K. (C) Creep experiments at 293 K for different protein concentrations (as indicated). (D) Combined frequency sweeps and converted creep experiments from Figures 3.3A and C.

In all cases the elastic behaviour (G') dominates over the viscous behaviour (G"). The storage modulus does not depend on frequency in the range between 0.01 and 100 rad/s. The loss modulus initially decreases with frequency, goes through a minimum and then increases again. We note that gelatin has a similar viscoelastic response (Figure 3.3B).

In order to gain insight into the system on time scales above 100 s, creep experiments were done. A constant stress was applied to the gel and the resulting deformation was measured as a function of time. Deformation is expressed as a time dependent compliance J(t) (strain divided by applied stress). Creep curves (Figure 3.3C) are characterized by a rapid

elastic response followed by a slow viscous response. When the stress is removed, the elastic response is recovered. The creep curves are rather accurately, although not exactly, described by a single-relaxation time Maxwell model, $J(t)=1/G_0+t/\eta$, where $G_0$ is the plateau elastic modulus and $\eta$ is the zero-shear viscosity. This was expected, since many transient networks obey Maxwell behaviour [6]. The creep data were converted to the frequency domain by a method described by Ferry [18]. Together with the frequency sweeps presented in Figure 3.3A, this gives the viscoelastic behaviour of the system over a broad frequency range, comprising six decades (Figure 3.3D).

From the data presented in Figure 3.3, we obtain the plateau modulus $G_0$, the zero-shear viscosity $\eta$ (the inverse slope of J=f(t) at long deformation times), and the relaxation time of the gels $\tau$ ($\eta$ divided by $G_0$). These parameters are plotted as a function of concentration and temperature in Figures 3.4 and 3.5. In these figures, the symbols represent the experimental data, while the solid lines correspond to model calculations, described in section 3.4.

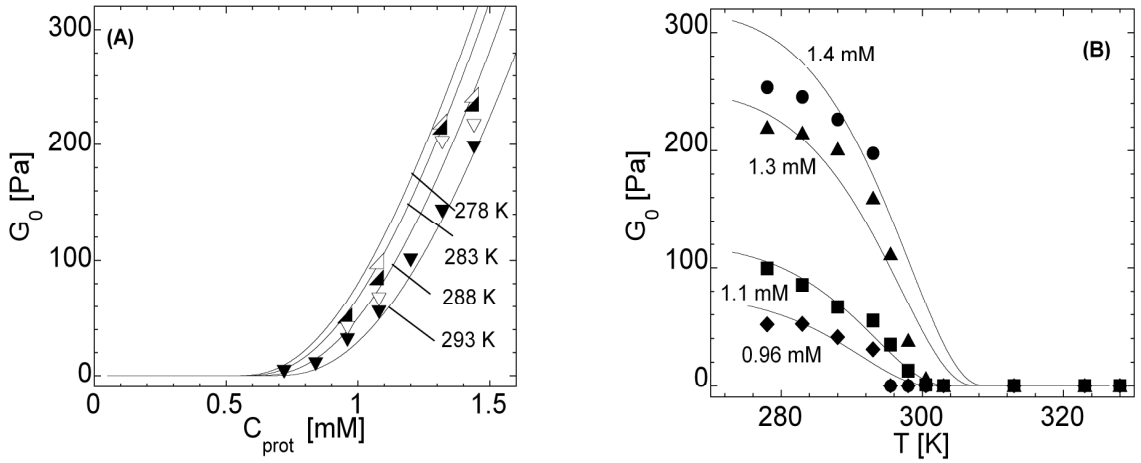


Figure 3.4 (A) Plateau storage modulus as a function of concentration of protein ($C_{prot}$) at different temperatures: (▼) 293 K, (▽) 288 K, (◢) 283 K, (◿) 278 K. (B) Plateau storage modulus as a function of temperature for different protein concentrations ($C_{prot}$): (●) 1.4 mM, (▲) 1.3 mM, (■) 1.1 mM, (◆) 0.96 mM. In both figures, solid lines correspond to model calculations described in section 3.4.

Figure 3.4A shows the plateau modulus ($G_0$) as a function of the concentration at different temperatures. Clearly, the storage modulus depends strongly on concentration. Below $C_{prot}$~0.9 mM the gel is very weak, as being close to a percolation threshold. At a concentration of 1.4 mM it has already a significant storage modulus of ~250 Pa. The temperature dependency is presented in Figure 3.4B. At T>310 K there is no measurable storage modulus, while at low temperatures the modulus stabilizes at a plateau. Note that the

temperature at which the gel properties disappear is lower than the melting temperature of the triple helices, measured with calorimetry (Chapter 5).

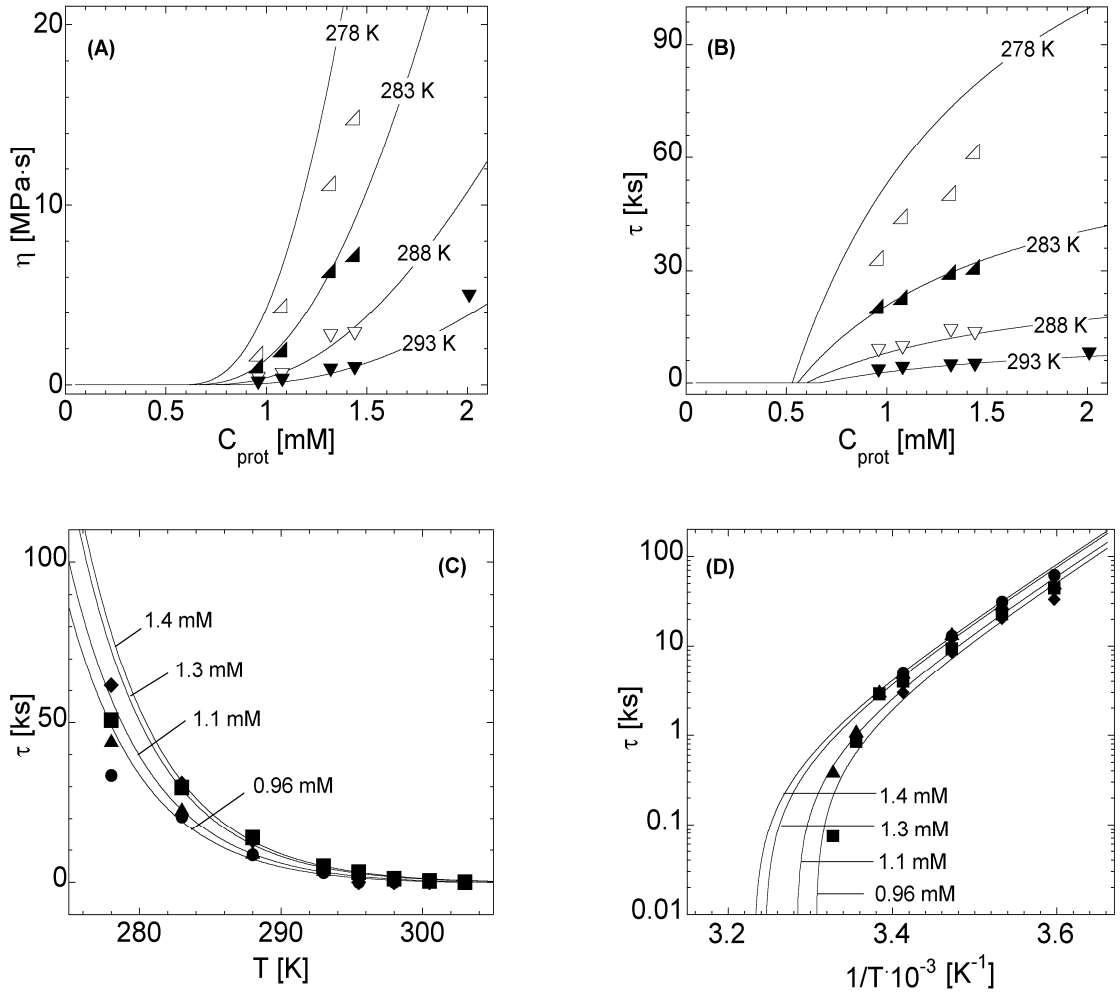


Figure 3.5 (A) η as a function of protein concentration at different temperatures: (▼) 293 K, (▽) 288 K, (◢) 283 K, (◿) 278 K. (B) τ as a function of protein concentration at the same temperatures. (C) τ as a function of temperature for different protein concentrations: (●) 1.4 mM, (▲) 1.3 mM, (■) 1.1 mM, (◆) 0.96 mM. (D) Arrhenius plot of τ for the same concentrations. In all figures, the solid lines correspond to model calculations described in section 3.4.

As can be seen in Figure 3.5, both η and τ, increase with decreasing temperature and increasing protein concentration ($C_{prot}$). Figure 3.5D is an Arrhenius plot of the relaxation time, showing that dissociation of triple helices is an activated process, characterized by an activation barrier.

The dependence of the storage modulus on the protein concentration is much stronger than for commonly known physical gels such as gelatin [19] or pectins [20]. According to classical gel theory, the modulus is proportional to the concentration of elastically active

chains, *i.e.* chains that bridge two crosslinks in the gel. Our results therefore indicate that the fraction of chains that are active increases strongly with increasing concentration.

Moreover, the concentration dependence of the relaxation time (Figure 3.5B) indicates that the relaxation time is not simply determined by the dissociation of a single triple helix. There must be other factors contributing to stress relaxation. Experiments above the melting temperature and experiments with the R4 block without helix-forming blocks showed that entanglements do not contribute to the elasticity of the gels. Rather, we believe that the detailed structure of the network is responsible for the strong concentration dependence. To test this, we developed a model based on the classical network theory of Flory [21] and Stockmayer [22], which accounts, explicitly, for the well-defined functionality of the network.

## 3.4 Model

Each triple helix is formed by association of three end blocks. The equilibrium constant for this process is written as:

$$K_H = \frac{C_H}{C_F^{\,3}} \qquad \text{(Eq. 3.1)}$$

where $C_H$ is the concentration of triple helices and $C_F$ the concentration of free end blocks. (Note that the detailed structure of the triple helix (all ends parallel or two parallel and one antiparallel) is not important for the mechanical properties of the gel because the middle block is relatively long). There are two possibilities to form a triple helix. It can be formed either by three end blocks from three different chains, or by three end blocks from two different chains, such that two side blocks come from the same polypeptide. The first case leads to the junction points of the network, while the second case corresponds to loops. Loops, in addition to free (dangling) ends, act as gel stoppers (see Figure 3.1C). Obviously, $C_H=C_J+C_L$ with $C_J$ the concentration of junctions and $C_L$ that of loops.

The probability to form a junction (with volume $\upsilon$), is $(C_F\cdot\upsilon)^3$, because three free end groups have to meet in a volume $\upsilon$ The probability to form a node involved in a loop is $[(C_F\cdot\upsilon)^2]\cdot[\upsilon/V_{coil}]\cdot[C_F/2C_{prot}]$. Here, the first factor is the probability that two free end groups of different chains meet, the second factor is the probability that the other end of one of these chains is also situated in the volume $\upsilon$ (with $V_{coil}$ the volume of a polymer coil), and the third factor is the probability that this end is not (yet) involved in a helix, with $C_{prot}$ the total concentration of chains. It follows that:

$$C_L = \frac{C_J}{2 \cdot C_{prot} \cdot V_{coil}} \approx \frac{C_J \cdot C^*}{2 \cdot C_{prot}} \qquad \text{(Eq. 3.2)}$$

where $C^* \approx 1/V_{coil}$ is the overlap concentration. Loops are predominant below the overlap concentration C*, while junctions are predominant for $C_{prot} > C^*$.

For given $K_H$ and $C_{prot}$, the concentrations of free end groups (dangling ends), loops, and junctions can be calculated using equations 3.1 and 3.2. The probability for a certain end group to be involved in a junction point is equal to $p = 3C_J/2C_{prot.}$ According to classical gel theory, the critical gelation (or percolation) threshold for a trifunctional network is at p=1/2. For p>1/2, a certain fraction of chains is connected to an infinite cluster. Dangling ends or loops are termination points for the cluster. The probability β that a given branch, emanating from a junction point is not connected to the infinite cluster can be calculated from the probability p. In a mean-field approximation β=(1-p)/p [23]. The probability that all three emanating chains are connected to the infinite cluster is $(1-\beta)^3$, while the probability that only two out of three chains are linked to the gel is $3\beta(1-\beta)^2$.

Only junction points with all three branches linked to the gel network connect elastically active chains. Junction points with only two of their chains linked to the gel merely elongate the active chains and are responsible for the formation of so-called “superchains”, active chains consisting of more than one molecule (Figure 3.1C) [23].

The total number of elastically active chains can be calculated as $\nu_{eff} = 1.5 \cdot C_J (1-\beta)^3$ where the factor 1.5 takes into account that each junction has three active chains and that each active chain connects two junction points. This gives for the elastic modulus:

$$G_0 \approx F \cdot \nu_{eff} \cdot R \cdot T = F \cdot 1.5 \cdot C_J \cdot (1-\beta)^3 \cdot R \cdot T = \frac{F \cdot \left[ C_{prot} \cdot (2p-1)^3 \cdot R \cdot T \right]}{p^2} \qquad \text{(Eq. 3.3)}$$

here RT is the thermal energy per mole, and F is a pre-factor, the so-called front factor. In the classical, affine network theory, F=1 [21], while for the phantom network model F=1/3 in the case of nodes with multiplicity of three [24]. For p=1/2 (percolation threshold), the modulus vanishes, while for p=1 (all junctions active) we recover the classical rubber-like scaling $G_0 = F \cdot C_{prot} \cdot R \cdot T$.

The total number of chains involved in links, *i.e.* junction points connected with at least two strands to the gel, is:

$$n = C_J \cdot [1.5 \cdot (1-\beta)^3 + 3 \cdot \beta \cdot (1-\beta)^2] \qquad \text{(Eq. 3.4)}$$

From this we obtain for the average length of an active chain:

$$< N >= \frac{n}{\nu_{eff}} = \frac{1}{2p-1} \qquad \text{(Eq. 3.5)}$$

Just above the network threshold (p=1/2), that is, slightly below the melting temperature or at low concentrations, the effective active chains are much longer than a single polymer chain (we call these superchains, see Figure 3.1C); for p close to unity, <N> goes to unity.

Stress relaxation occurs when an elastically active chain breaks. Here, this happens when a triple helix (junction point) dissociates. A superchain consisting of N molecules can break in N places, so its relaxation time is expected to be N times shorter than the life time $\tau_0$ of a single helix:

$$\tau - \frac{\tau_0}{< N >} = \tau_0 \cdot (2p-1) \qquad \text{(Eq. 3.6)}$$

We note that $\tau_0$ is related to the thermal dissociation rate of a triple helix $\tau_0 = k_d^{-1}$ with $k_d$ the dissociation rate constant. For $k_d$ we assume Arrhenius behaviour:

$$k_d = k_{d,0} \cdot \exp\left[\frac{-E_a}{RT}\right] \qquad \text{(Eq. 3.7)}$$

where $E_a$ is the activation energy. Dissociation becomes faster as the temperature increases. The equilibrium constant of helix formation is also a function of the temperature. This temperature dependence can be expressed by Van‘t Hoff’s equation:

$$K_H = K_{H,0} \cdot \exp\left[\frac{-\Delta H}{RT}\right] \qquad \text{(Eq. 3.8)}$$

where $\Delta H$ is the molar enthalpy of helix formation. Since helix formation is an exothermic process ($\Delta H<0$), $K_H$ decreases with increasing temperature. The shift in equilibrium constant brings changes in $C_F$, $C_J$, and $C_L$ and thus changes in the storage modulus, the relaxation time, and the viscosity.

The model described in this section describes the linear viscoelasticity of the network with six parameters: F, C*, $E_a$, $k_{d,0}$, $\Delta H$, and $K_{H,0}$. The front factor F was chosen as 0.5 as a trade-off between the classical affine network theory and the phantom network model. The overlap concentration C* can be calculated from the dimension of the chains. The radius of gyration $R_g$ is estimated to be ~7 nm, based on a master curve for $R_g$ as a function of the

number of residues proposed by Fritzkee [25]. Knowing that $V_{coil}=4/3\pi R_g^3$, and that the mass of a single chain is $M_{prot}/N_A$, where $M_{prot}$ ~42 kDa and $N_A$ is Avogadro's number, we calculated the overlap concentration as C*~1 mM. To obtain a value for the molar enthalpy of helix formation, we performed differential scanning calorimetry measurements (see Chapter 5). The measured enthalpy is approximately -192 kJ per mole of triple helices. This value corresponds very well with results obtained by Frank *et al.* [16], who found an enthalpy of -8.9 kJ per mole of tripeptide, corresponding to -220-250 kJ per mole of end blocks in triple helices form. From the calorimetry data, we also obtain the prefactor $K_{H,0:}$ 1.7·10-29 $l^2/mol^2$ (see Chapter 5). The activation energy $E_a$ and the prefactor $k_{d,0}$ that specify the dissociation rate, finally, are obtained from the data in Figure 3.5D. Assuming Arrhenius behavior for $\tau_0$ (Equation 3.7), we find $E_a=112 \pm 4$ kJ/mol and $k_{d,0}\sim10^{16}$ 1/s.

With no further adjustable parameters, we can compute $G_0$, $\tau$, and $\eta(=G_0\cdot\tau)$ as a function of concentration and temperature. The results of these calculations are shown in Figures 3.4 and 3.5 (solid lines). All these curves (both concentration and temperature dependencies) are in very good agreement with the experimental data.

From the model, we deduce the internal structure of the gel in terms of the fractions of end groups involved in triple helices (junctions or loops) and free ends. In Figure 3.6 we present how each fraction depends on temperature and concentration.

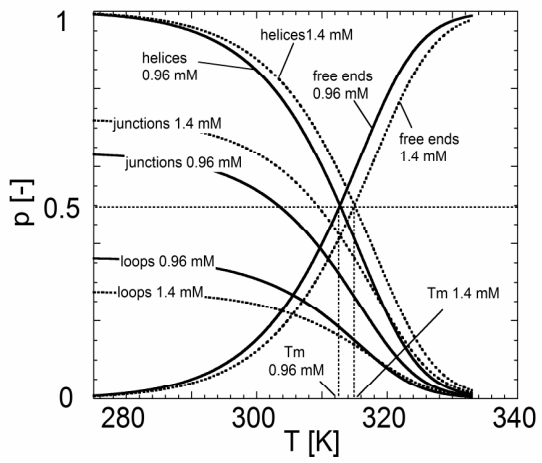


Figure 3.6 Dependency of the fractions of triple helices, loops, junctions and dangling ends (as indicated) on protein concentration and temperature. Dotted curves: 1.4 mM, full curves: 0.96 mM.

With increasing temperature, the fraction of helices decreases and that of free ends increases. Half of the helices have melted at a temperature of 315 K for a 1.4 mM solution and at 313 K for 0.96 mM. These melting temperatures were confirmed with differential scanning calorimetry (Chapter 4 and 5) and with measurements of the helical content using

circular dichroism [14]. By contrast, the elastic properties of the networks are lost at much lower temperatures; around 300 K (see Figure 3.4B). The reason for this is that only helices involved in junctions contribute to the elastic properties; helices in loops do not. As can be seen in Figure 3.6, the fraction of chain ends in junctions reaches the critical value of 1/2 at significantly lower temperatures than the total helix fraction. This effect is stronger for low polymer concentrations, because the fraction of loops increases with decreasing concentration. The latter also explains the strong concentration dependence of the modulus (Figure 3.4A).

## 3.5 Concluding remarks

In this chapter, we investigated a new type of telechelic polymers that self-assemble reversibly into transient networks with a node multiplicity of exactly three. The well-defined multiplicity made it possible to develop a theoretical model based on classical gel theory, which allows calculation of the complete (linear) viscoelastic behaviour of the network from a limited set of input parameters that can all be measured independently. The model calculations were in quantitative agreement with experiments, showing that the structure of our physical gels is rather well-described by classical gel theory, at least not too close to the percolation threshold.

As far as we know, this is the first report, which describes the internal structure of a network formed by telechelic polymer with such well-defined multiplicity. Telechelics with a multiplicity of 2 have been reported in literature, based on hydrogen-bonding [26], complementary strands of DNA [27], or coordination bonds [28], but these molecules form only linear chains and no networks. Conventional telechelics, such as PEO chains with hydrophobic side blocks, have higher node multiplicity and do form networks. However, the number of chains emanating from a node in these systems can fluctuate around an average value. This eliminates the special features associated with a precise node multiplicity, and makes quantitative modeling more difficult.

In this chapter, we considered only one polypeptide sequence, but the precise molecular design can be varied easily by changing the design of the underlying DNA template (see Chapter 4). By varying the length of the different blocks, for example, we can modify the rheological and structural properties of the networks. The collagen-inspired telechelic polypeptides studied here thus form a class of physical gels with highly controllable and predictable properties.

## References


[1] M. Sutter, J. Siepmann, W.E. Hennink, W. Jiskoot, Recombinant gelatin hydrogels for the sustained release of proteins. Journal of Controlled Release 119(3) (2007) 301-312.

[2] B. Balakrishnan, M. Mohanty, P.R. Umashankar, A. Jayakrishnan, Evaluation of an in situ forming hydrogel wound dressing based on oxidized alginate and gelatin. Biomaterials 26(32) (2005) 6335-6342.

[3] J. Kim, S.S. Kim, K.H. Kim, Y.H. Jin, S.M. Hong, S.S. Hwang, B.G. Cho, D.Y. Shin, S.S. Im, Applications of telechelic polymers as compatibilizers and stabilizers in polymer blends and inorganic/organic nanohybrids. Polymer 45(10) (2004) 3527-3533.

[4] K.T. Nijenhuis, On the nature of crosslinks in thermoreversible gels. Polymer Bulletin 58(1) (2007) 27-42.

[5] S.C. Lee, Y.W. Cho, K. Park, Control of thermogelation properties of hydrophobically-modified methylcellulose. Journal of Bioactive and Compatible Polymers 20(1) (2005) 5-13.

[6] T. Annable, R. Buscall, R. Ettelaie, D. Whittlestone, The rheology of solutions of associating polymers-comparison of experimental behavior with transient network theory. Journal of Rheology 37(4) (1993) 695-726.

[7] J. Sprakel, E. Spruijt, M.A.C. Stuart, N.A.M. Besseling, M.P. Lettinga, J. van der Gucht, Shear banding and rheochaos in associative polymer networks. Soft Matter 4(8) (2008) 1696-1705.

[8] E.R. Wright, V.P. Conticello, Self-assembly of block copolymers derived from elastin-mimetic polypeptide sequences. Advanced Drug Delivery Reviews 54(8) (2002) 1057-1073.

[9] K. Nagapudi, W.T. Brinkman, B.S. Thomas, J.O. Park, M. Srinivasarao, E. Wright, V.P. Conticello, E.L. Chaikof, Viscoelastic and mechanical behavior of recombinant protein elastomers. Biomaterials 26(23) (2005) 4695-4706.

[10] W.A. Petka, J.L. Harden, K.P. McGrath, D. Wirtz, D.A. Tirrell, Reversible hydrogels from self-assembling artificial proteins. Science 281(5375) (1998) 389-392.

[11] S.B. Kennedy, K. Littrell, P. Thiyagarajan, D.A. Tirrell, T.P. Russell, Controlled structure in artificial protein hydrogels. Macromolecules 38(17) (2005) 7470-7475.

[12] F. Tanaka, S.F. Edwards, Viscoelastic properties of physically crosslinked networks-transient network theory. Macromolecules 25(5) (1992) 1516-1523.

[13] F. Tanaka, Theoretical study of molecular association and thermoreversible gelation in polymers. Polymer Journal 34(7) (2002) 479-509.

[14] M.W.T. Werten, H. Teles, A. Moers, E.J.H. Wolbert, J. Sprakel, G. Eggink, F.A. de Wolf, Precision Gels from Collagen-Inspired Triblock Copolymers. Biomacromolecules 10(5) (2009) 1106-1113.

[15] G.N. Ramachandram, Biochemistry of Collagen, Plenum Press, New York, 1976.

[16] S. Frank, R.A. Kammerer, D. Mechling, T. Schulthess, R. Landwehr, J. Bann, Y. Guo, A. Lustig, H.P. Bachinger, J. Engel, Stabilization of short collagen-like triple helices by protein engineering. Journal of Molecular Biology 308(5) (2001) 1081-1089.

[17] M.W.T. Werten, W.H. Wisselink, T.J.J. Jansen-van den Bosch, E.C. de Bruin, F.A. de Wolf, Secreted production of a custom-designed, highly hydrophilic gelatin in Pichia pastoris. Protein Engineering 14(6) (2001) 447-454.

[18] J.D. Ferry, Viscoelastic Properties of Polymers, Wiley, New York, 1980.

[19] K.T. Nijenhuis, Investigation into the aging process in gels of gelatin-water systems by the measurement of their dynamic moduli. Mechanism of the aging process. Colloid and Polymer Science 259(10) (1981) 1017-1026.

[20] E.E. Braudo, I.G. Plashchina, V.B. Tolstoguzov, Structural characterisation of thermoreversible anionic polysaccharide gels by their elastoviscous properties. Carbohydrate Polymers 4 (1984) 23-48.

[21] P.J. Flory, Principles of Polymer Chemistry Cornell University Press, New York, 1953.

[22] W.H. Stockmayer, Journal of Chemical Physics 12 (1944) 125-136.

[23] L.C. Case, Branching in polymers. Network defects. Journal of Polymer Science 45(146) (1960) 397-404.

[24] H.M.J.a.E. Guth, Journal of Chemical Physics 11 (1943) 455-467.

[25] N.C. Fitzkee, G.D. Rose, Reassessing random-coil statistics in unfolded proteins. Proceedings of the National Academy of Sciences of the United States of America 101(34) (2004) 12497-12502.

[26] R.P. Sijbesma, F.H. Beijer, L. Brunsveld, B.J.B. Folmer, J. Hirschberg, R.F.M. Lange, J.K.L. Lowe, E.W. Meijer, Reversible polymers formed from self-complementary monomers using quadruple hydrogen bonding. Science 278(5343) (1997) 1601-1604.

[27] D.C. Chow, W.K. Lee, S. Zauscher, A. Chilkoti, Enzymatic fabrication of DNA nanostructures: Extension of a self-assembled oligonucleotide monolayer on gold arrays. Journal of the American Chemical Society 127(41) (2005) 14122-14123.

[28] T. Vermonden, J. van der Gucht, P. de Waard, A.T.M. Marcelis, N.A.M. Besseling, E.J.R. Sudholter, G.J. Fleer, M.A.C. Stuart, Water-soluble reversible coordination polymers: Chains and rings. Macromolecules 36(19) (2003) 7035-7044.

# Chapter 4

# Influence of middle block design on gel properties formed by telechelic polypeptides

*Abstract*

In this chapter we study the influence of the middle block design on gel properties, formed by telechelic polypeptides, with collagen-like end blocks and a random coil-like middle block. We compare architecture and melting properties of networks formed by molecules comprising middle blocks of 400 and 800 amino acids (42 and 78 kDa, respectively). In addition to length, we examine the influence of amino acids sequence in a non-trimer forming domain. Rheological tests show that the storage modulus strongly depends on the coil size, which is determined by the molecular weight and the flexibility of the polymer. At the same protein molar concentration (thus the same amount of crosslink-forming end blocks), the storage modulus of gels formed by longer and stiffer polypeptides is much higher than that of the shorter and more flexible polymers. These results indicate that the elastic properties of the network can be tuned not only by changing polymer concentration and temperature but also by altering the middle block design. All experimental data could be accurately described by an analytical model, which accounts for the internal gel architecture.

Published in modified form as: H. Teles, P.J. Skrzeszewska, M.W.T Werten, J. van der Gucht, G. Eggink and F.A. de Wolf, Influence of molecular size on gel-forming properties of telechelic collagen-inspired polymers. Soft Matter 6(19) (2010) 4681-4687

## 4.1 Introduction

Protein-based hydrogels have proven to be effective biomaterials in a variety of medical and pharmaceutical applications [1-3]. Despite the success of these materials, which are mostly derived from animal fibrillar proteins, their use is often limited by the characteristics of the available protein, and it may be influenced by batch to batch or source to source variations. Furthermore, materials isolated from mammalian sources often have a risk of infectious agents transmission [4].

Traditional gelatin, commonly used as a protein gel, consists of a multitude of different, partially degraded, and chemically modified fragments of animal collagen, resulting in gels with ill-defined molecular composition and complex network-forming properties. This complexity, in combination with the impossibility to change the molecular structure at will, limits the possibilities to determine structure-function relationship, and has prompted the need for exploration of synthetic strategies that allow exquisite control over the monomer sequence and polymer length [4].

In the past decade recombinant DNA techniques became a tool to develop genetically engineered protein polymers with defined composition and structure, that offer safe biocompatibility and full control over the length and sequence of biopolymers [5]. Recently, we reported on the recombinant production and characterisation of a new class of gel-forming telechelic triblock polypeptides with controllable and predictable properties [6, 7]. Gel formation is obtained by combining collagen-inspired $(Pro\text{-}Gly\text{-}Pro)_n$ end blocks (abbreviated as T) with highly hydrophilic random coil middle blocks that define the distance between the trimer forming T end blocks. Contrary to natural gelatin, this new class of synthetic collagenous gels has a well-defined junction multiplicity of exactly three and predictable physicochemical properties [7]. So far, two of such triblock copolymers, denoted as TR4T and TP4T, have been produced and characterised [6, 7]. These polymers consisted of nine repeating units of (Pro-Gly-Pro) in T blocks and a middle block made of a tandem repeat of four highly hydrophilic 9 kDa blocks (R4 or P4) that assume a random conformation. The polar P block with a collagen-inspired designer sequence, consists of (Gly-Xaa-Yaa) repeats, while the R block has the same amino acid composition, but a quasi random amino acid sequence. The mass of the entire TR4T or TP4T is 42 kDa. By changing the underlying DNA template, we doubled the length of the middle block and in this chapter, we report on the biosynthesis and characterisation of the resulting 78 kDa triblock copolymers, TR8T and TP8T. In Chapter 3, which is focused on TR4T hydrogels, we showed that the network-

forming properties are strongly dependent on protein concentration and temperature [7]. By taking into consideration the formation of loops and dangling ends, we were able to develop an analytical model that accurately described the network structure and truly reproduced the observed relationships between the storage modulus and the relaxation time as a function of temperature and concentration, without a need of adjustable parameters other than quantities that could be verified by experimental measurements [7]. In this chapter, besides concentration and temperature, we study the influence of middle block length and amino acid sequence on the viscoelastic properties of the networks. The amino acid sequence appears to have an influence on the flexibility of the middle block and, consequently, on the overlap concentration. We use the model developed in Chapter 3 to interpret the experimental data for TR8T and TP8T and show that small changes in polymer structure significantly influence the mechanical properties of the network.

## 4.2 Material and Methods

***Expression vectors and Pichia pastoris transformation***

The construction of the vectors encoding the genes TP4T and TR4T is described in detail in Chapter 2 and in references 6 and 8. The previously described vectors pMTL23-P4T, pMTL23-R4T, pMTL23-P4, pMTL23-R4, and pCR4-TOPO-T [6] were used to construct the genes encoding TP8T and TR8T. Vectors pMTL23-P4T and pMTL23-R4T [6] were digested with *Dra*III (5´ to the P4T or R4T genes) and dephosphorylated. P4- and R4-DNA fragments, obtained from *Dra*III/*Van*91I-digested pMTL23-P4 and pMTL23-R4 were inserted into the previously digested pMTL23-P4T and pMTL23-R4T, respectively, so as to yield pMTL23-P8T and pMTL23-R8T. These vectors were then digested with *Dra*III (5´ to the P8T and R8T genes) and dephosphorylated. A T block DNA, obtained from *Dra*III/*Van*91I-digested pCR4-TOPO-T, was inserted into pMTL23-P8T and pMTL23-R8T, so as to yield vectors pMTL23-TP8T and pMTL23-TR8T. TP8T and TR8T fragments were then cloned into *Pichia pastoris* expression vector pPIC9 (Invitrogen) using *Xho*I/*Eco*RI. The entire R4, P4, TR4T, TP4T, TR8T and TP8T DNA sequences (and translated amino acid sequences) have been deposited in the GenBank under accession numbers EU834225-EU834230. The expression vectors were linearized with *Sal*I and transformed into the *his4* GS115 strain [9]. Transformation and strain selection of transformants were as described earlier [10].

***Fermentation of Pichia pastoris***

Fermentation of *Pichia pastoris* strains was performed as described by Zhang *et al.* [11]. Strains were cultured in minimum basal salts medium in a 3-l Bioflo 3000 fermenter (New Brunswick Scientific). The fermentation was run at 30 °C and the pH was kept at 3 by addition of ammonium hydroxide. The methanol level in the fermentation broth was kept constant at ~0.2 % (w/v) by using a home-made semiconductor gas sensor controller, similar to that described by Katakura *et al*. [12]. The methanol fed-batch phase was prolonged for approximately 2-3 days. The cells were removed by centrifugation for 30 min at 20,000 xg in a SLA-3000 rotor (Sorval), followed by microfiltration of the supernatant.

***Protein Purification***

Protein purification was done by ammonium sulphate precipitation as described in more detail in Chapter 2.

***SDS-PAGE***

Fermentation supernatants and pure products were analysed by SDS-page using the NuPAGE Novex system (Invitrogen), with 10 % Bis-Tris gels, MES SDS running buffer and SeeBlue Plus2 prestained molecular mass markers. Gels were stained in Coomassie SimplyBlue SafeStain (Invitrogen) and destained in MQ water. N-terminal sequencing analysis was determined by Edman degradation as described previously [10]. Protein sequencing was preformed by Midwest Ananlytical (St. Louis, Mo).

***Matrix Assisted Laser Desorption/Ionization (MALDI) Mass Spectrometry (MS)***

MALDI-TOF was performed using an Ultraflex mass spectrometer (Bruker). Samples were prepared by the dried droplet method on a 600 μm AnchorChip target (Bruker), using 5 mg/ml 2,5-dihydroxyacetophenone, 1.5 mg/ml diammonium hydrogen citrate, 25 % (v/v) ethanol and 1 % (v/v) trifluoroacetic acid as matrix. Measurements (20 Hz) were made in the positive, linear mode, with the following parameters: ion source 1, 20000 V; ion source 2, 18450 V; lens, 5000 V; pulsed ion extraction, 550 ns. Protein Calibration Standard II (Bruker) was used for external calibration.

***Differential Scanning Calorimetry (DSC)***

Differential scanning calorimetry experiments were performed with a MicroCal VP-DSC instrument. 0.51 ml degassed protein solutions (2.4 mM) prepared in phosphate buffer (pH 7,

I=10 mM) were loaded at 50 ºC into the calorimeter. For each experiment, the protein solutions were equilibrated for 10-15 hours at 20 ºC to allow complete helix formation. Then, the temperature was raised from 20 ºC to 65 ºC at a scan rate of 0.25 K/min. At this protein concentration both the melting temperature and the enthalpy are scan rate independent (Chapter 5). After recording the DSC trace, the sample was cooled to 20 ºC and left for 10 hours for helix reformation. The DSC trace was then recorded again in an identical manner. The calorimetric transition enthalpy was obtained by integration of the area under the excess heat capacity peak. The flooring of the thermogram was done by fitting the thermogram baseline with a third order polynomial function.

***Rheology***

The rheological measurements where preformed with an Anton Paar Physica MCR301 rheometer, equipped with a cone and plate geometry of 50 mm diameter. Temperature control was insured by a Peltier system, which allows fast heating and cooling. Protein solutions of different molar concentrations were prepared in phosphate buffer (pH 7, I=10 mM), heated for half an hour at 50 ºC and then introduced in the preheated geometry. The system was subsequently quenched to 20 ºC to induce gel formation for 15 hours. A solvent trap was used to prevent evaporation. Gelation was monitored by measuring the storage modulus (G'), as well as the loss modulus (G") at a frequency of 1 Hz and a strain of 1 %. Two types of rheological measurements were done at different temperatures (between 20 ºC and 40 ºC). At each temperature the system was equilibrated for 5 hours before doing the measurements. First, viscoelastic characterization of the equilibrated gel was performed in the frequency range 0.001-20 Hz (0.00628-125 rad/s) and a deformation amplitude of 1 %. Second, creep experiments were carried out and converted to the frequency domain using methods described by Ferry [13]. For TP4T, the applied stress was varied between 5 Pa and 20 Pa and for TR8T and TP8T, between 5 Pa and 300 Pa. The stress values were chosen not to go beyond the linear regime. The deformation and recovery phases were followed each for a period of 1800 s.

***Dynamic Light Scattering***

Protein solutions of 0.5 mg/ml prepared in phosphate buffer (pH=7, I=10 mM) were pipetted into light scattering cuvettes of 45 µl The data were acquired at 20 °C using a Malvern Zetasizer Instrument (Nano series). The light source was a 4 mW He-Ne laser with wavelength 633 nm. The scattering angle θ was fixed at 173º.

## 4.3 Experimental results

***Biosynthesis and molecular characterisation of the protein polymers***

*Pichia pastoris* strains containing the genes encoding the ~78 kDa collagen-like triblock copolymers, TR8T and TP8T, were cultured in bioreactors and the proteins were purified from the fermentation supernatant. Cell-free TR8T and TP8T fermentation broths and purified products were analysed by SDS-PAGE (Figure 4.1A). All purified proteins migrated as single bands indicating a high purity and intactness, although TR8T and TP8T showed anomalous migration behaviour in SDS-PAGE, similar to the migration behaviour found previously for TR4T, TP4T and P4 [6, 8]. The molecular weights of TR8T and TP8T were determined by MALDI-TOF MS. Figure 4.1B shows that the experimental values are in good agreement with the expected value of 78.176 kDa for both TR8T and TP8T. Furthermore, N-terminal sequencing of the SDS-PAGE bands confirmed the identity of the proteins.

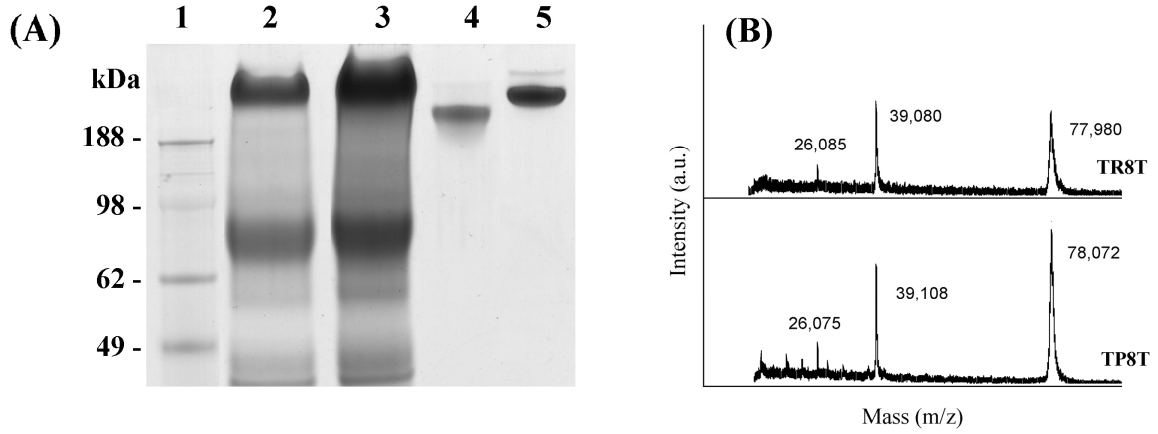


Figure 4.1 Production of protein polymers. (A) SDS-PAGE: lane 1, molecular weight marker; lane 2 cell-free TR8T fermentation broth; lane 3 cell-free TP8T fermentation broth; lane 4 purified TR8T; lane 5 purified TP8T; 15 µl of cell-free fermentation broth and ~20 µg of purified protein was applied. (B) MALDI-TOF of purified TR8T and TP8T. Single and doubly charged molecular ions are indicated.

The volumetric productivity of TR8T and TP8T was estimated to be 1-3 g/l of clarified broth. These values are very similarly to the production yields previously reported for TR4T, TP4T and P4 [6, 8]. We can deduce from these results that an increase in total protein size did not have an influence on the proteins' intactness and yield.

***Enthalpy and melting temperature***

Endothermic transitions occurred upon melting TR8T and TP8T with a ΔCp maximum at 315.3 K and 315.6 K, respectively (Figure 4.2). The calorimetric transition enthalpies were calculated by integration of the area under the excess heat capacity peaks. The calculated enthalpies were 202±11 kJ per mole of triple helices and 229±20 kJ per mole of triple helices for TR8T and TP8T, respectively. The experimental enthalpy values correlate well with the expected melting enthalpy value of 223 kJ per mole of triple helices for a $(Pro\text{-}Gly\text{-}Pro)_9$ end blocks calculated on the basis of the results obtained by Frank *et al*. [14] and Engel *et al.* [15]. These results are consistent with the earlier reported values of $T_m$ and enthalpy for TR4T and TP4T [6, 16]. This confirms our previous findings that the trimer-forming end blocks (T) are solely responsible for trimerization.

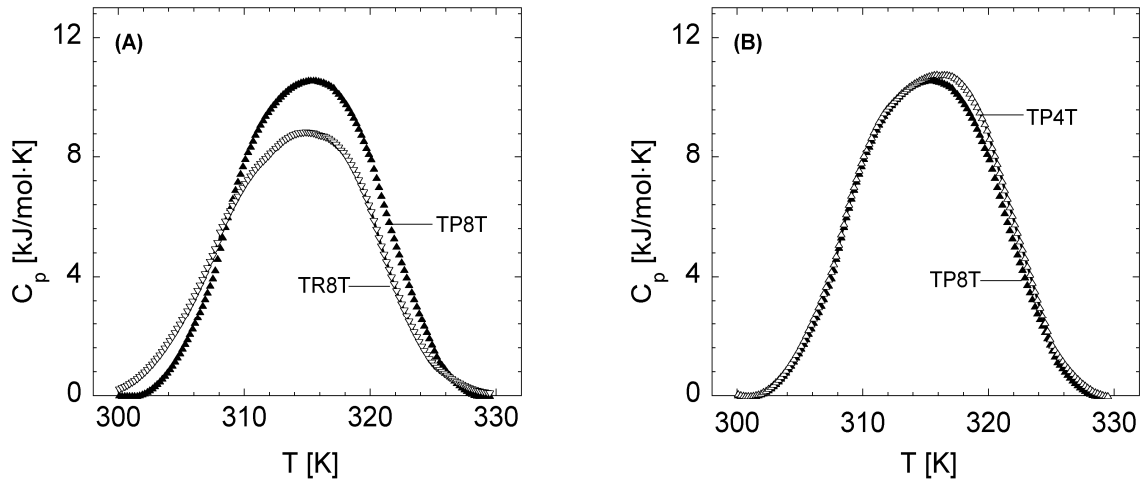


Figure 4.2 (A) DSC thermogram of TR8T and TP8T. (B) DSC thermogram of TP8T and TP4T. Protein concentration for all cases was 2.4 mM and scan rate was 0.25 K/min.

***Hydrogel formation***

In line with the previous studies (Chapter 3) the gel-forming behaviour of TR4T and TP4T, TR8T and TP8T was investigated by means of dynamic rheology. Several concentrations of the four different protein gels were investigated. At 20 ºC, a physical gel is formed due to triple helix formation, exclusively by the collagen-like end blocks (T). In the beginning of the gelation process viscous properties are predominant but with time, as the protein network develops, the elastic properties prevail. A steady-state storage modulus is reached after 5-6 hours. All four different proteins show the same course of network

formation. Because the end blocks do not contain charged amino acids, and the middle block contains only 4 mol% negative and 3 mol% positive charges, electrostatic contributions to the modulus were neglected. Figure 4.3A shows the development of the storage (G') and loss (G") moduli for a 1.2 mM solution of TR8T and TP8T. Similar gelation behaviour was found for TR4T (Chapter 3) and TP4T [6]. The occurrence of a steady G' value contrasts with traditional animal gelatin, in which the G' continues to evolve during more than 100–1000 hours [17, 18]. The fact that we have a steady state G' is probably related to the presence of only a single type of short helix-forming domains in the triblock polymers, as opposed to gelatin, in which a range of structures with different thermal stabilities is present [19].

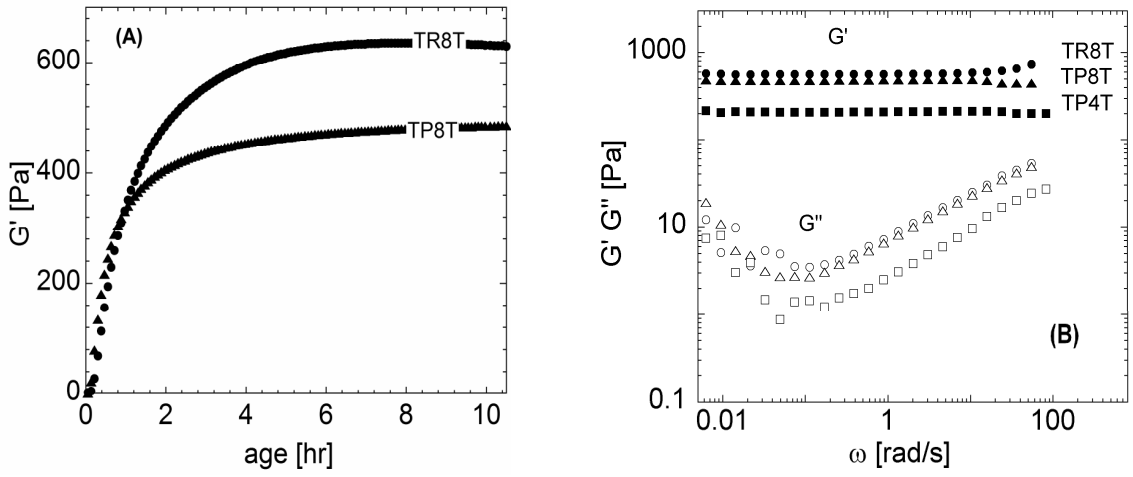


Figure 4.3 Storage modulus for 1.2 mM TR8T (●) and TP8T (▲) as a function of age (1 Hz, γ=1 %). (B) Frequency sweeps at 293 K for 1.2 mM TR8T (●) and TP8T (▲) and for 2.3 mM TP4T (■).

When the steady-state value of G' was reached for TP4T, TR8T and TP8T gels, the G' and G" values were measured as a function of frequency (Figure 4.3B). Within the available frequency range, the elastic behaviour (G') dominates over the viscous behaviour (G"). The storage modulus does not depend on the frequency in this range, while the loss modulus decreases with frequency and reaches a minimum around 0.1 rad/s and then increases again (Figure 4.3B). The frequency independence of the G' is in agreement with measurements done with natural gelatin solutions [17].

To obtain insight into the gel system at frequencies below 0.01 rad/s, creep measurements were performed. A fixed stress was applied to the gel after it reached a steady-state storage modulus, and the resulting deformation was followed as a function of time. We converted the creep results to the frequency domain by a method described by Ferry [13] and combined them with the oscillatory data. Figure 4.4A shows creep curves and Figure 4.4B

shows the resulting frequency-dependent storage and loss moduli for three different concentrations of TR8T. Similar results were found for TR4T (Chapter 3), TP4T and TP8T (Supplementary information in reference [20]).

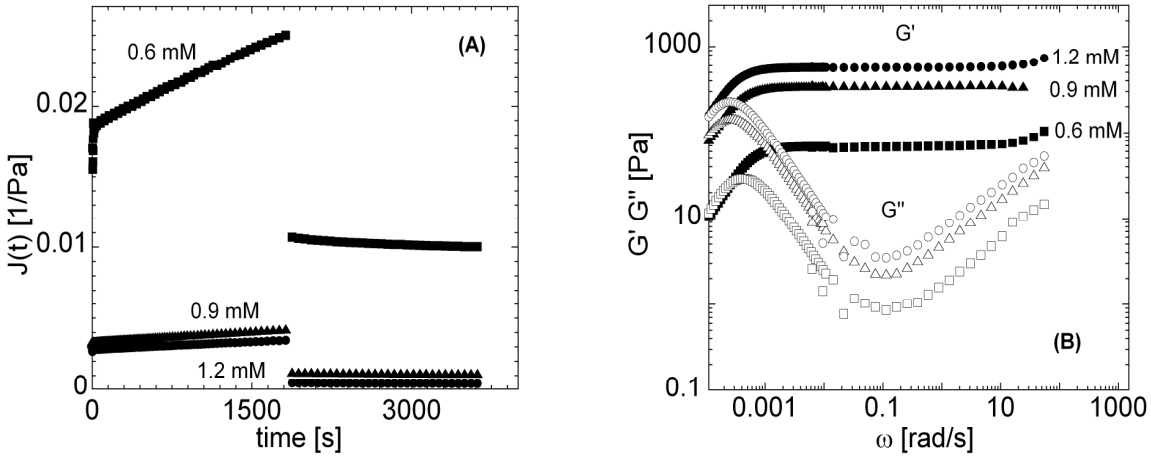


Figure 4.4 (A) Creep experiments and (B) combined frequency sweeps and converted creep experiments at 293 K for TR8T at different concentrations: (●) 1.2 mM (▲) 0.9 mM and (■) 0.6 mM.

Both frequency sweeps and creep experiments allowed us to determine the plateau storage modulus $G_0$ and relaxation time $\tau$ at different concentrations (symbols in Figure 4.5A and 4.5B, respectively).

The plateau storage modulus of all studied proteins depends strongly on the protein concentration. Furthermore, the longer versions of the collagen-like protein polymers, *i.e.*, TR8T and TP8T had a considerably higher plateau storage modulus ($G_0$) than their shorter counterparts, TR4T and TP4T at comparable molar concentration (Figure 4.5A). While a storage modulus of ~700 Pa is obtained at a protein concentration of 1.2 mM with TR8T, a comparable value is only reached at a concentration of ~2 mM with TR4T gels.

This difference is most probably related to the fact that longer chains are less likely to form intramolecular loops, and therefore lead to a higher density of trimolecular (network-building) junctions at the same polymer concentration [7, 21]. In the next section we provide a more consistent and thorough interpretation of these observations, by using a model developed in Chapter 3.

Except for TP4T, the present gelatin-like polymers, which can maximally contain ~4.6 g helix per mmol protein (4.6 g/l at 1 mM), appear to reach a storage modulus (Figure 4.5A) that is 5–200 times higher than traditional gelatins [22], at a comparable w/v helix concentration (g/l). The highest values are again reached with TR8T and TP8T, probably because they are less prone to loop formation. The difference between the triblock

copolymers and traditional gelatin can be explained by the design of our triblock copolymers, in which each triple helix is very short. It follows that at comparable w/v helix content a larger number of discrete triple helices are formed than in traditional gelatin. As far as those triple helices also represent crosslinks, it is clear that this will lead to a comparatively higher crosslink density and thus, a higher storage modulus. At comparable protein concentration (g/l) the triblock gelatins do not have a higher storage modulus than the traditional animal material, because the helix-forming end blocks only represent a small portion of the entire triblock polymer chain.

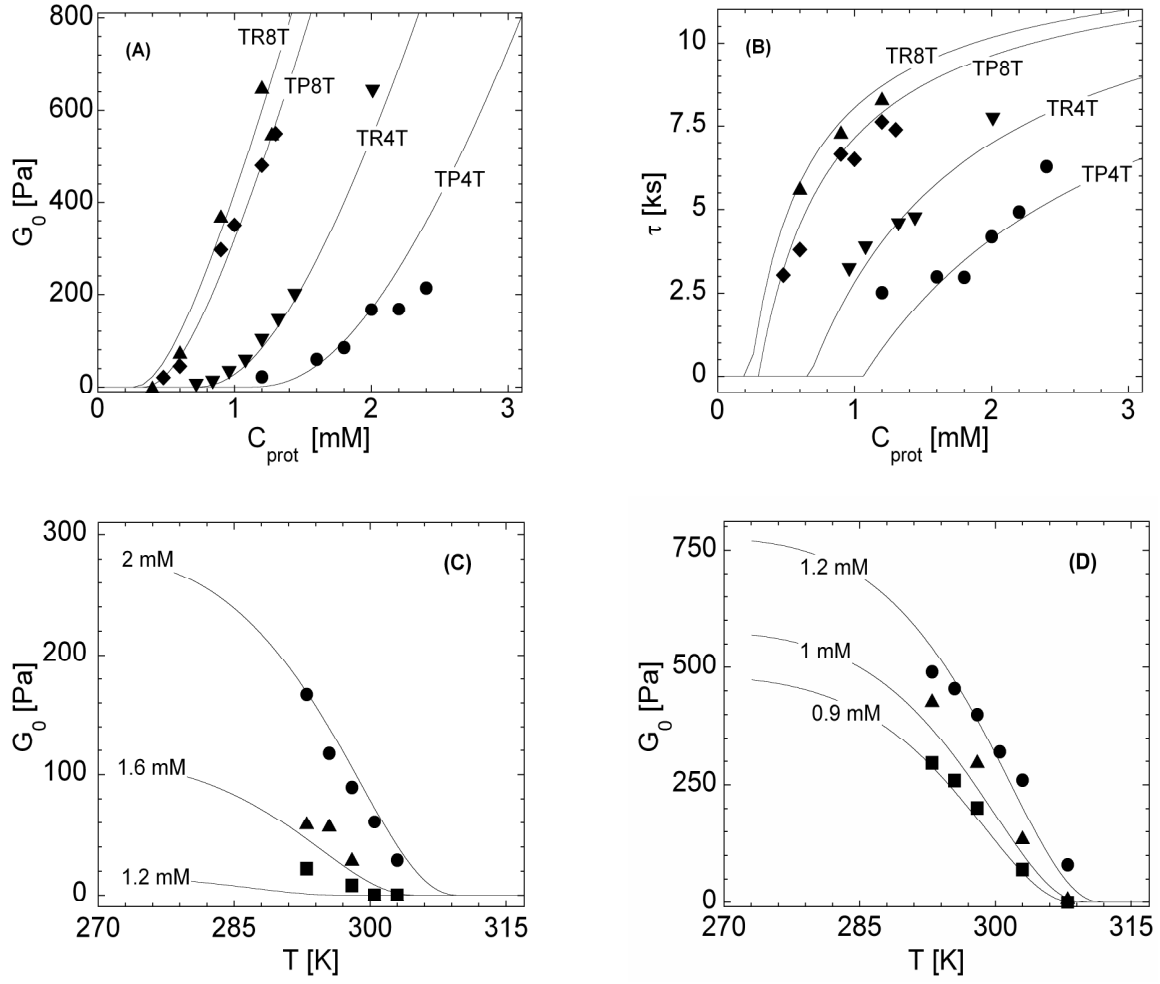


Figure 4.5 (A) Plateau storage modulus as a function of protein concentration at 293 K. (B) Relaxation time (τ) as a function of protein concentration at 293 K. Symbols correspond to experimental data: (▲) TR8T, (◆) TP8T, (▼) TR4T (●) TP4T and solid lines correspond to model calculations described in next section. (C and D) Plateau storage modulus as a function of temperature for different concentrations of TP4T: (●) 2 mM, (▲) 1.6 mM, (■) 1.2 mM; and of TP8T: (●) 1.2 mM, (▲) 1 mM, (■) 0.9 mM. Solid lines correspond to model calculations presented in section 4.4.

## 4.4 Network modeling and discussion

In an attempt to provide a consistent and more thorough interpretation of the experimental observations, we use the analytical model developed in Chapter 3. The model is based on the classical gel theory by Flory [23] and Stockmayer [24]. It takes into account the equilibrium between helix formation and free ends by the trimer-forming end blocks (T). The formation of helices can occur in two ways: a triple helix is formed by three T end blocks coming from three different chains (a junction) or by two T end blocks coming from the same chain and a third one from a different chain (a loop). Only junctions with all three branches linked to the gel network contribute effectively to the elastic properties. Junction points with only two of their chains linked to the gel merely elongate the active chains and are responsible for the formation of so-called "superchains". In Chapter 3 we demonstrated that the junctions/ loops ratio increases with protein concentration. Here we show that it also depends strongly on the size of the middle block. The probability that an end block is part of a junction ($p_J$=p) can be expressed as a function of the total protein concentration ($C_{prot}$), the overlap concentration (C*) and the fraction of end blocks involved in a triple helix ($p_H$) (see Chapter 3):

$$p = \frac{2 \cdot p_H \cdot C_{prot}}{2 \cdot C_{prot} + C^*} \qquad \text{(Eq. 4.1)}$$

where C* is related to the dimension of the chains and can be estimated as $C^* \sim 1/(4/3\pi R_g^3)$ with $R_g$ the radius of gyration.

Using the classical network theory of Flory and Stockmayer [23, 24], the following equation for the plateau storage modulus was derived in Chapter 3:

$$G_0 \approx \frac{F \cdot \left[ C_{prot} \cdot (2p-1)^3 \cdot R \cdot T \right]}{p^2} \qquad \text{(Eq. 4.2)}$$

where RT is the thermal energy per mole and F is the front factor, taken to be 0.5.

Stress relaxation occurs when an elastically active chain breaks. Here, this happens when a triple helix (junction point) dissociates [7, 16]. The average network relaxation time is given by the following equation (see Chapter 3):

$$\tau = \frac{\tau_0}{< N >} = \tau_0 \cdot (2p-1) \qquad \text{(Eq. 4.3)}$$

where $\tau_0$ is the lifetime of a single helix. Dissociation of helices is also a function of temperature. The higher the temperature the faster the helices dissociate. This temperature dependence can be described by the Arrhenius correlation (Chapter 3).

For the model calculations with middle block other than R4 it was necessary to recalculate the overlap concentration (C*), which is related to the dimensions of the protein chain. All the other parameters, determined experimentally, were kept constant with respect to the previous chapter. For more details on the model calculations please see Chapter 3.

To have a good estimation of the dimension of the protein chains in solution we used dynamic light scattering to measure the size of P4 and R4 blocks. The results obtained indicate an ~8 % lower hydrodynamic radius ($R_H$) for the P4 block (5.7 ± 0.3 nm) as compared to the R4 block (6.2 ± 0.4 nm). The measured hydrodynamic radius of R4 is smaller than the radius of gyration ($R_g$) of ~7 nm estimated earlier [7] based on a master curve for $R_g$ as a function of the number of residues, proposed by Fritzkee *et al.* [25]. However, the hydrodynamic radius is usually slightly lower than the radius of gyration for random coil proteins [26, 27]. Assuming $R_g$ to be ~1 % higher than $R_H$, the calculated overlap concentrations for TP4T and TR4T are ~1.6 mM and ~1.1 mM, respectively.

We assumed the $R_g$ to scale with the residue number ($N_r$) as $R_g \sim N_r^{0.6}$ as for polymers in a good solvent [26, 27]. Accordingly, we estimated the $R_g$ of the polypeptides with the longer middle blocks, P8 and R8, to be ~10 and ~11 nm, respectively. The corresponding values of the overlap concentrations (C*) of TP8T and TR8T were ~0.38 mM and ~0.3 mM, respectively. Having determined the overlap concentration (C*) of all four proteins, we could model the network. Figures 4.5A and B show a very good agreement between the experimental data (symbols) and model calculations (solid lines) for all proteins. However, in Figure 4.5C and D (dependence of the storage modulus on temperature), there are some differences between model and experimental data: the model appears to describe the experimental data only qualitatively. Probably this is because the temperature dependence is very sensitive to the measured values of melting entropy and enthalpy.

It is clear from the model that the polymers with longer middle blocks have a higher storage modulus because a longer midblock leads to a bigger radius of gyration ($R_g$) and thus to a lower overlap concentration. A bigger $R_g$ decreases the probability that two end blocks from the same molecule associate with each other, and form a loop. The consequence of fewer loops in the system is a higher storage modulus. Figure 4.6A shows the dependency of the fraction of junctions ($p_J$) and nodes involved in loops ($p_L$) on the concentration for all four proteins, based on model calculations. In this figure it is clearly shown that the fraction of

loops present in the system is considerably higher for the shorter triblock copolymers, TR4T and TP4T at each concentration. It should be noted that the effect of additional transient entanglements due to the increase in effective concentration of the random coil middle blocks, contributing to the higher storage modulus of the protein polymers with longer middle blocks, can be neglected. Entanglements would not disappear upon melting, and if present would contribute to the storage modulus and viscosity above the melting temperature of the gels. Both $G_0$ (Figure 4.5C and D ) and viscosity (data not shown) reach very small values above the melting temperature of the gels.

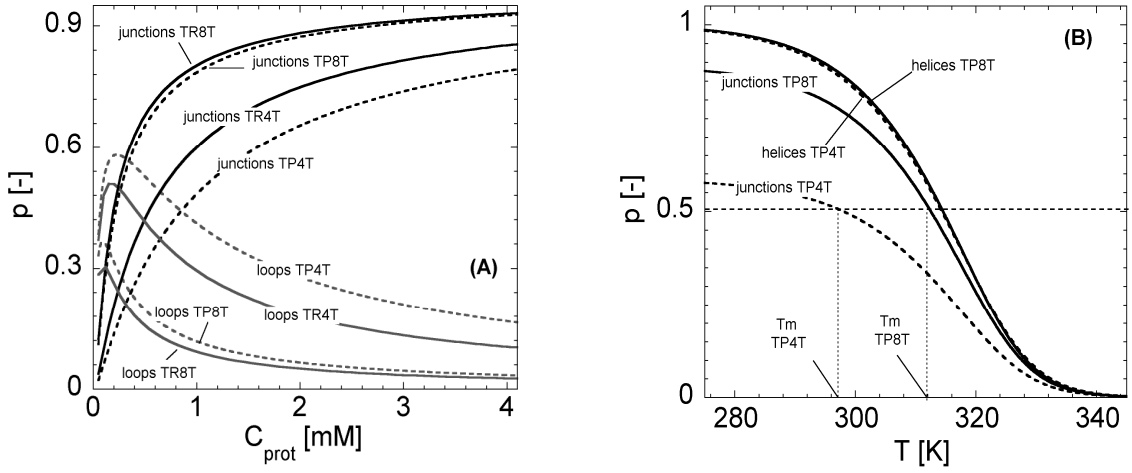


Figure 4.6 (A) Dependency of fraction of junctions ($p_J$) and loops ($p_L$) on protein concentration at temperature 293 K. (B) Dependency of fraction of triple helices ($p_H$) and junctions ($p_J$) on temperature for TP4T and TP8T at a protein concentration of 1.2 mM.

In addition, we observed that the R series, TR4T and TR8T, also show a higher storage modulus than their corresponding P series counterparts, TP4T and TP8T. The explanation for this is difference in coil flexibility. Although, P and R blocks have exactly the same composition, their amino acid sequence is different. Fitzkee *et al.* [25] have shown that even a polypeptide chain that assumes a random coil conformation still has locally folded conformations that contribute to the overall flexibility of the chain. Apparently, this leads to a smaller radius of gyration for the P middle block than for the R middle block and thus to higher predisposition of loops formation. This effect is stronger for the proteins with the shorter middle blocks, because the fraction of loops decreases strongly with increasing polymer length (Figure 4.6A).

***Melting behaviour of the network***

In order to compare the melting behaviour of the four proteins, creep and frequency sweeps were carried out at higher temperatures (293–323 K). As an example, Figure 4.5C and D show the plateau storage modulus ($G_0$) of TP4T and TP8T as a function of temperature, at different concentrations. Contrary to what emerged from DSC measurements (Figure 4.2B) the temperature at which the $G_0$ value approaches zero and the gel completely loses its elastic properties varies with the length of the middle block. For the same molar concentration, *e.g.* 1.2 mM, this temperature is ~298 K for TP4T and ~313 K for TP8T. According to classical gel theory those temperatures should correspond approximately to the temperature at which 50 % of all the T end groups available in the system are involved in trimolecular junctions and thus, the junction probability $p=3C_J/2C_{prot}=0.5$.

In Figure 4.6B we plot the fraction of triple helices ($p_H$) and the fraction of junctions ($p_J$) obtained from model calculations as a function of temperature for TP4T and TP8T at a concentration of 1.2 mM. The total amount of triple helices (junctions and loops together) does not depend on the length of the midblock and reaches ~50 % at ~315 K for both TP4T and TP8T. However, the fraction of junctions ($p_J$) is significantly higher for molecules with a longer middle block. The 50 % value, reached at 297 K for TP4T and at 313 K for TP8T, is in good agreement with the temperature dependence of $G_0$ shown in Figure 4.5C and D as discussed above

## 4.5 Concluding remarks

In order to explore the relationship between the middle block size and hydrogel-forming properties of telechelic polypeptides with trimer-forming collagen-like end blocks, four versions of this class of polymers, differing only in their middle block length or amino acid sequence, were studied. The temperature-dependent measurement of the storage modulus (reflecting the elasticity of the gels) showed that, besides polymer concentration [7], the length of the random coil middle blocks is also a predominant factor governing the viscoelastic properties of the hydrogels. The gel strength depends not only on the helix content of the system but also on the ratio between loops and junctions. Longer polymer chains render higher gel strength, because the probability is lower that they form a loop. A consequence of fewer loops in the system is a higher number of elastically active chains, effectively contributing to the elastic properties of the network. The experimental results were supported by an analytical model based on classical gel theory, showing, once more, that the

well-defined multiplicity of the network of this particular class of hydrogels allows the prediction of the complete viscoelastic behaviour of the network, when the polymer structure is well-known.

Our results suggest that, by controlling the structure of the present type of hydrogel-forming polymers through genetic engineering, their physicochemical properties can not only be controlled and predicted but also developed in order to match a variety of different applications.

## References

[1] C. Yang, P. Hillas, J. Tang, J. Balan, H. Notbohm, J. Polarek, Development of a recombinant human collagen-type III based hemostat. Journal of Biomedical Materials Research Part B-Applied Biomaterials 69B(1) (2004) 18-24.

[2] D. Olsen, C.L. Yang, M. Bodo, R. Chang, S. Leigh, J. Baez, D. Carmichael, M. Perala, E.R. Hamalainen, M. Jarvinen, J. Polarek, Recombinant collagen and gelatin for drug delivery. Advanced Drug Delivery Reviews 55(12) (2003) 1547-1567.

[3] C.H. Lee, A. Singla, Y. Lee, Biomedical applications of collagen. International Journal of Pharmaceutics 221(1-2) (2001) 1-22.

[4] R. Langer, D.A. Tirrell, Designing materials for biology and medicine. Nature 428(6982) (2004) 487-492.

[5] W. Shen, J.A. Kornfield, D.A. Tirrell, Structure and mechanical properties of artificial protein hydrogels assembled through aggregation of leucine zipper peptide domains. Soft Matter 3(1) (2007) 99-107.

[6] M.W.T. Werten, H. Teles, A. Moers, E.J.H. Wolbert, J. Sprakel, G. Eggink, F.A. de Wolf, Precision Gels from Collagen-Inspired Triblock Copolymers. Biomacromolecules 10(5) (2009) 1106-1113.

[7] P.J. Skrzeszewska, F.A. de Wolf, M.W.T. Werten, A.P.H.A. Moers, M.A. Cohen Stuart, J. van der Gucht, Physical gels of telechelic triblock copolymers with precisely defined junction multiplicity. Soft Matter 5(10) (2009) 2057-2062.

[8] M.W.T. Werten, W.H. Wisselink, T.J.J. Jansen-van den Bosch, E.C. de Bruin, F.A. de Wolf, Secreted production of a custom-designed, highly hydrophilic gelatin in Pichia pastoris. Protein Engineering 14(6) (2001) 447-454.

[9] J.M. Cregg, K.J. Barringer, A.Y. Hessler, K.R. Madden, Pichia Pastoris as a host system for transformations. Molecular and Cellular Biology 5(12) (1985) 3376-3385.

[10] M.W.T. Werten, T.J. Van den Bosch, R.D. Wind, H. Mooibroek, F.A. De Wolf, High-yield secretion of recombinant gelatins by Pichia pastoris. Yeast 15(11) (1999) 1087-1096.

[11] W.H. Zhang, M.A. Bevins, B.A. Plantz, L.A. Smith, M.M. Meagher, Modeling Pichia pastoris growth on methanol and optimizing the production of a recombinant protein, the heavy-chain fragment C of botulinum neurotoxin, serotype A. Biotechnology and Bioengineering 70(1) (2000) 1-8.

[12] Y. Katakura, W.H. Zhang, G.Q. Zhuang, T. Omasa, M. Kishimoto, W. Goto, K.I. Suga, Effect of methanol concentration on the production of human beta(2)-glycoprotein I domain V by a recombinant Pichia pastoris: A simple system for the control of methanol concentration using a semiconductor Gas Sensor. Journal of Fermentation and Bioengineering 86(5) (1998) 482-487.

[13] J.D. Ferry, Viscoelastic Properties of Polymers, Wiley, New York, 1980.

[14] S. Frank, R.A. Kammerer, D. Mechling, T. Schulthess, R. Landwehr, J. Bann, Y. Guo, A. Lustig, H.P. Bachinger, J. Engel, Stabilization of short collagen-like triple helices by protein engineering. Journal of Molecular Biology 308(5) (2001) 1081-1089.

[15] J. Engel, H.T. Chen, D.J. Prockop, H. Klump, Triple helix reversible coil conversion of collagen-like polypeptides in aqueous and non aqueous solvents-comparison of thermodynamic parameters and binding of water to (L-Pro-L-Pro-Gly)n and (L-Pro-L-Hyp-Gly)n Biopolymers 16(3) (1977) 601-622.

[16] P.J. Skrzeszewska, F.A. de Wolf, M.A. Cohen Stuart, J. van der Gucht, Kinetics of network formation by telechelic polypeptides with trimeric nodes. Soft Matter 6(2) (2010) 416-422.

[17] K.T. Nijenhuis, Investigation into the aging process in gels of gelatin-water systems by the measurement of their dynamic moduli. Mechanism of the aging process. Colloid and Polymer Science 259(10) (1981) 1017-1026.

[18] V. Normand, S. Muller, J.C. Ravey, A. Parker, Gelation kinetics of gelatin: A master curve and network modeling. Macromolecules 33(3) (2000) 1063-1071.

[19] W.Y. Aalbersberg, R.J. Hamer, P. Jasperse, H.H.J. de Jongh, C.G. de Kruif, P. Walstra, F.A. de Wolf, Progress in Biotechnology; Industrial Proteins in Perspective, Elsevier, New York, 2003.

[20] H. Teles, P.J. Skrzeszewska, M.W.T. Werten, J. van der Gucht, G. Eggink, F.A. de Wolf, Influence of molecular size on gel-forming properties of telechelic collagen-inspired polymers. Soft Matter 6(19) (2010) 4681-4687.

[21] T. Annable, R. Buscall, R. Ettelaie, D. Whittlestone, The rheology of solutions of associating polymers-comparison of experimental behavior with transient network theory. Journal of Rheology 37(4) (1993) 695-726.

[22] C. Joly-Duhamel, D. Hellio, A. Ajdari, M. Djabourov, All gelatin networks: 2. The master curve for elasticity. Langmuir 18(19) (2002) 7158-7166.

[23] P.J. Flory, Principles of Polymer Chemistry Cornell University Press, New York, 1953.

[24] W.H. Stockmayer, Journal of Chemical Physics 12 (1944) 125-136.

[25] N.C. Fitzkee, G.D. Rose, Reassessing random-coil statistics in unfolded proteins. Proceedings of the National Academy of Sciences of the United States of America 101(34) (2004) 12497-12502.

[26] D.K. Wilkins, S.B. Grimshaw, V. Receveur, C.M. Dobson, J.A. Jones, L.J. Smith, Hydrodynamic radii of native and denatured proteins measured by pulse field gradient NMR techniques. Biochemistry 38(50) (1999) 16424-16431.

[27] C. Tanford, Physical Chemistry of Macromolecules, John Wiley & Sons, Inc., New York, 1961.

# Chapter 5

# Kinetics of network formation by telechelic polypeptides with trimeric nodes

*Abstract*

In this chapter we study the kinetics of transient network formation by monodisperse telechelic polypeptides with collagen-like end blocks and a random coil middle block. Upon cooling, the end blocks associate reversibly into triple helices, leading to gels with well-defined, trimeric crosslinks. Formation of triple helices occurs in two steps: nucleation and propagation. At low protein concentrations, when a simultaneous encounter of three end blocks is rather infrequent, the limiting step is nucleation. With increasing concentration, propagation of triple helix becomes rate-limiting. The rate of helix formation controls the gelation process and the development of mechanical (rheological) properties. Not all helices contribute to the developing network: a certain fraction forms mechanically irrelevant loops, particularly at low concentrations. We show, however, that it is possible to predict the time-dependent gel properties with the help of an analytical model, which accounts for loops and dangling ends. A connection between helix content and storage modulus can be established. Using this model we can accurately account for the experimental data.

Published in modified form as: P.J. Skrzeszewska, F.A. de Wolf, M.A. Cohen Stuart, J. van der Gucht, Kinetics of network formation by telechelic polypeptides with trimeric nodes. Soft Matter 6(2) (2010) 416-422

## 5.1 Introduction

Hydrogels, *i.e.* crosslinked polymer networks swollen with water, find applications such as drug delivery systems [1], wound dressing materials [2], tissue engineering materials [3] and rheological regulators in polymer blends [4]. The nature of the crosslinks and the supramolecular structure of the network determine the mechanism and dynamics of the gelation process.

In case of permanent gels, the junctions consist of covalent bonds, which can be formed by exposure to, *e.g.* heat, radiation [5-7], or by adding reactive crosslinking agents [8]. In physical gels the nodes are created in a reversible manner, due to weak non-covalent interactions such as hydrogen bonds, van der Waals forces, hydrophobic or electrostatic interactions. Accordingly, they respond to changes in pH [9], ionic strength or temperature [10], depending on the nature of the bonds. In gels made out of biological macromolecules weak interactions, stabilizing nodes formed by secondary and tertiary structures, play a crucial role. A well-known example is gelatin, which upon cooling, forms gels by change of conformation from coil to triple helix [11].

The evolution of a gel begins when the first crosslink is formed. One by one the molecules assemble. First, small clusters appear. With time these grow either by accumulating more molecules, or by aggregating into bigger clusters. The moment a giant sample-spanning cluster appears is called the gel or percolation threshold [12]. At this stage, there are still many small aggregates present in the sol phase. With time they progressively link to the network, leading to an increase of system elasticity until, finally, a steady-state is reached.

The gelation process can be followed directly, by monitoring mechanical properties, or indirectly, in terms of crosslinks formation. Very often, it is assumed that all detected crosslinks equally contribute to the gel strength. In general it is not possible to justify this assumption. Moreover, it is obviously not correct for associative telechelic polymers [9, 13-15], which tend to form inactive loops to an extent depending on total polymer concentration. As examples we may mention not only synthetic associative thickeners [15], but also, polypeptide chains having leucine zipper [9], elastin [16] or collagen-like domains at their ends [14, 17].

The network structure determines the mechanical properties of the system. Unfortunately, for most gels it is rather difficult to precisely know the network structure because the node multiplicity (number of strands coming together in a node) is unknown or not well-defined [18], so that the topology (*e.g.* number of loops) is unknown as well. In some

cases the elucidation of a structure-property relationship is possible, but it requires very advanced numerical calculations or simulations [13, 19]. However, for gels with a low and precisely-known node multiplicity, like the presently described material, the structure can be estimated rather accurately, so that this problem is circumvented. The lowest multiplicity, at which a network can appear, is three. Since this is also the simplest possible case, we decided to analyze it in detail.

In Chapter 3 we developed an analytical model for our systems that accounts accurately for internal gel structure with loops, bridges and dangling ends (see Figure 5.1) and gives predictions for the rheological properties of the network.

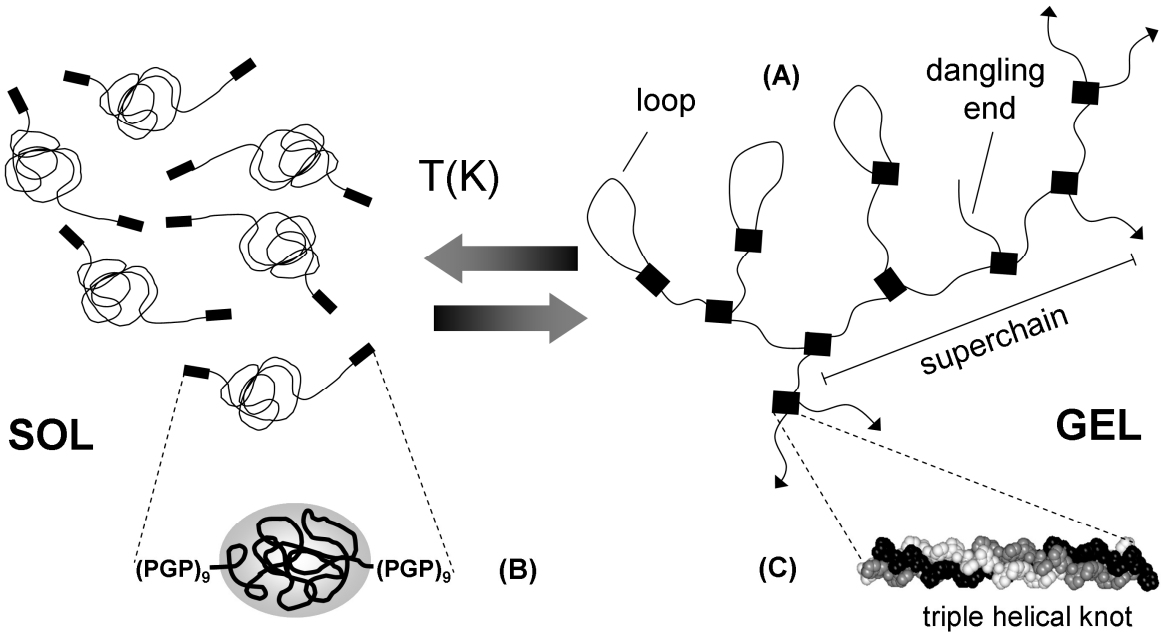


Figure 5.1 Gel network formation by telechelic polypeptides. (A) Gel network formed reversibly upon cooling. Chains terminated with an arrow are connected to the percolated gel network. (B) Single polypeptide consisting of a random coil-like middle block flanked by collagen-like end blocks (G-glycine, P-proline). (C) Triple helical knot formed by three end blocks.

We compared the model predictions to experimental results on solutions of telechelic polypeptides (TR4T) with collagen-inspired end blocks (T) that consist of nine consecutive Pro-Gly-Pro amino acid triplets. Three of these end blocks can co-assemble into triple helices. The middle block (R4) with a length of about 400 amino acids, is very hydrophilic and assumes a random conformation at any temperature. These protein polymers thus form physical gels with a node multiplicity of exactly three (see Figure 5.1). The melting temperature of the gels is about 40-47 °C, depending on protein concentration. Quantitative

agreement was found between the predictions of the model and the rheological measurements on the TR4T network (Chapter 3).

The results presented in Chapter 3 concerned stable TR4T gels that had approached a steady-state after approximately 15 hours. In this chapter we study the kinetics of the system during the gelation. We experimentally characterize both the amount of triple helix in time (by calorimetry) and the mechanical properties of the gel (by rheology). To describe the experimental data, we modify the model presented in Chapter 3 to include the kinetics of nucleation and propagation of triple helices.

## 5.2 Materials and methods

***Recombinant protein***

The construction of genes encoding TR4T protein with molecular weight of ~42 kDa, their transfection to the production host (the yeast *Pichia pastoris*) and the production and purification of the protein polymer have been described in Chapter 2 and in reference [17]. The complete amino acid sequence of the molecule has been deposited in GenBank [20] under accession number ACF33479.

All samples used to study gel formation were prepared in the same way. A given amount of protein was dissolved in phosphate buffer (pH 7, I=10 mM) and then heated at 50 °C for half an hour, allowing the protein to dissolve completely, under conditions where no triple helices are formed.

***Differential Scanning Calorimetry (DSC)***

Differential scanning calorimetry (DSC) was performed in a MicroCal VP DSC calorimeter with a cell volume of 0.51 ml. Several protein concentrations were tested (0.6~2.38 mM). In order to follow the development of triple helices in time, we used the following protocol. The sample was loaded to preheated measuring cell and then rapidly cooled in the DSC cell to 20 °C (at 3 K/min) and then left to equilibrate for a given time, varying from 0 to 15 hours. The amount of triple helices formed during this equilibration time was measured by increasing the temperature (at 0.6 K/min) and measuring the heat flow. In order to analyze the kinetics, we added an extra time of 45 minutes to the equilibration time, which accounts for the time needed to cool the sample from the approximate melting temperature (~42 °C) to 20 °C, and for the time needed to reach the melting temperature in

the upscan. After each upscan we waited 1 minute at 65 °C, before a new temperature quench was done.

***Rheology***

Five different concentrations of protein were tested (0.83, 0.96, 1.1, 1.3, 1.4 mM). All measurements were made using an Anton Paar Physica MCR 301 rheometer equipped with a cone and plate geometry of 50 mm diameter. The temperature was controlled by a Peltier system, which allowed fast heating and cooling. A solvent trap was used to minimize evaporation. Before adding the warm protein solution, the plate was preheated at 50 °C. After lowering the cone, the system was quenched to 20 °C. Gel formation was monitored by carrying out oscillatory measurements during the gelation process. For 0.83, 0.96 and 1.1 mM protein, frequency sweeps were performed during the gelation process, in a frequency range 0.1-20 Hz (0.628-125 rad/s) and with a deformation amplitude of 1 %, well within the linear response regime. The duration of each frequency sweep was fifteen minutes. At protein concentrations of 1.3 and 1.4 mM, where gelation was fast, the gel formation was monitored at a single frequency (1 Hz).

## 5.3 Experimental Results

***Triple helix formation during the gelation process***

The melting of the triple helices is an endothermic process. The heat effect is easily measured with differential scanning calorimetry (DSC). To melt a gel equilibrated during 15 hours, 107~128 kJ per mole of protein had to be introduced into the system (Figure 5.2A). The measured enthalpy (ΔH) did not depend on the scan rate (Figure 5.2B filled symbols). With increasing concentration, the enthalpy per mole of protein increased and reached a plateau of ~128 kJ/mole of protein at the highest concentration (Figure 5.2C). Assuming that this plateau value corresponds to ~100 % of triple helices, this corresponds to 192 kJ per mole of triple helices or 7.68 kJ per mole of hydrogen bonded tripeptides. This is in good agreement with the findings of Engel [21] and Frank [22]. At lower concentrations, the fraction of free end groups (or mismatched helices) is higher, and therefore the enthalpy per mole of protein is lower. The apparent melting temperature increases slightly with increasing concentration (Figure 5.2B open symbols). This has been found before for triple helices and can be explained on the basis of the reaction stoichiometry under equilibrium conditions [21, 23]. Except for the highest concentration, the apparent melting temperature revealed a

dependence on the scan rate, indicating that it was not possible to maintain equilibrium during the heating step (Figure 5.2A and 5.2B). At the highest concentration there is no scan-rate dependence, possibly because melting occurs at a higher temperature in this case, where the dissociation kinetics are faster [14, 24].

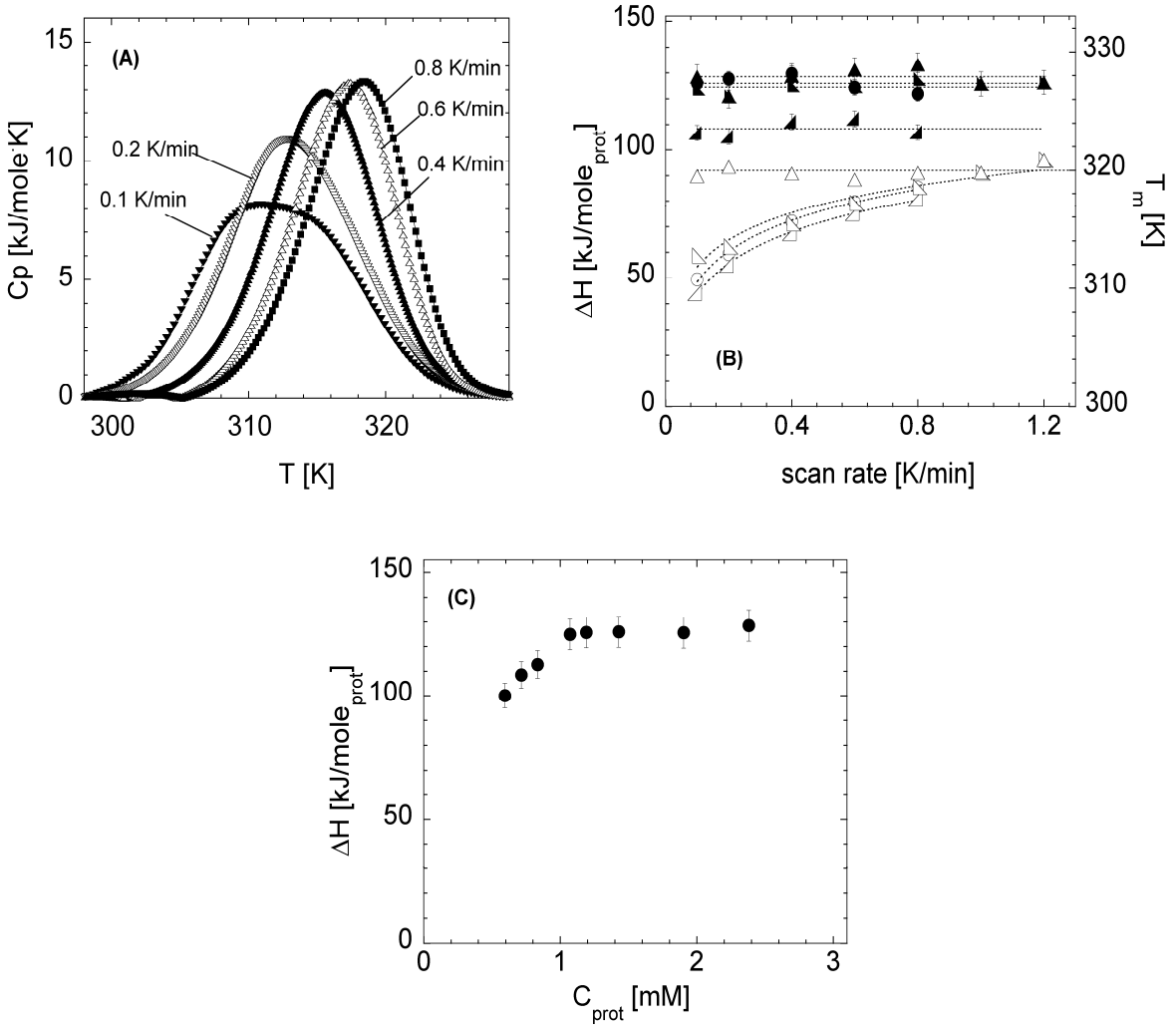


Figure 5.2 (A) DSC upscans with different scan rates (as indicated) for 1.42 mM after 15 hr of equilibration at 20 °C. (B) Enthalpy (filled symbols) and apparent melting temperatures (open symbols) as a function of scan rate for different concentrations after 15 hours of equilibration at 20 °C: (◢◿) 0.71 mM, (●○) 1.42 mM, (◣◺) 1.9 mM, (▲△) 2.38 mM. (C) Enthalpy change per mole of protein as a function of protein concentration.

Knowing that measured heat of melting corresponds to amount of triple helices in the system [17], we can analyze the kinetics of helix formation by measuring the enthalpy as a function of the equilibration time (*i.e.* the time that the sample was allowed to gel at 20 °C). An example of this (for 1.4 mM) is shown in Figure 5.3A. As can also be seen in this figure, the first and last (control) scan, both performed after 15 hours of equilibration, showed

exactly the same results. This indicates that the repeated cooling and heating did not affect the formation of triple helices.

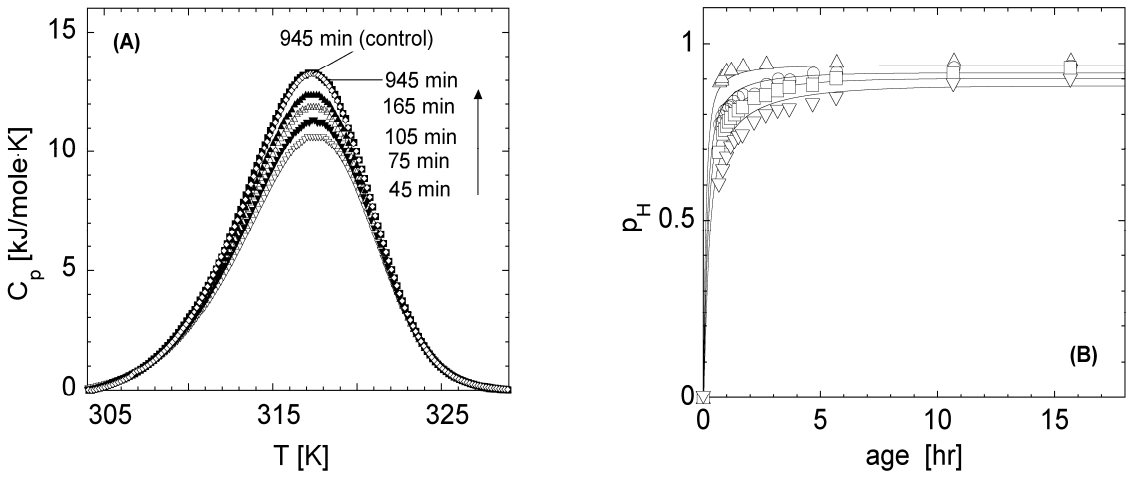


Figure 5.3 (A) DSC upscans with scan rate 0.6 K/min for 1.4 mM after different equilibration times (as indicated). (B) Development of triple helices in time for different concentrations: (▽) 0.83 mM, (□) 1.1 mM, (○) 1.4 mM, (△) 2.38 mM. Symbols correspond to experimental data and solid lines to model data, discussed in section 5.4.

The obtained enthalpies were normalized by the "plateau" enthalpy $\Delta H_0$=128 kJ per mole of protein, measured at the highest concentration after 15 hours of equilibration at 20 °C. Assuming that at this concentration and temperature the T blocks were nearly qualitatively converted to triple helices, the normalized enthalpy corresponds directly to the helicity of the system $p_H=C_H/C_{H,max}=3C_H/2C_{prot}$, where $C_H$ and $C_{prot}$ are the concentrations of triple helices and the total protein c, respectively. The formation kinetics of triple helices, as deduced from DSC data, is shown in Figure 5.3B.

To determine the reaction order, the initial rate of triple helix formation $(dC_H/dt)_0$ was plotted as a function of the total concentration of end groups $C_{F,0}=2\cdot C_{prot}$ on a double-logarithmic scale. The results are presented in Figure 5.4. At low concentrations, the order approaches three, while at higher concentrations it is closer to one. Such a change of reaction order has been reported earlier for triple helix formation [24]. It suggests that triple helix formation is a two-step mechanism, as will be discussed in detail in section 5.4. The rate constants, estimated by extrapolation of the experimental data for each of these steps (two solid lines in Figure 5.4), are: $k_{a1}$=25 to 600 $M^{-2}\cdot s^{-1}$ and $k_{a2}=1\cdot 10^{-4}$ to $2\cdot 10^{-3}$ $s^{-1}$. Respectively, these values cannot be estimated very accurately, however, as they are rather sensitive to the way of extrapolation.

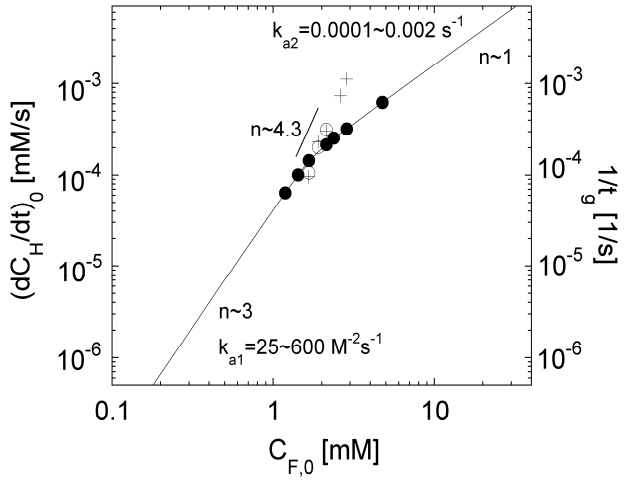


Figure 5.4 (●) Initial rate of triple helix formation as a function of end group concentration. The reaction order (n) changes from 3 to 1 with increasing concentration. (○) Reciprocal of the gel time, based on frequency resolved oscillatory experiments, (+) reciprocal of the gel time obtained from a G'(t)/G"(t) crossover, as a function of total end blocks concentration.

### *Changes in rheological properties during gelation*

In order to compare how the formation of triple helices affects the rheological properties of the system, we followed the kinetics of gel formation with rheology. The gel point ($t_g$) (critical point) for our system was determined by means of oscillatory experiments (Figure 5.5).

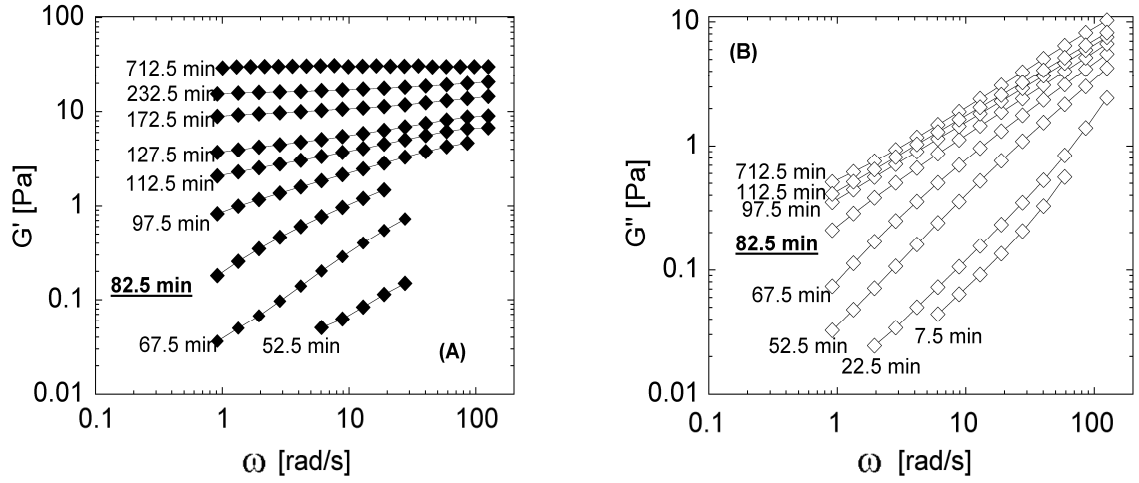


Figure 5.5 Oscillatory experiments for protein concentration $C_{prot}$=0.96 mM at different times after cooling to 20 °C. (A) Frequency sweeps for storage modulus. (B) Frequency sweeps for loss modulus. The critical exponent Δ~0.7 occurs at $t_g$=82.5 minutes.

Many experimental [25] and theoretical studies [26] have shown that at the gel point the storage modulus (G') and the loss modulus (G") both show power law behavior as a function of frequency: $G' \sim G'' \sim \omega^{\Delta}$. Figure 5.5 shows the storage (A) and the loss (B) moduli as a function of the deformation frequency, at various gel ages for a 0.96 mM TR4T solution. In the beginning, viscous properties are predominant. The loss modulus increases linearly with frequency in this regime, and the storage modulus is not detectable until the age of 52.5 minutes. As the gel point ($t_g$) is approached, the elastic properties start to play a more significant role. At t=82.5 minutes, both G'(ω) and G"(ω) show very similar power law behavior with a critical exponent Δ~0.70 (Figure 5.5 and 5.6).

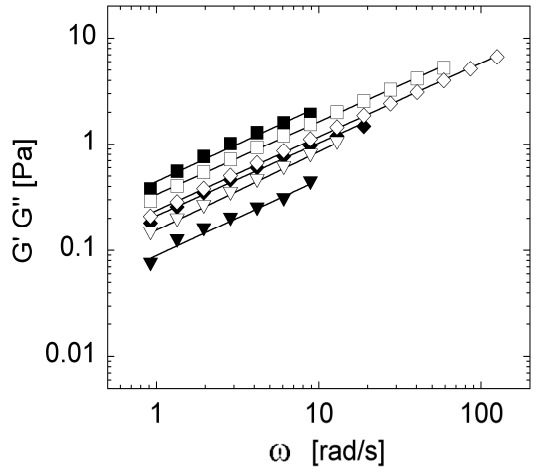


Figure 5.6 Gel thresholds for different protein concentrations: (▽,▼) 0.83 mM, $t_g$=157.5 minutes; (◇,◆) 0.96 mM, $t_g$ =82.5 minutes; (□,■) 1.1mM, $t_g$ =52.5 minutes. Open symbols represent G"(ω) and filled G'(ω).

As shown in Figure 5.6, the critical exponent hardly depends on the protein concentration. The exponent of 0.7 is in very good agreement with values found for biological gel-forming macromolecules such as gelatin or pectins [25, 27], and also with values predicted by percolation theory [12, 27]. As prescribed by the Kramers-Kronig relations, the loss tangent, tanδ=G"/G', should equal tan(Δπ/2)≈2 at the critical gel point [28]. As observed in Figure 5.6, this is approximately what we find at low concentrations, but at higher concentrations we find a smaller ratio. This is probably due to the difficulty in capturing the exact gel point at high concentrations, where gelation is fast (while each frequency sweep takes approximately 15 minutes).

At $t>t_g$, the gel becomes more elastic. As we have shown in previous chapters, using creep experiments, the system forms a soft, transient network with a characteristic relaxation

time on the order of several thousand seconds [14], which is too long to be observed in dynamic measurements in the available frequency range.

For concentrations of 1.3 and 1.4 mM, the system evolved too quickly through the gel point to capture the critical gel behavior by dynamic shear experiments. In this case, the gel time $t_g$ was estimated as the crossover of G'(t) and G"(t) at a frequency of 6.28 rad/s. This should be a reliable estimate, since gel points determined as a crossover, for concentrations lower than 1.1 mM, are all very close to values obtained from frequency sweeps (Figure 5.4).

As a second measure of the gelation kinetics, the reciprocal of the gel time $t_g$ is plotted versus the logarithm of the concentration of free end blocks ($C_{F,0}$) in Figure 5.4. Note that $t_g^{-1}$ increases much faster with $C_{F,0}$ than the initial rate $(dC_H/dt)_0$ of triple helix formation. This is an indication that, for our system, the helix content is not simply proportional to the network progress. As can be seen more clearly in Figure 5.7 the relation between the elastic properties (G') and helix content ($p_H$) of the system varies significantly with protein concentration.

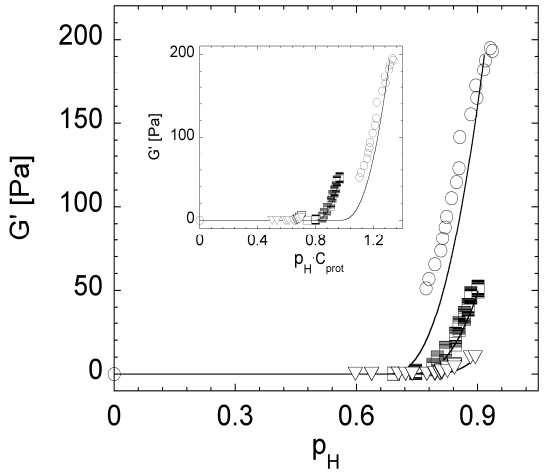


Figure 5.7 Storage modulus (G') as a function of triple helix fraction ($p_H$) for different protein concentrations: (▽) 0.83 mM, (□) 1.1 mM, (○) 1.4 mM. Solid lines present model data (section 5.4). Inset presents storage modulus (G') as a function of triple helix concentration ($p_H \cdot C_{prot}$). For 0.83 and 1.1 mM, the storage moduli at all frequencies between 1 and 10 rad/s are shown; for 1.4 mM, all data are at 6.28 rad/s.

Contrary to gelatin [29], no master curve between storage modulus and system helicity can be drawn. This is due to the loop formation that occurs in this particular gel, and that depends strongly on the protein concentration. At high concentrations, elastically active bridges are more likely to occur, while loops are more abundant at low concentrations.

## 5.4 Gelation model and discussion

The observed shift in reaction order from three to one, at increasing concentration (Figure 5.4), has also been observed by Boudko *et al*. [24]. Such a dependency is characteristic for collagen-like polypeptides. In natural collagen, non-collagenous globular domains (NC-domains) are essential for proper alignment of the chains forming triple helices [30]. They bind together and align the three chains, and thus initiate trimerization. Without NC-domains, the formation of triple helical nuclei is much slower, and mismatched helices can be formed [23, 31].

To form triple helix nuclei, our molecules, which lack NC domains, require simultaneous collision of three mutually aligned T blocks. At low concentrations, when such a simultaneous collision is rather infrequent, nucleation is rate-limiting (Figure 5.8A). Probably, a dimeric nucleus $C_{D*}$ first is formed [24]. However, the order of reaction at low concentrations being ~3 rather than ~2 suggests that double helices are not stable, and the limiting step is the formation of triple helical nuclei. For more concentrated solutions, when nucleation is relatively fast, propagation of triple helices becomes rate-limiting (Figure 5.8B). The propagation of triple helices is probably limited by *cis-trans* isomerization of peptide bonds in which proline residues are involved [32], and by readjustment of misalignments. The high incidence of proline in the end block will result in a high number of *cis* bonds in the monomeric state. In order to form a triple helix these have to be converted to the *trans* conformation. The activation energy of *cis-trans* isomerization slightly depends on the type of collagen, but is around ~80 kJ/mole [32].

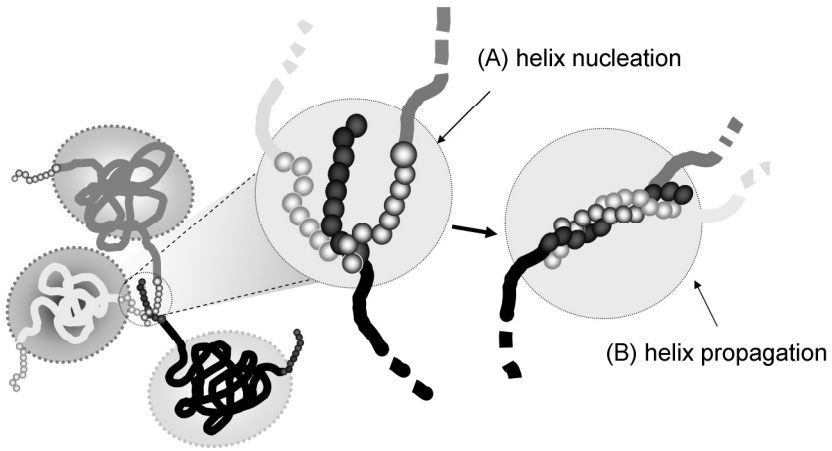


Figure 5.8 Two step kinetics of triple helix formation: (A) helix nucleation and (B) helix propagation.

In order to describe the formation of triple helices, we propose the following two-step kinetic model:

$$3C_F \underset{k_{d1}}{\overset{k_{a1}}{\rightleftharpoons}} C_{H^*} \underset{k_{d2}}{\overset{k_{a2}}{\rightleftharpoons}} C_H \qquad \text{(Eq. 5.1)}$$

where, $C_F$ is the concentration of free side groups, $C_{H^*}$ the concentration of helical nuclei (*i.e.* nuclei consisting of three chains that have formed an initial bond), and $C_H$ the concentration of fully developed triple helices; $k_{a1}$ and $k_{a2}$ are rate constants for nucleation and propagation, respectively, and $k_{d1}$ and $k_{d2}$ are the corresponding dissociation constants. On the basis of this scheme, the following kinetic equations can be written:

$$r_{H^*} = \frac{dC_{H^*}}{dt} = k_{a1} \cdot C_F{}^3 - k_{d1} \cdot C_{H^*} - k_{a2} \cdot C_{H^*} + k_{d2} \cdot C_H \qquad \text{(Eq. 5.2)}$$

$$r_H = \frac{dC_H}{dt} = k_{a2} \cdot C_{H^*} - k_{d2} \cdot C_H \qquad \text{(Eq. 5.3)}$$

Assuming this two step mechanism to hold, we can model the development of triple helices in time (Figure 5.3B solid lines).

The best fit to our data is obtained taking $k_{a1}$, $k_{a2}$ to be respectively 350 $M^{-2}\cdot s^{-1}$ and $2.7\cdot10^{-3}$ $s^{-1}$. These values are within the range estimated from the initial rates (solid lines in Figure 5.4). Values reported by Boudko [24] for short $(Pro\text{-}Pro\text{-}Gly)_{10}$ peptides at 7 °C are around 800 $M^{-2}\cdot s^{-1}$ and $7\cdot10^{-4}$ $s^{-1}$, respectively. With an artificial attached nucleation domain (trimetric foldon domain of T4 phage or the crosslinking domain of collagen III), the propagation constants of the same blocks are respectively $1.97\cdot10^{-3}$ $s^{-1}$ and $3.3\cdot10^{-4}$ $s^{-1}$ at 20 °C. Our findings are consistent with these published data. The dissociation rate constants $k_{d1}$ and $k_{d2}$ that gave the best agreement with experimental data are $5\cdot10^{-4}$ $s^{-1}$ and $2.2\cdot10^{-5}$ $s^{-1}$, respectively. These values are close to the dissociation rate of a single triple helix at 20 °C that we measured previously [14]: $k_d=\tau_0^{-1}\sim7\cdot10^{-5}$ $s^{-1}$.

In Chapter 3, we showed that the rheological properties of the gel can be described by a model that takes into account both the equilibrium between triple helices and free ends, and the distribution of helices over junctions (where all three T blocks come from different chains) loops (where two out of the three T groups come from the same molecule) (Figure 5.1). The ratio between junctions and loops increases with concentration [14]. The probability to form a junction ($p=p_J$) can be expressed as a function of total protein concentration ($C_{prot}$),

overlap concentration (C*) (which was estimated as ~1 mM in Chapter 3) and fraction of triple helices ($p_H$) as follows:

$$p = \frac{2 \cdot p_H \cdot C_{prot}}{2 \cdot C_{prot} + C^*} \qquad \text{(Eq. 5.4)}$$

Using the classical network theory of Flory [33] and Stockmayer [34], the following equation for the plateau modulus was derived:

$$G_0 \approx \frac{F \cdot \left[ C_{prot} \cdot (2p-1)^3 \cdot R \cdot T \right]}{p^2} \qquad \text{(Eq. 5.5)}$$

where RT is the thermal energy per mole, and F is the so-called front factor, taken to be 0.5. [14]

Using equation 5.4 we could convert the fraction of triple helices ($p_H$) in the system during the gelation process (from Figure 5.3B) into a fraction of network junctions ($p=p_J$), and then, with equation 5.5, we could calculate the elastic modulus ($G_0$). This allowed us to model the time-dependent rheological properties during the gelation process. The results of this calculation are shown in Figure 5.9, together with the experimental data.

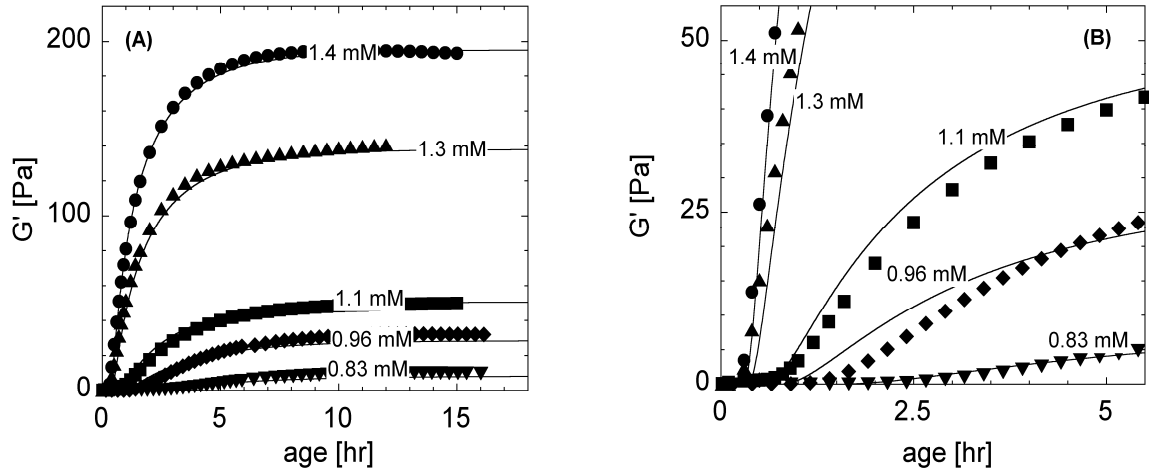


Figure 5.9 (A) Storage modulus as a function of gel age. (B) Storage modulus as a function of gel age at short times. Symbols represent experimental data and solid lines results from the model.

The agreement is very good, except in the initial stages of gelation (Figure 5.9B). The reason for these deviations at short times is that the mean field description does not give a good description of the critical gel state. As seen in Figure 5.5, the modulus depends on frequency in this regime, which is not accounted for by the model.

Assuming the critical gel fraction $p_c$ to be 0.5 (in our case gel fraction corresponds to junctions fraction) as proposed by the classical theory, the gel points ($t_g$) for different concentrations can be determined from the model data. Although the calculated values show a similar trend as the experimentally determined values, they are significantly lower (Figure 5.10). Such a deviation is probably caused by the fact that the analytical model developed by us, is based on classical gel theory [33], which neglects the formation of multimolecular loops. This is not valid close to the gel point. The critical gel fraction $p_c$ predicted by percolation theory for a system as ours should be higher than the $p_c$ predicted by classical theory [35].

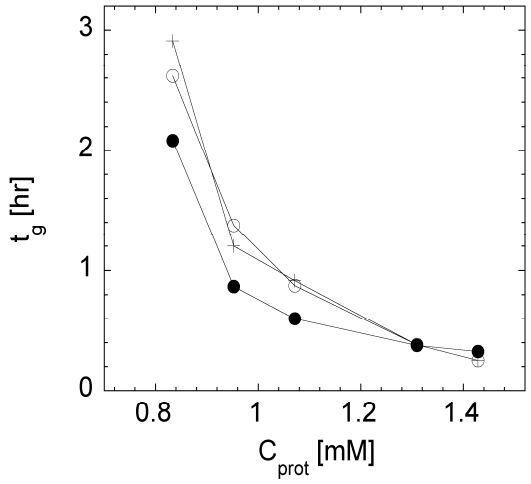


Figure 5.10 Gel time as a function of total protein concentration: (○) determined from oscillatory experiments, (+) determined from G'(t)/G"(t) crossover; (●) estimated from model, assuming pc=0.5.

## 5.5 Concluding remarks

In this chapter we analyzed the network formation by telechelic polypeptides with collagen-like end blocks, which form triple helices upon cooling. The development of triple helices can be described by a two-step kinetic model. Prior to triple helix propagation, a trimeric nucleus has to be formed. For dilute systems, the formation of trimeric nuclei is slow, and nucleation is the limiting step, resulting in an apparent reaction order of three. At higher concentrations, the limiting step is triple helix propagation, probably restricted by *cis-trans* isomerization of proline peptide bonds [32], and the apparent reaction order is close to unity.

The kinetics of triple helix formation reflects the kinetics of gel network formation, but in an indirect way. Due to loop formation, the gel strength depends not only on the helix

content of the system but also on the ratio between loops and junctions. This ratio depends on the overall protein concentration.

Owing to the well-defined node multiplicity in this system it was possible to calculate the loops/junctions ratio and, hence, to link the kinetics of triple helix formation to changes in the network structure and mechanical properties of the gel.

## References

[1] M. Sutter, J. Siepmann, W.E. Hennink, W. Jiskoot, Recombinant gelatin hydrogels for the sustained release of proteins. Journal of Controlled Release 119(3) (2007) 301-312.

[2] B. Balakrishnan, M. Mohanty, P.R. Umashankar, A. Jayakrishnan, Evaluation of an in situ forming hydrogel wound dressing based on oxidized alginate and gelatin. Biomaterials 26(32) (2005) 6335-6342.

[3] B.S. Kim, D.J. Mooney, Development of biocompatible synthetic extracellular matrices for tissue engineering. Trends in Biotechnology 16(5) (1998) 224-230.

[4] J. Kim, S.S. Kim, K.H. Kim, Y.H. Jin, S.M. Hong, S.S. Hwang, B.G. Cho, D.Y. Shin, S.S. Im, Applications of telechelic polymers as compatibilizers and stabilizers in polymer blends and inorganic/organic nanohybrids. Polymer 45(10) (2004) 3527-3533.

[5] M. Wang, L. Xu, X.C. Ju, J. Peng, M.L. Zhai, J.Q. Li, G.S. Wei, Enhanced radiation crosslinking of carboxymethylated chitosan in the presence of acids or polyfunctional monomers. Polymer Degradation and Stability 93(10) (2008) 1807-1813.

[6] B. Singh, S. Kumar, Synthesis and characterization of psyllium-NVP based drug delivery system through radiation crosslinking polymerization. Nuclear Instruments & Methods in Physics Research Section B-Beam Interactions with Materials and Atoms 266(15) (2008) 3417-3430.

[7] F. Cataldo, O. Ursini, E. Lilla, G. Angelini, Radiation-induced crosslinking of collagen gelatin into a stable hydrogel. Journal of Radioanalytical and Nuclear Chemistry 275(1) (2008) 125-131.

[8] T.H. Chen, H.D. Embree, L.Q. Wu, G.F. Payne, In vitro protein-polysaccharide conjugation: Tyrosinase-catalyzed conjugation of gelatin and chitosan. Biopolymers 64(6) (2002) 292-302.

[9] W. Shen, J.A. Kornfield, D.A. Tirrell, Structure and mechanical properties of artificial protein hydrogels assembled through aggregation of leucine zipper peptide domains. Soft Matter 3(1) (2007) 99-107.

[10] S.C. Lee, Y.W. Cho, K. Park, Control of thermogelation properties of hydrophobically-modified methylcellulose. Journal of Bioactive and Compatible Polymers 20(1) (2005) 5-13.

[11] K.T. Nijenhuis, On the nature of crosslinks in thermoreversible gels. Polymer Bulletin 58(1) (2007) 27-42.

[12] P.G. de Gennes, Scaling Concepts in Polymer Physics, Cornell University Press, Ithaca London, 1979.

[13] T. Annable, R. Buscall, R. Ettelaie, D. Whittlestone, The rheology of solutions of associating polymers-comparison of experimental behaviour with transient network theory. Journal of Rheology 37(4) (1993) 695-726.

[14] P.J. Skrzeszewska, F.A. de Wolf, M.W.T. Werten, A.P.H.A. Moers, M.A. Cohen Stuart, J. van der Gucht, Physical gels of telechelic triblock copolymers with precisely defined junction multiplicity. Soft Matter 5(10) (2009) 2057-2062.

[15] J. Sprakel, E. Spruijt, M.A.C. Stuart, N.A.M. Besseling, M.P. Lettinga, J. van der Gucht, Shear banding and rheochaos in associative polymer networks. Soft Matter 4(8) (2008) 1696-1705.

[16] E.R. Wright, V.P. Conticello, Self-assembly of block copolymers derived from elastin-mimetic polypeptide sequences. Advanced Drug Delivery Reviews 54(8) (2002) 1057-1073.

[17] M.W.T. Werten, H. Teles, A. Moers, E.J.H. Wolbert, J. Sprakel, G. Eggink, F.A. de Wolf, Precision Gels from Collagen-Inspired Triblock Copolymers. Biomacromolecules 10(5) (2009) 1106-1113.

[18] S.B. Rossmurphy, Incipient behaviour of gelatin gels. Rheologica Acta 30(5) (1991) 401-411.

[19] F. Tanaka, S.F. Edwards, Viscoelastic properties of physically cross-linked networks-transient network theory. Macromolecules 25(5) (1992) 1516-1523.

[20] http://www.ncbi.nlm.nih.gov/Genbank/, GenBank.

[21] J. Engel, H.T. Chen, D.J. Prockop, H. Klump, Triple helix reversible coil conversion of collagen-like polypeptides in aqueous and non aqueous solvents - comparison of thermodynamic parameters and binding of water to (L-Pro-L-Pro-Gly)n and (L-Pro-L-Hyp-Gly)n Biopolymers 16(3) (1977) 601-622.

[22] S. Frank, R.A. Kammerer, D. Mechling, T. Schulthess, R. Landwehr, J. Bann, Y. Guo, A. Lustig, H.P. Bachinger, J. Engel, Stabilization of short collagen-like triple helices by protein engineering. Journal of Molecular Biology 308(5) (2001) 1081-1089.

[23] A.V. Persikov, Y.J. Xu, B. Brodsky, Equilibrium thermal transitions of collagen model peptides. Protein Science 13(4) (2004) 893-902.

[24] S. Boudko, S. Frank, R.A. Kammerer, J. Stetefeld, T. Schulthess, R. Landwehr, A. Lustig, H.P. Bachinger, J. Engel, Nucleation and propagation of the collagen triple helix in single-chain and trimerized peptides: Transition from third to first order kinetics. Journal of Molecular Biology 317(3) (2002) 459-470.

[25] C. Michon, G. Cuvelier, B. Launay, Concentration-dependence of the critical viscoelastic properties of gelatin at the gel point. Rheologica Acta 32(1) (1993) 94-103.

[26] J.E. Martin, D. Adolf, J.P. Wilcoxon, Viscoelasticity of near-critical gels. Physical Review Letters 61(22) (1988) 2620-2623.

[27] G. Forgacs, S.A. Newman, B. Hinner, C.W. Maier, E. Sackmann, Assembly of collagen matrices as a phase transition revealed by structural and rheologic studies. Biophysical Journal 84(2) (2003) 1272-1280.

[28] H.H. Winter, F. Chambon, Analysis of Linear Viscoelasticity of a Cross-Linking Polymer at the Gel Point. Journal of Rheology 30(2) (1986) 367-382.

[29] C. Joly-Duhamel, D. Hellio, A. Ajdari, M. Djabourov, All gelatin networks: 2. The master curve for elasticity. Langmuir 18(19) (2002) 7158-7166.

[30] W.Y. Aalbersberg, R.J. Hamer, P. Jasperse, H.H.J. de Jongh, C.G. de Kruif, P. Walstra, F.A. de Wolf, Progress in Biotechnology ; Industrial Proteins in Perspective, Elsevier, New York, 2003.

[31] J. Engel, D.J. Prockop, The zipper-like folding of collagen triple helices and the effects of mutations that disrupt the zipper Annual Review of Biophysics and Biophysical Chemistry 20 (1991) 137-152.

[32] H.P. Bachinger, P. Bruckner, R. Timpl, J. Engel, Role of cis-trans isomerization of peptide-bonds in coil reversible triple helix conversion of collagen. European Journal of Biochemistry 90(3) (1978) 605-613.

[33] P.J. Flory, Principles of Polymer Chemistry Cornell University Press, New York, 1953.

[34] W.H. Stockmayer, Journal of Chemical Physics 12 (1944) 125-136.

[35] C.J. Brinker, G.W. Scherer, Sol-gel science: the physics and chemistry of sol-gel processing, Academic Press, Inc, San Diego, 1990.

# Chapter 6

# Fracture and self-healing in a well-defined self-assembled polymer network

*Abstract*

In this chapter we study shear-induced fracture and self-healing of well-defined transient polymer networks formed by telechelic polypeptides, with nodes formed by collagen-like triple helices. When these gels are sheared at a rate, which is higher than the inverse relaxation time of the nodes, fracture occurs at a critical stress, which increases logarithmically with increasing shear rate. When a constant stress is applied, fracture occurs after a delay time, which decreases exponentially with increasing stress. These observations indicate that fracture in these systems is due to stress-activated rupture of triple helical junctions. After rupture, the physical gels heal completely.

Published as: P.J. Skrzeszewska, J. Sprakel, F.A. de Wolf, R Fokkink, M.A. Cohen Stuart and J. van der Gucht, Fracture and self-healing in a well-defined self-assembled polymer network. Macromolecules 43 (7) (2010) 3542–3548.

## 6.1 Introduction

Physical (transient) gels are solvent-filled networks, formed by reversibly crosslinked polymers, in which weak interactions such as hydrogen bonds, hydrophobic interactions, Van der Waals forces or electrostatic interactions are responsible for crosslinks formation. Due to the transient character of the junctions, physical gels, contrary to covalent networks, are able to relax applied stresses by dissociation and reformation of junctions. This plastic relaxation makes them capable of healing after damage, which is impossible in case of permanent gels [1]. Consequently, physical networks offer unique advantages for many applications. They can be used as controlled drug delivery systems [2], rheological regulators in polymer blends [3], coatings, food, and cosmetics, or as matrix materials for tissue engineering [4]. Also in nature fibrous tissues, such as cartilage, are formed by (partially) non-covalently crosslinked biopolymers. The self-healing capacity of these networks plays an important role in wound healing. Physical gels are viscoelastic, with a characteristic relaxation time that is determined by the lifetime of the physical junctions in the network. When a small stress or strain rate is applied to a physical gel, the natural relaxation mechanism of the material is able to keep up with the deformation, and the system responds linearly. Experiments in this regime, although very useful to understand the internal structure and transient character of the network [5], often do not correspond to realistic application conditions. Depending on their practical or biological function, hydrogels are exposed to deformations and stresses, which go far beyond the linear regime. Under these large deformations, viscoelastic materials can undergo several macroscopic instabilities such as yielding or breaking. While fracture of brittle solids, such as metals or ceramics, has been widely studied, the failure of solvent-filled viscoelastic polymer networks is still poorly understood. So far, most of the work on failure of viscoelastic networks was done for gels formed by classical telechelic polymers, consisting of a hydrophilic chain modified with two hydrophobic end groups [6-9], or by natural biopolymers [10-12]. However, the internal architecture and the crosslink dynamics are rather poorly defined in most of these systems. This renders understanding the failure process in terms of molecular parameters problematic. To avoid such difficulties, we consider physical gels with very well-defined topology and junction dynamics; these are gels formed by biosynthetic telechelic polypeptides, consisting of rather short collagen-like end blocks $(Pro\text{-}Gly\text{-}Pro)_9$ flanking a water-soluble, random coil-like domain (399 amino acids long) [13]. At ambient temperature, the end blocks of this polymers assemble into triple helices [13], forming a network with a node multiplicity of exactly three [5]. Linear rheology showed that this

network obeys, to a good approximation, Maxwell behaviour. The relaxation time was found to be in the kilo-seconds range, and to depend strongly on concentration and temperature, as does the elastic shear modulus (Chapter 3). The experimental results could be described quantitatively and without adjustable parameters by an analytical model, based on classical gel theory. This model accounts for the internal gel structure, with bridges, loops, and dangling ends, and uses available thermodynamic data for the formation and decay of triple helices.

In this chapter, we focus strongly on non-linear properties such as fracturing and self-healing. By carrying out shear start-up experiments we determine the critical stress for gel failure and the steady-state stress after fracture, both as a function of shear rate. We also investigate delayed network rupture under a fixed applied stress. To get more insight into the mechanism and nature of network disintegration, we carried out particle image velocimetry (PIV). The two-dimensional velocity maps determined from these experiments confirm a shear-induced fracture, which we elaborate in more detail using the activated bond rupture theory proposed by Chaudhury and Evans [14, 15]. Finally, we investigated self-healing of the system after rupture by following the recovery of the storage modulus in time. The experiments showed that the system can fully heal after different fracture histories.

## 6.2 Material and methods

### *Recombinant protein*

The construction of genes encoding the TR4T protein with a molecular weight of 42 kDa, the transfection to the production host (the yeast *Pichia pastoris*), and the production and purification of the protein polymer have been described in Chapter 2.

### *Non-linear rheology*

All measurements were conducted on an Anton Paar Physica MCR 301 rheometer equipped with Couette geometry (CC10) with an outer diameter of 10.84 mm and a bob size of 10 mm. Samples were always prepared in the same way. A given amount of protein was dissolved in phosphate buffer (pH 7, I=10 mM) and then heated at 50 °C for half an hour, allowing the protein to dissolve completely under conditions where no triple helices are formed. Before inserting the warm protein solution in the Couette cell, the geometry was preheated to 50 °C. After lowering the bob, the system was quenched to 20 °C. Prior to actual experiments, the sample was equilibrated for 15 hours to form a stable gel. A solvent trap was

used to minimize evaporation. Shear start-up experiments were conducted in a wide range of applied shear rates ($10^{-6}$ up to $10^{3}$ $s^{-1}$). The stress was monitored for several hours, which is much longer than the relaxation time of the networks (on the order of 1000 seconds as shown in Chapter 3). In an alternative experiment, a constant stress was applied to the sample and the resulting deformation was measured as a function of time.

The network healing was monitored by applying a sinusoidal deformation of small amplitude (frequency f=1 $s^{-1}$ and strain $\gamma$=1 %) to follow the recovery of the elastic modulus (G') in time.

***PIV (Particle Image Velocimetry)***

The local fluid velocity in the gap of the Couette cell is measured by particle image velocimetry (PIV). Tracer particles (0.02 % w/v of 10 μm Spherotech Fluorescent Nile Red latex particles) were added to the solution for flow visualization. The set up used to perform PIV is presented in Figure 6.1.

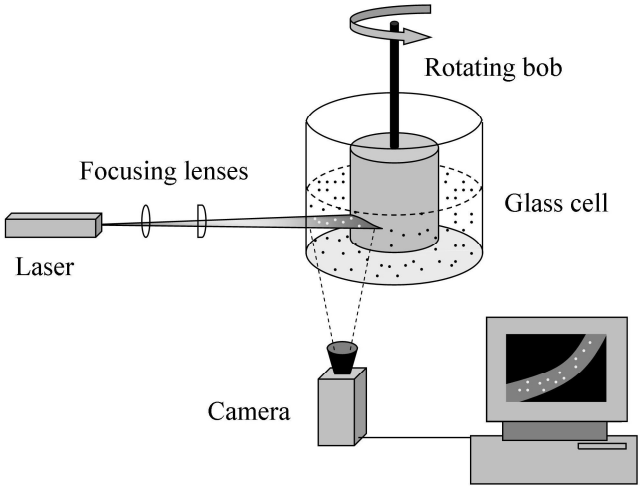


Figure 6.1 Particle image velocimetry (PIV) set up.

An Anton Paar Physica MCR 300 rheometer was equipped with a Couette cell with transparent walls, with an outer diameter of 36 mm and gap size of 2 mm. A DPSS (Diode Pump Solid State) laser beam with wavelength of 532 nm was passed through two lenses: a spherical lens (Opto Sigma 011-1275, Ø 15 mm FL-120 mm, Molenaar Optics) and a cylindrical lens (Thorlabs LK1087L2 FL-6.4 mm H-6.0 mm L-12.0 mm), in order to generate a laser sheet that illuminates a thin section of the gap in the flow-gradient plane. The estimated thickness of the laser sheet is 155 μm. A CCD camera mounted below the gap

records the images, focussed on the plane illuminated by the laser sheet. In order to obtain the velocity vectors at each position, two images taken at a given time interval were cross-correlated using a multi-pass, multi-grid FFT algorithm, as implemented in the open source package JPIV [16]. Time intervals were different for different shear rates: 100, 7, 1.4, 0.6, and 0.26 s respectively for $\dot{\gamma}\cdot\tau$=1.92, 32, 160, 320, and 1600.

## 6.3 Results and discussion

In this chapter, we consider TR4T solutions at three different concentrations. The values of the plateau storage modulus $G_0$ and of the viscoelastic relaxation time $\tau$ for these concentrations are given in Table 6.1. They were determined in Chapter 3 by means of linear creep experiments.

| $C_{prot}$ [mM] | $G_0$ [Pa] | $\tau$ [s] |
|---|---|---|
| 0.96 | ~35 | ~3200 |
| 1.1 | ~58 | ~3800 |
| 2 | ~600 | ~7700 |

Table 6.1 Elastic plateau modulus and relaxation time for different TR4T concentrations.

Figure 6.2 shows the stress response after start-up of steady shear flow for a TR4T gel at a concentration of 0.96 mM at 20 °C, for different applied shear rates. The results are plotted as stress ($\sigma$) versus strain ($\gamma=\dot{\gamma}\cdot t$).

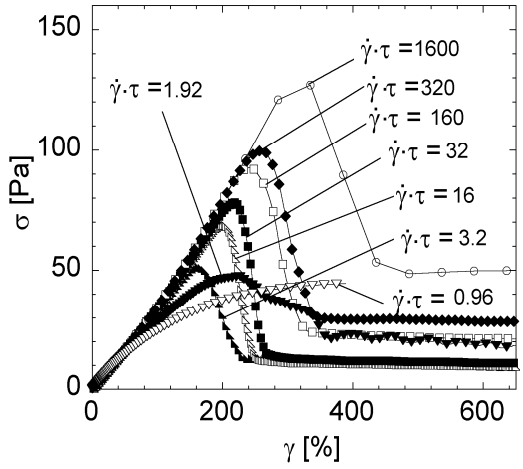


Figure 6.2 Time-resolved stress response as a function of strain ($\gamma=\dot{\gamma}\cdot t$) after start-up of steady shear for a 0.96 mM TR4T gel at 20 °C. The reduced shear rates ($\dot{\gamma}\cdot\tau$) are indicated near the lines, with $\tau$ equal to 3200 s.

For shear rates below the inverse relaxation time ($\dot{\gamma}\cdot\tau$<1), the stress increases gradually with increasing strain towards its steady-state value. In this regime, the natural relaxation of the transient nodes can keep up with the applied deformation and the material flows homogeneously. However, for higher shear rates, $\dot{\gamma}\cdot\tau$>1, the stress first rises to a pronounced maximum, before it decreases rapidly to a lower steady-state value. This decrease in the stress indicates failure of the network. As we will show below, steady-state velocity profiles measured with particle image velocimetry (PIV) show an inhomogeneous flow with a fracture zone. The transient stress curves at high shear rates resemble those for a fracturing brittle solid: an initial elastic response followed by failure at a critical stress. Only for shear rates slightly above the inverse relaxation time ($\dot{\gamma}\cdot\tau$=3.2 in Figure 6.2), some plastic deformation is observed, which appears as a quasi-plateau before actual breaking. Note that the stress and strain, at which failure occurs, depend on the applied shear rate. This is in contrast to observations by Berret [7] for fracture in a network of associative polymers. Recent simulations for a similar system, however, also show such a shear rate dependence [9]. In the next section we will discuss the kinetics of failure in more detail. First, we consider the initial elastic response.

***Initial elastic response***

At low strains, all stress/strain curves in Figure 6.2 superimpose. Initially, the stress increases linearly with increasing strain with a slope equal to the plateau modulus $G_0$. For strains larger than ~50 %, deviations from the linear response can be observed. At low shear rates ($\dot{\gamma}\cdot\tau$<1), the stress deviates downwards, because of plastic relaxation in the physical gel (dissociation and reformation of triple helices). At higher shear rates, there is no such relaxation and the response is purely elastic. In this case, we see that before failure the stress deviates slightly upwards, indicating that the network undergoes weak strain hardening. This strain hardening is probably related to the finite extensibility of the bridging middle blocks. As shown in Figure 6.3, strain hardening is also observed in oscillatory shear experiments with increasing strain amplitude. For a protein concentration of 0.96 mM, the modulus increases by about 15 % with increasing strain before the gel ruptures. At a protein concentration of 2 mM no strain hardening is observed. Probably the regime of strain hardening could not be reached at these higher concentrations, because these gels break already at much smaller strains. For our system, network stiffening is much weaker than for gels formed by gelatin [17], silk/collagen-like block polymers [18] or by classical associative

telechelics [6], where the storage modulus increases by as much as a factor 2-5 before fracture occurs. This difference may be due to the fact that we have very long, flexible middle blocks and relatively short node-forming end blocks. This could reduce considerably the non-linear force extension relation due to finite chain extensibility.

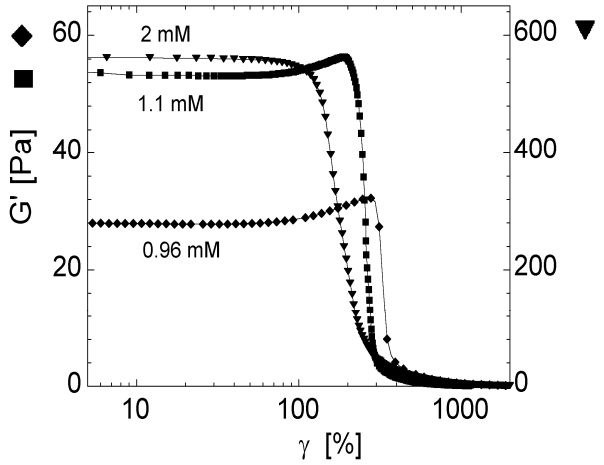


Figure 6.3 Storage modulus as a function of strain amplitude in an oscillatory shear experiments at a frequency of 6.28 rad/s. Data for 0.96 and 1.1 mM refer to the left axis, those for 2 mM to the right axis.

***Fractured flow at steady state***

After the transient stress response upon start-up of shear flow, the stress finally reaches a steady-state (Figure 6.2). This steady-state stress is plotted as a function of the applied shear rate in Figure 6.4 for three different TR4T concentrations at 20 °C (we refer to these plots as "flow curves").

In order to compare gels formed at different protein concentrations, the data from Figure 6.4A were rescaled by plotting the dimensionless stress $\sigma/G_0$ versus the reduced shear rate $\dot{\gamma}\cdot\tau$ (Figure 6.4B), with $G_0$ and $\tau$ as given in Table 6.1. Along the flow curves several regimes can be observed. At low shear rates, $\dot{\gamma}\cdot\tau<1$, the shear stress increases linearly with the shear rate. The system behaves like a Newtonian liquid with constant zero-shear viscosity. This region was explored in more in Chapter 3. For $\dot{\gamma}\cdot\tau$ larger than 1, the flow curves are non-monotonic: the steady-state stress first decreases with increasing shear rate and then increases again at higher shear rates. This non-monotonic loop indicates a flow instability with an associated change in structure [6, 19]. As discussed above, the transient stress response in this regime is characterized by a large overshoot (Figure 6.2).

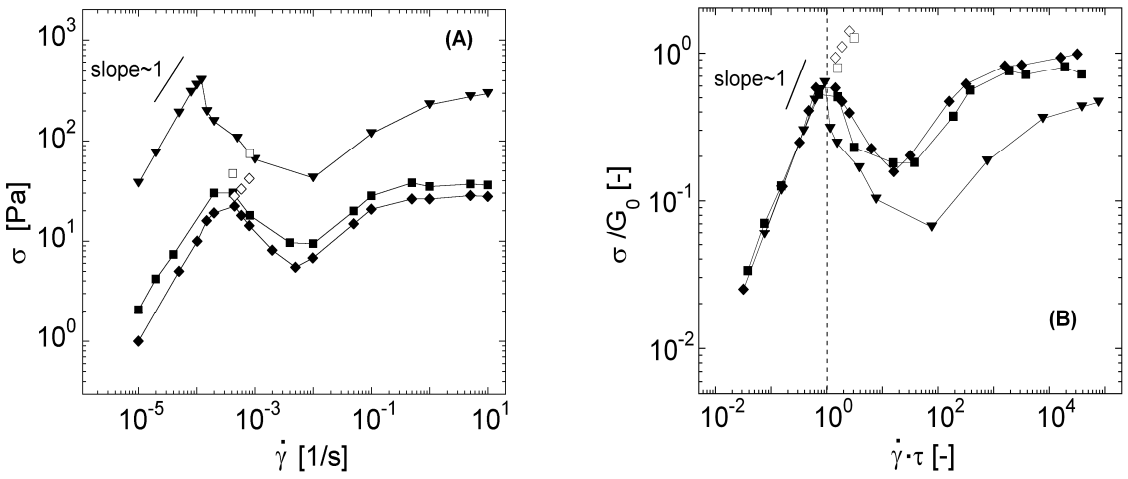


Figure 6.4 Steady-state flow curves at controlled shear rate for different protein concentrations: (◆) 0.96 mM, (■) 1.1 mM, and (▼) 2 mM. Open symbols denote metastable values. (A) Steady-state shear stress as a function of shear rate. (B) Reduced steady-state shear stress ($\sigma/G_0$) versus reduced shear rate ($\dot{\gamma}\cdot\tau$) with $G_0$ and $\tau$ indicated in Table 6.1.

To examine the nature of the failure that occurs at high deformation rates, we measured the velocity profiles in the Couette cell using particle image velocimetry (PIV). In Figure 6.5A, we present snap shots of the velocity field at the steady-state for several applied shear rates.

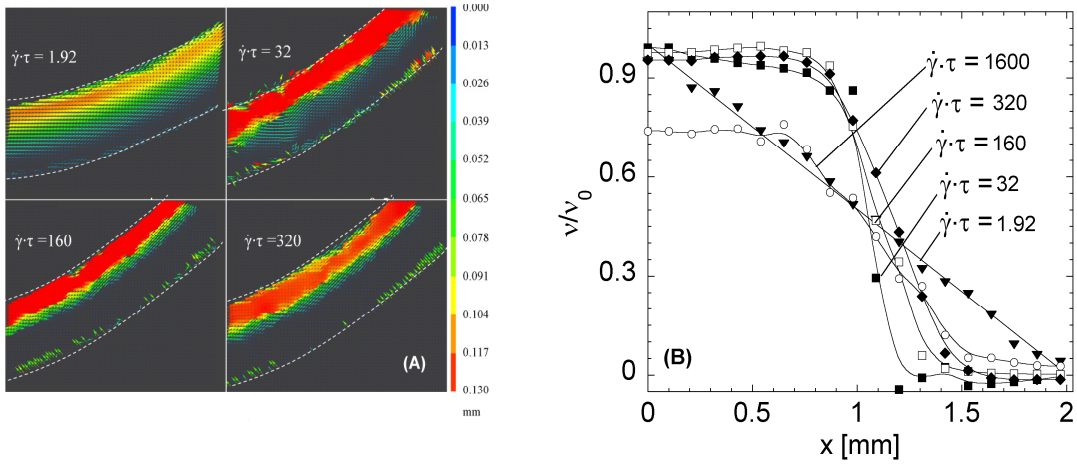


Figure 6.5 (A) Snap shots of the velocity vector field at the steady-state for several applied shear rates (as indicated) for protein concentration 0.96 mM. The colour scale indicates the displacement (in mm) of tracked particles between two frames. Time interval between frames: 100 s for $\dot{\gamma}\cdot\tau$=1.92; 7 s for $\dot{\gamma}\cdot\tau$=32; 1.4 s for $\dot{\gamma}\cdot\tau$=160; and 0.6 s for $\dot{\gamma}\cdot\tau$=320. (B) Calculated velocity profiles (v(x)) normalized by velocity of the wall ($v_0$).

At low shear rates, $\dot{\gamma}\cdot\tau$~1, the velocity profile is homogeneous: the velocity decreases linearly from the inner, rotating wall to the outer, stationary wall. At higher shear rates however, the velocity profile is strongly non-linear. The gel is broken into two parts: one part close to the moving wall that moves with almost constant velocity and one part at the stationary wall, which is not moving at all. In the region between these two phases, the local shear rate is very high. This region is a fracture zone, where all, or most, of the crosslinks are ruptured. It can be seen in Figure 6.5 that this fracture zone has an irregular shape and is rather wide, on the order of a few hundred microns, which is much wider than the average distance between crosslinks (which is on the order of several nm). This was also observed by Berret and Serero in a similar system of telechelic polymers [6]. It indicates that some fluidization occurs in the region where the two gel phases slide past each other. With increasing overall shear rate, the width of the fracture zone increases. The stress in this region, which dominates the macroscopically measured stress, is due to viscous dissipation in the fluidized zone and elastic stresses that arise due to mutual movement of the irregular fracture surfaces. With increasing shear rate, the apparent viscosity decreases, which may indicate that the fracture surfaces become smoother or that the gel locally breaks in smaller fragments.

Note that the position of the fracture zone in the gap is different for every experiment. However, we have never observed it near one of the two walls of the Couette cell (which would result in wall slip). This indicates that the polymer sticks strongly to the Couette wall. Only at very high shear rates (*e.g.* for $\dot{\gamma}\cdot\tau$=1600 in Figure 6.5B) we observe some slip at the inner cylinder after the gel has fractured. Before fracture this slip is absent. The position of the fracture zone remains stable for at least 3 hours.

***Fracture at constant applied stress***

Another approach to study the failure of gels is to apply a constant stress and follow the resulting deformation as a function of time (Figure 6.6). For stresses that are smaller than the elastic modulus $G_0$, the gel creeps homogeneously (Chapter 3). For larger stresses, however, fracture occurs, leading to an inhomogeneous velocity profile with a very high apparent (overall) shear rate. If the applied stress is much larger than the elastic modulus $G_0$, the network fractures almost immediately after applying the load. A different situation is observed for stresses not too far above $G_0$. In this case, fracture does not occur immediately, but is delayed. Moreover, the delay time is not constant but varies significantly from one experiment to another, suggesting a stochastic fracture mechanism. Figure 6.7 shows the time

before fracture ($t_b$) as a function of the applied stress. With increasing stress, the average delay time decreases rapidly.

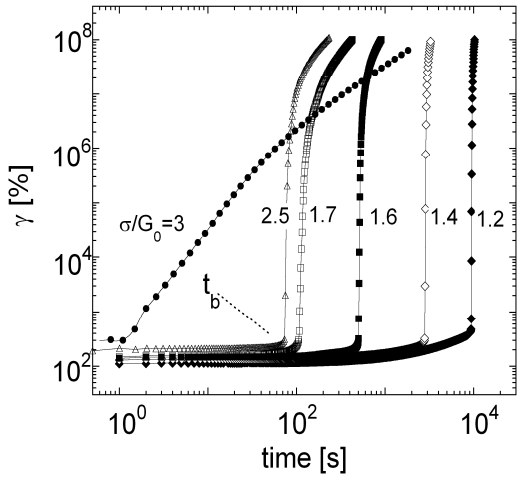


Figure 6.6 Delayed fracture of a 1.1 mM network at different applied stresses. Initially, the sample responds elastically to the deformation ($\gamma \sim \sigma/G_0$), but after a lag time $t_b$, which varies from one experiment to another, the gel breaks, leading to a very rapid increase of the overall strain.

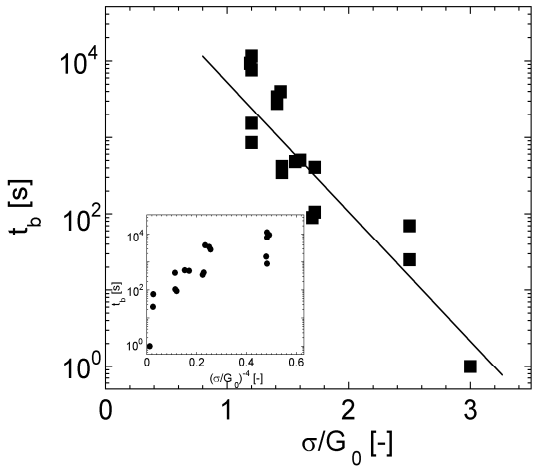


Figure 6.7 Breaking time ($t_b$) as a function of the applied stress ($\sigma/G_0$). Inset shows data plotted as $t_b$ versus $\sigma^{-4}$.

Delayed fracture has been observed before for soft rubbers, glassy materials, and associative polymer networks [8, 12, 20]. It has been explained using a crack nucleation model proposed by Pomeau [21]. Essentially, this model is based on Griffith's theory for brittle fracture, which compares the elastic energy released upon crack nucleation to the cohesive energy in the gel [22]. This theory predicts a critical size, at which cracks start to grow catastrophically for a given stress. Smaller cracks are stable and do not grow. It was

proposed by Pomeau that the crack nucleation time corresponds to the time needed for a crack of this critical size to appear. Associated with this is an energy barrier, which decreases very strongly with the applied stress: $U_a \sim 1/\sigma^4$, so that the rupture time is expected to decrease as $t_b \sim \exp(\text{const}/\sigma^4)$ [8, 12, 20]. Our data in Figure 6.7 cannot be fitted by such a relation, however (see inset in Figure 6.7), suggesting that this crack nucleation picture does not apply to our system. This is furthermore confirmed by our observation that the critical shear stress depends on the applied shear rate (see Figure 6.2). This cannot be explained by the Griffith theory. It should be kept in mind, however, that the Griffith theory is based on equilibrium considerations, so that it is not clear that it can be applied to dynamic fracture [23]. An alternative approach to describe the dynamics of fracture of polymeric materials is based on activated bond rupture [14]. When a constant stress is applied to the gel, the triple helical nodes in the gel experience a force *f* pulling on them. As predicted by Kramers [15, 24], this leads to an enhanced dissociation rate:

$$k_D' = k_D \cdot \exp\left[\frac{f \cdot \delta}{kT}\right] \qquad \text{(Eq. 6.1)}$$

where $k_D$ is the rate, at which elastically active chains relax in the absence of force (equal to $1/\tau$ with $\tau$ the linear relaxation time) and $\delta$ is a length that characterizes the width of the bond potential. It is on the order of the length of the junction, 9 nm, so that the typical force scale $k \cdot T/\delta$ is on the order of a few pN.

Due to the presence of defects (small pre-existing cracks) in the network, originating from thermal density fluctuations, the stress is not homogeneous throughout the material. The stress is concentrated near the tip of a pre-existing crack, so that crosslinks just ahead of such a crack experience the highest force and therefore the highest dissociation rate. This leads to steady-state, stress-enhanced propagation of such cracks ("subcritical crack growth"). Once a crack reaches the critical crack size (the so-called Griffith length), catastrophic fracture follows. This model thus predicts a rupture time, which decreases exponentially with increasing stress [25, 26]:

$$t_b \sim 1/k_D' \sim \exp\left[-\Omega \cdot \sigma\right] \qquad \text{(Eq. 6.2)}$$

where the factor $\Omega$ incorporates the factor $\delta/k \cdot T$, but also takes into account the stress concentration near the pre-existing cracks. As shown in Figure 6.7, the exponential decrease

of $t_b$ with increasing stress agrees well with our data, with $\Omega \approx 3.75/G_0$. The large scatter in the experimentally determined rupture times reflects the stochastic nature of this process.

***Shear rate-dependence of rupture***

Above, we considered dissociation kinetics under a constant applied force. In order to describe fracture at constant shear rate, we need to account for the fact that the deformation increases linearly with time. Such a description of bond rupture kinetics has been presented by Evans for single bonds [15] and for adhesive rupture by Chaudhury *et al.* [14]. Here, we follow their approach to describe cohesive failure inside the gel. Assuming affine deformation, each bridging chain in the network is stretched by the shear flow at a speed $\xi \cdot \dot{\gamma}$, where $\xi$ is the typical distance between junctions in the network. Treating the bridging chains as Gaussian chains with spring constant $k \cdot T/\xi^2$, we find that the force acting on a sheared crosslink increases as $f(t)=K(k \cdot T/\xi)\dot{\gamma} \cdot t$ (here, we assume that initially, before the shear is started, the force is zero). The factor K accounts for local stress intensification that occurs in the vicinity of the crack tip. Substituting this time-dependent (transient) force into equation 6.1, we find that the bond dissociation rate increases exponentially with time. The survival probability of a bond P(t) can then be written as [15]:

$$P(t) = \exp\left\{-\int_0^t k_D'\left[f(t)\right]dt\right\} = \exp\left\{\frac{\xi}{K \cdot \delta \cdot \dot{\gamma} \cdot \tau} \cdot \left[1 - \exp\left(\frac{K \cdot \delta \cdot \dot{\gamma} \cdot t}{\xi}\right)\right]\right\} \qquad \text{(Eq. 6.3)}$$

where $\tau = 1/k_D$ is the linear relaxation time.

The average lifetime of a crosslink can be obtained from this as:

$$<\tau_0'> = \int_0^\infty P(t)\,dt \approx \begin{cases} \tau \cdot \left(1 - \frac{K \cdot \delta \cdot \dot{\gamma} \cdot \tau}{\xi}\right) \left(if\ \dot{\gamma} \cdot \tau << \frac{\xi}{K \cdot \delta}\right) \\ \frac{\xi}{K \cdot \delta \cdot \dot{\gamma}} \ln\left(\frac{K \cdot \delta \cdot \dot{\gamma} \cdot \tau}{\xi}\right) \left(if\ \dot{\gamma} \cdot \tau >> \frac{\xi}{K \cdot \delta}\right) \end{cases} \qquad \text{(Eq. 6.4)}$$

In the high shear rate regime ($\dot{\gamma} \cdot \tau >> 1$), reformation of crosslinks can be neglected. It follows that the gel will undergo a catastrophic rupture after a time $t_b' \approx <\tau_0'>$. The critical strain at rupture follows as:

$$\gamma_c = \dot{\gamma} \cdot t_b' \approx \frac{\xi}{K \cdot \delta} \ln\left[\frac{K \cdot \delta \cdot \dot{\gamma} \cdot \tau}{\xi}\right] \qquad \text{(Eq. 6.5)}$$

Hence, the critical strain is predicted to increase logarithmically with increasing shear rate. For $\dot{\gamma} \cdot \tau >> 1$ the stress-strain relation is approximately linear (neglecting the weak strain hardening), so that $\sigma_c/G_0 \approx \gamma_c$ should also increase proportionally to $\ln \dot{\gamma}$. Figure 6.8A shows the critical strain $\gamma_c$ as a function of $\dot{\gamma} \cdot \tau$ for three different concentrations. Indeed, for $\dot{\gamma} \cdot \tau > 1$, the critical strain increases logarithmically with increasing shear rate.

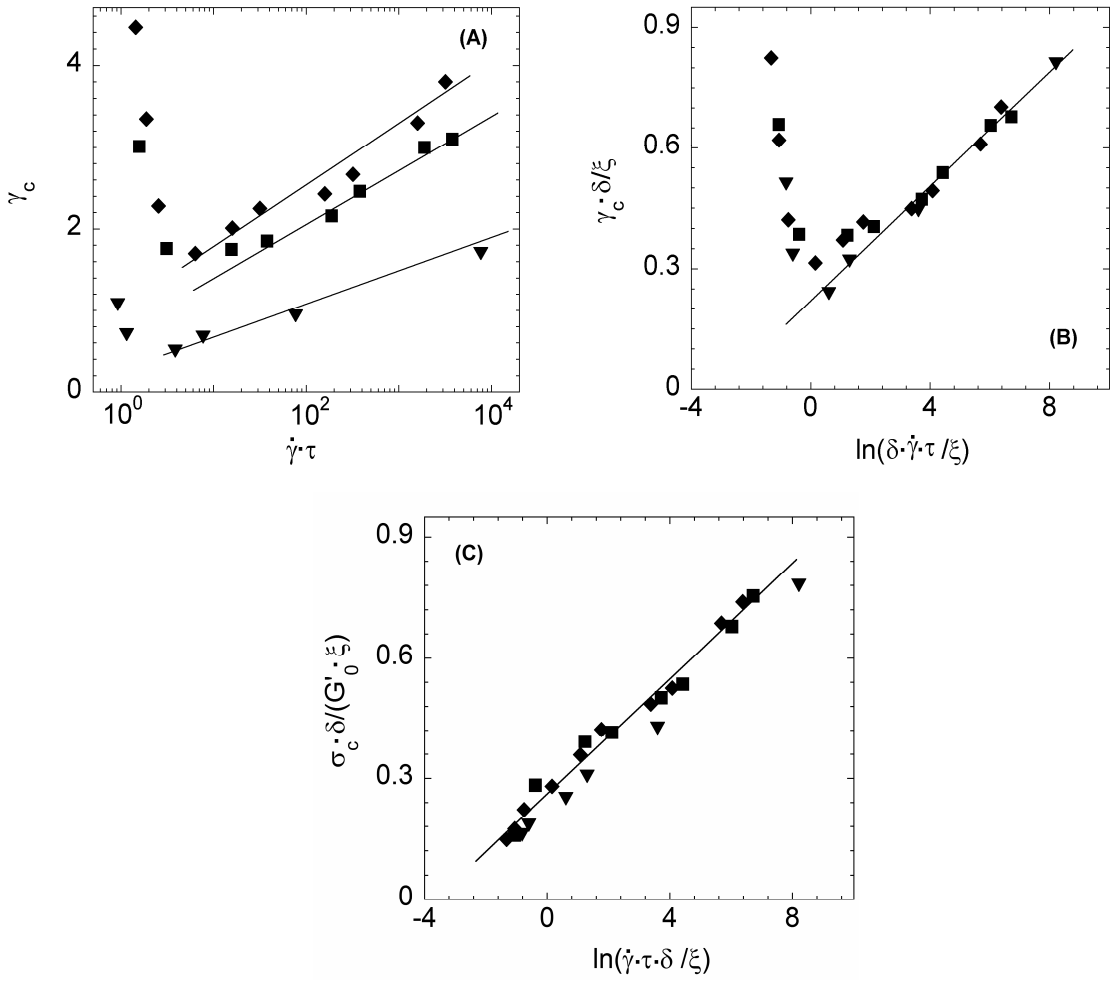


Figure 6.8 (A) Critical strain as a function of shear rate for different protein concentrations. (B) Normalized critical strain as a function of shear rate plotted in the form of Equation 6.5. (C) Same for critical stress. Protein concentrations: (◆) 0.96 mM, (■) 1.1 mM and (▼) 2 mM.

We now make a more quantitative comparison between experiment and model. As we have shown in Chapter 3, the values of $G_0$, $\xi$, and $\tau$ depend on the protein concentration (see also Table 6.1). At low concentrations the network contains many loops and relatively few

bridges. Most of these active bridges consist of more than one molecule, so-called superchains [5]. As a result, the modulus $G_0$ is low and the typical distance between junctions is large. We estimate the distance $\xi$ between junctions from the modulus, using: $G_0 \approx kT/\xi^3$. With increasing concentration it decreases from approximately 50 nm at 0.96 mM to 20 nm at 2 mM. For the value of $\delta$, we take the length of a triple helical junction, 9 nm. To test equation 6.5 we have plotted $\gamma_c \cdot \delta/\xi$ and $(\sigma_c \cdot \delta/(G_0 \cdot \xi)$ as a function of $\ln(\delta \cdot \dot{\gamma} \cdot \tau/\xi)$ in Figure 6.8B and C. Indeed, all curves are found to superimpose, and both the critical strain and the critical stress are increasing linearly with the logarithm of the shear rate at sufficiently high deformation rates. Hence, the experimental data are in very good agreement with the model, showing that gel fracture is indeed consistent with a stress-enhanced bond rupture process. From a fit to equation 6.5 we find $K \approx 35$, indicating significant stress intensification. At low shear rates ($\dot{\gamma} \cdot \tau$ only slightly above unity), deviations from linearity can be observed in Figure 6.8A and B. The reason for this is that, at these low shear rates, the network can heal by reformation of triple helices and undergo plastic deformation prior to fracture. This can also be seen in Figure 6.2 for $\dot{\gamma} \cdot \tau = 1.92$, where the stress first remains at a metastable value for some time, before fracture occurs. For $\dot{\gamma} \cdot \tau < 1$, no fracture is observed so that the critical strain diverges

***Self-Healing***

Contrary to covalently crosslinked gels, physical gels with a finite viscoelastic relaxation time can heal after the deformation is stopped. Figure 6.9 shows the recovery of the elastic properties after fracturing it by applying a constant shear rate (A) or shear stress (B). The system can recover up to 100 % of its initial elastic properties, even after several fracturing cycles (Figure 6.9C). Not only is the storage modulus recovered, but also the fracture strength. After healing the gel can be strained to the same maximum strain and stress (Figure 6.9D). We compare the kinetics of healing after rupture to the kinetics of gel formation upon cooling, which we investigated in detail in Chapter 5. The latter is characterized by a lag phase before elastic properties start to appear (see Figure 6.9A-C). This lag phase is consistent with the fact that at least 50-60 % of the end blocks should be involved in elastically active junctions [27] before a percolated network appears. Until that point, the storage modulus is almost undetectable.

In the curves that show the recovery after fracture, no such lag phase is observed and the storage modulus comes back to its original plateau value within ~1 hour after shearing or ~5 hours after applying stress. This is much faster than the initial gel formation upon cooling.

This indicates that outside the fracture zone, the junctions have not appreciably dissociated during the fracture processes. Healing then only requires the reformation of junctions that connect the undamaged pieces of network (gel clusters). Also, the formation of loops may be less likely in the fracture zone, because the second end of the same molecule is probably already connected to a floating piece of gel. Consequently, reformation of the same amount of triple helices leads to a more effective increase of the elastic properties.

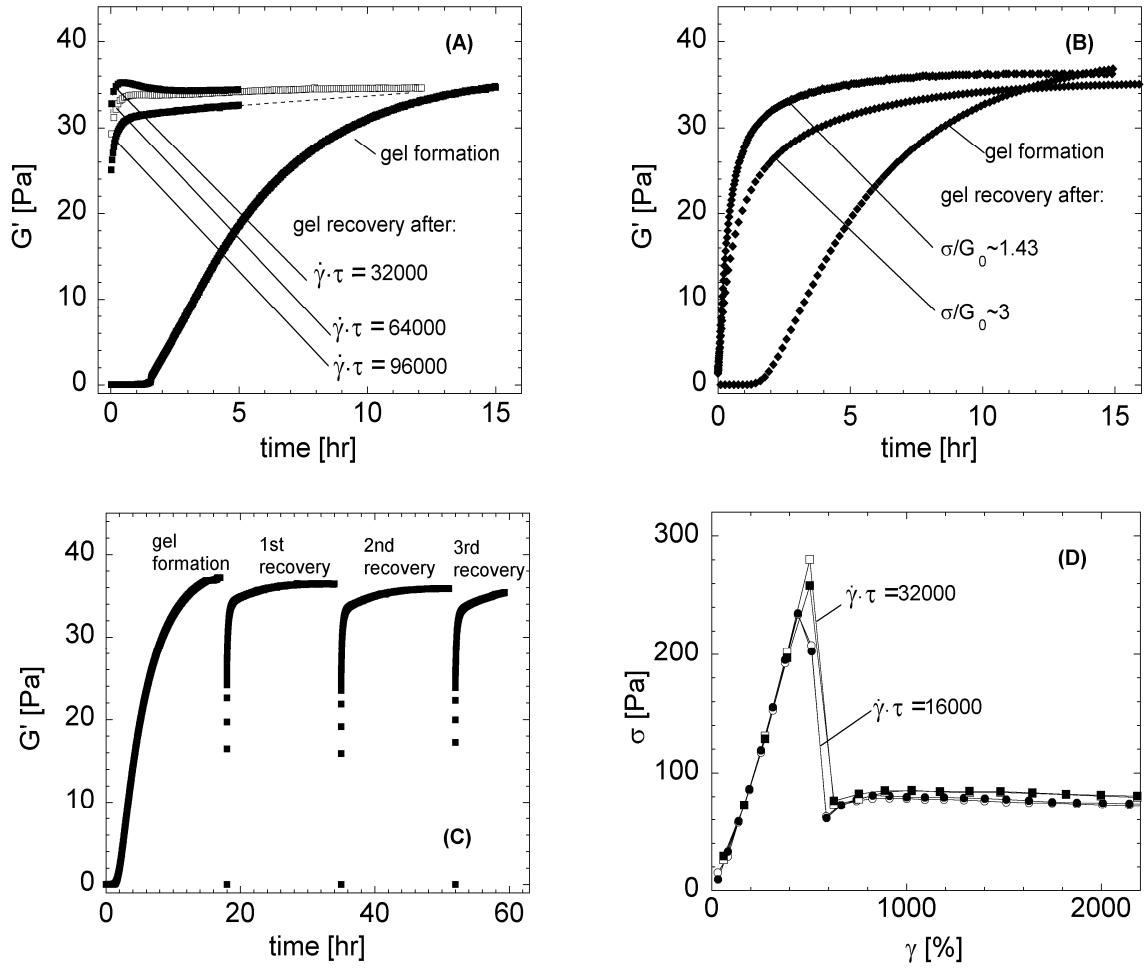


Figure 6.9 Healing of 0.96 mM gel after different fracture histories: (A) Storage modulus recovery after 1 hour of shearing with different shear rates (as indicated). (B) Recovery after applying stress of 50 Pa and 105 Pa for half an hour. (C) Multiple fracture-recovery cycles (with $\dot{\gamma}\cdot\tau$=96000). (D) Recovery of the fracture strength after fracture and healing for two shear rates. Filled symbols: before fracture; open symbols: after fracture followed by self-healing.

The rate of recovery $(dG'/dt)_0$ during healing depends on the applied deformation history. When the gel is fractured at a higher applied shear rate or stress, the recovery is slower (Figure 6.9A and B). As shown in Figure 6.5B, higher shear rates result in a wider fracture zone, which requires more time to heal.

## 6.4 Concluding remarks

In this chapter we have investigated the failure of physical networks formed by collagen-inspired telechelic polypeptides with well-defined node multiplicity. When a constant shear rate or shear stress is applied to these physical gels, the system undergoes a macroscopic fracture. This instability could be observed with PIV. The kinetics of fracture strongly suggests that gel fracture is due to stress-activated rupture of triple helical nodes in the network. When the applied stress or shear rate is taken away, the network recovers completely. The kinetics of this self-healing is much faster than the initial sol-gel transition upon cooling of a protein solution.

A similar shear-induced fracture has been observed in other transient polymer networks, formed by telechelic polymers with hydrophobic associating groups [7, 8]. In these systems, the critical strain, at which the gel ruptures was found not to depend on the applied shear rate [7], although the range of applied shear rates was not as large as in the present study. The critical rupture stress in these systems could be estimated using a quasi-static fracture model, based on classical Griffith theory. By contrast, our measurements do show a shear rate-dependence of the critical rupture strain. This cannot be explained with the static Griffith model and strongly suggests a dynamic fracture process that is governed by stress-activated bond rupture. We have no explanation for the different behaviours found in these transient networks. Possibly, the much longer relaxation time of our triple helix-based networks leads to more solid-like behaviour. We note that a similar shear rate dependence was found in coarse-grained Brownian dynamics simulations on failure in transient polymer networks [9].

## References


[1] Q. Wang, J.L. Mynar, M. Yoshida, E. Lee, M. Lee, K. Okuro, K. Kinbara, T. Aida, High-water-content mouldable hydrogels by mixing clay and a dendritic molecular binder. Nature 463(7279) (2010) 339-343.

[2] M. Sutter, J. Siepmann, W.E. Hennink, W. Jiskoot, Recombinant gelatin hydrogels for the sustained release of proteins. Journal of Controlled Release 119(3) (2007) 301-312.

[3] J. Kim, S.S. Kim, K.H. Kim, Y.H. Jin, S.M. Hong, S.S. Hwang, B.G. Cho, D.Y. Shin, S.S. Im, Applications of telechelic polymers as compatibilizers and stabilizers in polymer blends and inorganic/organic nanohybrids. Polymer 45(10) (2004) 3527-3533.

[4] B.S. Kim, D.J. Mooney, Engineering smooth muscle tissue with a predefined structure. Journal of Biomedical Materials Research 41(2) (1998) 322-332.

[5] P.J. Skrzeszewska, F.A. de Wolf, M.W.T. Werten, A.P.H.A. Moers, M.A. Cohen Stuart, J. van der Gucht, Physical gels of telechelic triblock copolymers with precisely defined junction multiplicity. Soft Matter 5(10) (2009) 2057-2062.

[6] J.F. Berret, Y. Sereo, B. Winkelman, D. Calvet, A. Collet, M. Viguier, Nonlinear rheology of telechelic polymer networks. Journal of Rheology 45(2) (2001) 477-492.

[7] J.F. Berret, Y. Serero, Evidence of shear-induced fluid fracture in telechelic polymer networks. Physical Review Letters 87(4) (2001) 048301-048304.

[8] H. Tabuteau, S. Mora, G. Porte, M. Abkarian, C. Ligoure, Microscopic Mechanisms of the Brittleness of Viscoelastic Fluids. Physical Review Letters 102(15) (2009).

[9] J. Sprakel, E. Spruijt, J. van der Gucht, J.T. Padding, W.J. Briels, Failure-mode transition in transient polymer networks with particle-based simulations. Soft Matter 5(23) (2009) 4748-4756.

[10] T. Baumberger, C. Caroli, D. Martina, Fracture of a biopolymer gel as a viscoplastic disentanglement process. European Physical Journal E 21(1) (2006) 81-89.

[11] T. Baumberger, O. Ronsin, From thermally activated to viscosity controlled fracture of biopolymer hydrogels. Journal of Chemical Physics 130(6) (2009).

[12] D. Bonn, H. Kellay, M. Prochnow, K. Ben-Djemiaa, J. Meunier, Delayed fracture of an inhomogeneous soft solid. Science 280(5361) (1998) 265-267.

[13] M.W.T. Werten, H. Teles, A. Moers, E.J.H. Wolbert, J. Sprakel, G. Eggink, F.A. de Wolf, Precision Gels from Collagen-Inspired Triblock Copolymers. Biomacromolecules 10(5) (2009) 1106-1113.

[14] M.K. Chaudhury, Rate-dependent fracture at adhesive interface. Journal of Physical Chemistry B 103(31) (1999) 6562-6566.

[15] E. Evans, K. Ritchie, Dynamic strength of molecular adhesion bonds. Biophysical Journal 72(4) (1997) 1541-1555.

[16] http://www.jpiv.vennemann-online.de/download.html.

[17] A. Bot, I.A. van Amerongen, R.D. Groot, N.L. Hoekstra, W.G.M. Agterof, Large deformation rheology of gelatin gels. Polymer Gels and Networks 4(3) (1996) 189-227.

[18] A.A. Martens, J. van der Gucht, G. Eggink, F.A. de Wolf, M.A.C. Stuart, Dilute gels with exceptional rigidity from self-assembling silk-collagen-like block copolymers. Soft Matter 5(21) (2009) 4191-4197.

[19] J. Sprakel, E. Spruijt, M.A.C. Stuart, N.A.M. Besseling, M.P. Lettinga, J. van der Gucht, Shear banding and rheochaos in associative polymer networks. Soft Matter 4(8) (2008) 1696-1705.

[20] N. Shahidzadeh-Bonn, P. Vie, X. Chateau, J.N. Roux, D. Bonn, Delayed fracture in porous media. Physical Review Letters 95(17) (2005).

[21] Y. Pomeau, Spontaneous breaking of 2-dimensional bent crystals. Comptes Rendus De L Academie Des Sciences Serie II 314(6) (1992) 553-556.

[22] A.A. Griffith, The Phenomena of Rupture and Flow in Solids. Philosophical Transactions of Royal Society A 221(221) (1921) 163-198.

[23] Y. Gan, Comment on "Delayed fracture in porous media". Physical Review Letters 96(25) (2006).

[24] H.A. Kramers, Brownian motion in a field of force and the diffusion model of chemical reactions. Physica 7(7) (1940) 284-304.

[25] S.N. Zhurkov, Kinetic concept of the strength of solids. International Journal of Fracture 26(4) (1984) 295-307.

[26] S. Santucci, L. Vanel, S. Ciliberto, Slow crack growth: Models and experiments. European Physical Journal-Special Topics 146 (2007) 341-356.

[27] P.J. Skrzeszewska, F.A. de Wolf, M.A. Cohen Stuart, J. van der Gucht, Kinetics of network formation by telechelic polypeptides with trimeric nodes. Soft Matter 6(2) (2010) 416-422.

# Chapter 7

# Shape-memory effects in biopolymer networks with collagen-like transient nodes

*Abstract*

In this chapter we study shape-memory behaviour of hydrogels, formed by biodegradable and biocompatible recombinant telechelic polypeptides, with collagen-like end blocks and a random coil-like middle block. The programmed shape of these hydrogels is achieved by chemical crosslinking of lysine residues present in the random coil. The chemical network can be stretched up to 200 % and "pinned" in a temporary shape by lowering the temperature and allowing the collagen-like end blocks to assemble into physical nodes. The deformed shape of the hydrogel can be maintained, at room temperature, for several days, or relaxed within a few minutes upon heating to 50 ºC or higher. The presented hydrogels could return to their programmed shape even after several thermo-mechanical cycles, indicating that they remember the programmed shape. The kinetics of shape recovery at different temperatures is studied in more detail and analyzed using a mechanical model composed of two springs and a dashpot.

Submitted in modified form for publication: P.J. Skrzeszewska, L.N. Jong, F.A. de Wolf, M.A. Cohen Stuart and J. van der Gucht, Shape-memory effects in biopolymer networks with collagen-like transient nodes.

## 7.1 Introduction

Shape-memory materials (SMMs) are stimuli responsive systems that can change their shape upon a change in external conditions such as pH or temperature [1-3]. They have many biomedical or sensory applications [4-6]. They can be used as smart medical devices, implants for minimally invasive surgery or heat-shrinking tubing and films [7]. Although the shape memory effect was observed already in the beginning of the 1950s, it was not fully appreciated until the nickel-titanium alloy Nitinol was discovered in 1963. For the next decades Nitinol has been extensively studied, and nowadays it is a commonly used commercial shape-memory alloy [8]. Twenty years later, shape-memory polymers were introduced [9]. Above its glass transition temperature ($T_g$), a polymeric material is in a rubbery state and can be easily deformed. It can be frozen in a temporary state by deforming it and cooling below $T_g$. The deformed state is maintained until the temperature is raised above $T_g$ again, after which the material returns to its initial shape. Most polymers, however, do not completely restore their elastic properties. By contrast, shape-memory polymers can recover almost 100 % of the deformation. They typically have a phase-segregated morphology, consisting of soft (switchable) and hard domains [9]. When cooled under deformation, the crystallization of the soft domains fixes the material in its temporary shape. Upon reheating the crystalline domains melt and the system recovers the programmed shape. Very well-known shape-memory polymers are polyurethane multiblock copolymers [10]. Their properties and the transition temperature can be tuned by changing the ratio between the soft and the hard domains. The higher the fraction of hard domains, the more difficult the crystallization of the soft domains and the lower the melting temperature [10]. Shape-memory behaviour is also observed for some hydrogels. This group of materials is of particular interest for biomedical applications, because they are soft and filled with water, which makes them more compatible with biological tissues [11]. An example of shape-memory hydrogels are networks formed by linear poly(vinyl alcohol) [12]. Poly(vinyl alcohol) forms physical hydrogels below 50 °C with transient nodes created through hydrogen bonding and crystallization. In order to make the system stable above this temperature the network is permanently crosslinked with glutaraldehyde. The chemical gel can be stretched up to 200 % and “pinned” in a temporary shape by immersing the sample in a poor solvent, deswelling and formation of the physical nodes. The programmed shape can be recovered by exposing the gel to boiling water [12]. Another shape memory hydrogel has been reported by Li *et al*. [13], composed of lightly crosslinked telechelic oligomers functionalized with ureidopyrimidinone

(UPy) side groups [13]. The Upy groups consist of a linear array of four H-bonding sites that can strongly associate into reversible nodes and maintain the gel in a temporary shape.

In this chapter we present shape memory effects in hydrogels that employ collagen-like triple helical assemblies to "pin" the temporary shape of a lightly, chemically crosslinked polymer network. The permanent network is composed of chemically crosslinked monodispersed, biodegradable and biocompatible telechelic polypeptides (abbreviated as TR4T) with a random coil-like middle block and collagen-like end blocks composed of nine amino acid triplets Pro-Gly-Pro. Upon cooling, these end blocks assemble into triple helical nodes [14-16]. The permanent shape is achieved by adding a crosslinking agent (glutaraldehyde) that connects lysine residues present in the middle block [17]. When cooled down under applied deformation, the formation of the triple helices fixes the material in its temporary shape (Figure 7.1). Once the system is exposed to a temperature, above which the triple helices melt (~45 ºC), it can return to its original, programmed, shape (Figure 7.1).

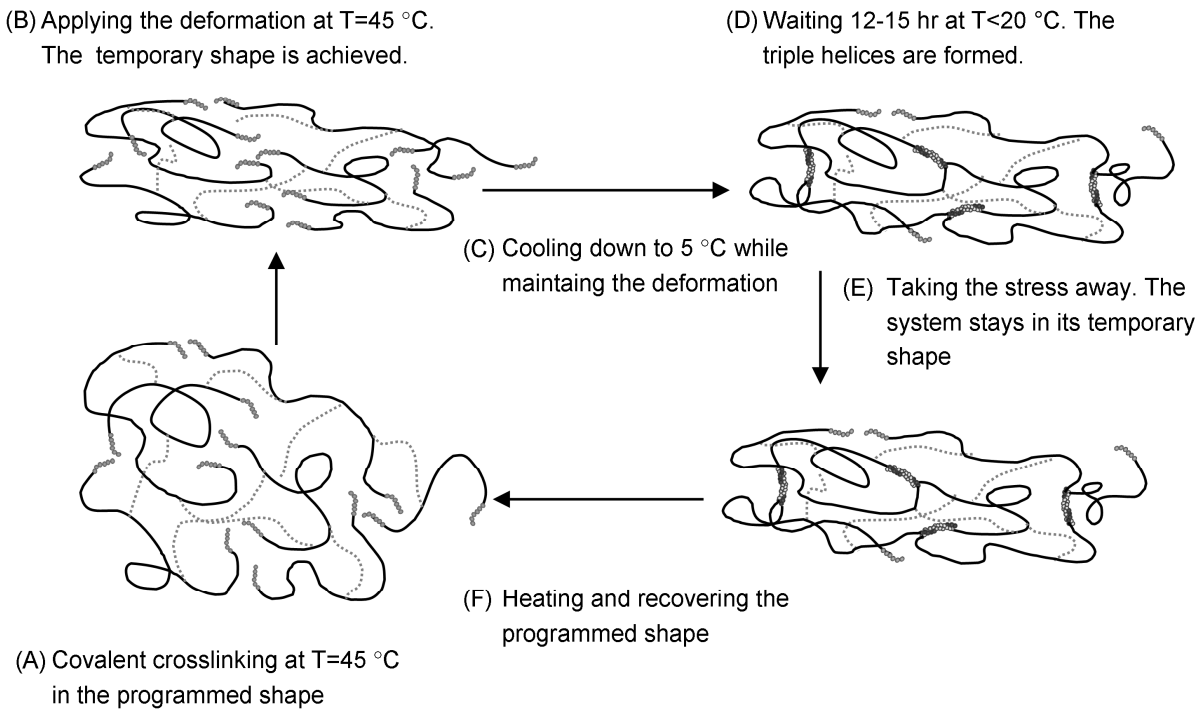


Figure 7.1 Schematic presentation of the shape-memory cycle.

We have tested several hydrogels, formed at various concentrations of TR4T and crosslinked with various concentrations of crosslinker. By carrying out thermo-mechanical cycles, as shown in Figure 7.1, we characterized the extent to which the physical bonds can

maintain these gels in a deformed state. The rate at which the gels return to their permanent shape was studied for different temperatures.

## 7.2 Materials and methods

***Recombinant telechelic protein***

The construction of genes encoding TR4T protein with molecular weight of ~42 kDa, its transfection to the host organisms (the yeast *Pichia pastoris*), the production and the purification of the protein polymer have been described in Chapter 2 and reference [18] The protein comprises three blocks. The end blocks, abbreviated as T (trimer-forming), consist of nine consecutive Pro-Gly-Pro triplets [18]. Upon cooling the T domains form collagen-like triple helices. The middle block R4 (399 amino acids) has a sequence that does not lead to any secondary or tertiary structure; it assumes a random coil configuration at any temperature. The middle block comprises 12 lysine residues that can be crosslinked with glutaraldehyde in order to form a lightly crosslinked chemical gel. The complete amino acid sequence of the molecule has been deposited in GenBank under accession number ACF33479.

***Shape memory cycles***

The shape-memory cycles were carried out using an Anton Paar, Physica MCR 301 rheometer equipped with Couette geometry (CC10) with an outer diameter of 10.84 mm and a bob size of 10 mm. The temperature was controlled by a Peltier system, which allowed fast heating and cooling. Four different concentrations of the protein were tested (together with different amounts of crosslinker (glutaraldehyde (GA)). Final protein concentrations after adding GA were 1.4, 1.9, 2.4 and 2.86 mM. All samples were prepared in the same way. A given amount of the protein was dissolved in phosphate buffer (pH=7, I=10 mM) and then heated at 50 °C for half an hour, allowing the protein to dissolve completely under conditions where end blocks did not form triple helices. Subsequently, 8.4 or 16.8 moles of crosslinker per mole of protein were added. After short vigorous mixing, the solution of polymer and the crosslinker was immediately transferred into the preheated rheometer. After lowering the bob, the system was held at 45 °C (above the melting temperature of the triple helices) for 6 hours, during which the chemical gel was formed. During the last hour of this step the storage and loss moduli of the permanent network were measured. The degree of chemical bonding depended on the amount of TR4T polypeptide and the amount of glutaraldehyde. When the storage modulus reached a plateau, the gel was subjected to the shape-memory cycles. Before each cycle the sample was equilibrated at 45 °C for 30-60 minutes without any load. After

that a shear strain was applied (20 and 60 %). The strain values were chosen not to go beyond the linear regime. After 30 minutes of holding the deformation at 45 °C, the temperature was lowered either to 20 °C or stepwise to 5 °C. The system was kept deformed at low temperature for 15 hours (either 15 hours at 20 °C or 6 hours at 20 ºC, 2 hours at 15 ºC, 2 hours at 10 ºC and 5 hours at 5 ºC). During this time the T blocks assembled into triple helices, and the temporary (strained) shape of the gel was fixed. Once the physical network was formed the load was taken away. The immediate response was monitored at 5 and 20 °C, for 1-10 hours. Then the network was heated up to 25, 30, 40, 45, 50 or 60 °C and the strain recovery was observed for the next 1.5-10 hours. For each sample 5-6 thermo-mechanical cycles were performed. After each cycle the storage modulus of the chemical network was checked at 45 ºC.

***Visualization of shape memory behavior***

In order to visualize the shape-memory effect of the hydrogels, we prepared a cylindrical piece of gel by crosslinking a 4.8 mM TR4T solution with 8.4 moles of glutaraldehyde per mole of protein. The chemical crosslinking was performed at 50 °C for 6 hours. During this time we observed that the hydrogel colour changed from transparent through yellow to very dark brown. Similar colouring has been observed before for many proteins crosslinked with glutaraldehyde [17, 19]. As shown by Hopwood *et al.* [17] the depth of colour (thus absorbance) increases with crosslinks density. As suggested by Tramezzani *et al.* the yellow compound is a Schiff base formed between glutaraldehyde and a primary amine (lysine) [20]. Before each thermo-mechanical cycle the sample was equilibrated at 60 °C for half an hour. Then, the deformation was applied. After 5 minutes of holding the deformation at 60 °C, the temperature was lowered to room temperature (~20 °C). The system was kept deformed at this temperature for 24 hours. After 24 hours the sample was either left at room temperature for a few days to investigate the slow relaxation process or heated up to 60 °C to observe fast shape recovery. The recovery observations were registered with the help of a video camera (Sony Cybershot). The thermo-mechanical cycles were repeated several times.

## 7.3 Results and discussion

***Chemical network formation***

The shape memory behaviour was tested for several concentrations of TR4T polypeptide, chemically crosslinked with different amounts of glutaraldehyde. The storage modulus of the fixed network ($G_f$) strongly depends on the protein concentration but also on

the amount of glutaraldehyde. Solutions of 1.4 mM of TR4T mixed with 8.4 or 16 moles of glutaraldehyde per mole of protein formed gels with a storage modulus of ~480 and ~2000 Pa, respectively. From these values, using classical gel theory [21], we could estimate the concentration of elastically active chemical bridges as 0.18 and 0.73 mM, respectively. These numbers are much lower than the expected value of 8.57 mM, estimated for a 1.43 mM gel by taking into account that the total number of reactive residues (lysine) in the polymer chain is 12. Such findings suggest that a large excess of glutaraldehyde is needed to form a maximally crosslinked network. That is because part of glutaraldehyde reacts with remaining impurities such as aromatic amino acids or ammonium sulphate or as suggested by Hopwood *et al.* [17] and Bowes *et al.* [22] three molecules of glutaraldehyde are bound per lysine residue.

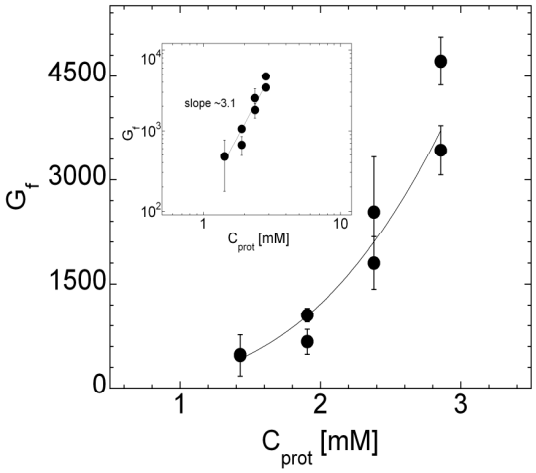


Figure 7.2 Storage modulus of the permanent (chemical) gel ($G_f$) at 45 °C as a function of total protein concentration ($C_{prot}$), crosslinked with 8.4 moles of glutaraldehyde per mole of protein.

On the other side, we have to keep in mind that not all chemical crosslinks have to be elastically active. As shown in Figure 7.2, the elastic modulus increases with increasing polymer concentration (at equal molar excess of crosslinker), roughly as $G_f \sim C_{prot}^3$. Such a non-linear increase can be attributed to network imperfections, such as loops or dangling ends that are more abundant at low concentrations.

***Shape memory thermo-mechanical cycles***

For each freshly prepared chemical network we carried out several shape-memory thermo-mechanical cycles. In Figure 7.3 we present the typical shape-memory cycle, for a hydrogel formed by a 2.4 mM solution of TR4T protein mixed with 8.4 moles of glutaraldehyde per mole of protein. The chemical gel with a plateau storage modulus of

~1800±375 Pa was formed at 45 ºC, which is above the melting temperature of the triple helical nodes [15], within 6 hours (data not shown).

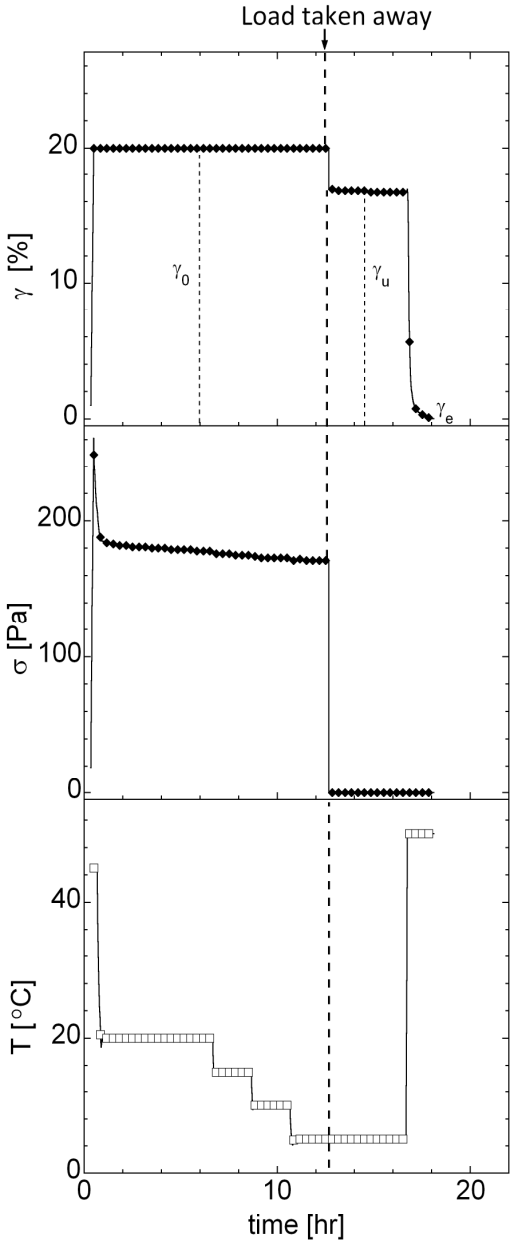


Figure 7.3 Typical shape-memory cycle for a hydrogel formed by a 2.4 mM protein solution mixed with 8.4 moles of glutaraldehyde per mole of protein.

Once the permanent network was formed a 20 % shear strain was applied to the system (at 45 ºC), resulting in an initial stress response of 261 Pa. This value slowly declined towards 208 Pa within the next half hour, and then slowly dropped further to 186 Pa upon cooling to 20 ºC. Further cooling caused a slight additional decrease in the stress and at 5 ºC its value

was 172 Pa. Similar behaviour was observed for all tested samples. Obviously, the measured stresses were larger for higher applied deformations. The stress decrease after the initial overshoot indicates that there are some bonds formed by glutaraldehyde that are not permanent but relax slowly.

After holding the system in the cooled state for 12 hours, during which the end T blocks assemble into triple helices, the load was taken away, leading to an immediate decrease of the strain from 20 % to 16.9 %. This initial response can be quantified by the strain-fixity ratio ($R_f$), which characterizes the material's capability to hold the temporary shape, and is defined as:

$$R_f(N) = \frac{\gamma_u(N)}{\gamma_0} \qquad \text{(Eq. 7.1)}$$

where $\gamma_u(N)$ is the strain value immediately after unloading in the Nth cycle and $\gamma_0$ is the applied strain, just before unloading.

The strain after unloading of a 2.4 mM TR4T gel did not decay further within the next three hours of observation. Upon subsequent heating to 50 ºC (above the melting temperature of the physical nodes) the samples assumed the final unstrained state, $\gamma_e$. The recovery of the sample in the $N_{th}$ cycle was quantified by the strain-recovery ratio ($R_r$), defined as:

$$R_r(N) = \frac{\gamma_0 - \gamma_e(N)}{\gamma_0 - \gamma_e(N-1)} \qquad \text{(Eq.7.2)}$$

where $\gamma_e(N)$ is the residual recorded strain at the end of the $N_{th}$ thermo-mechanical cycle; complete recovery implies $\gamma_e=0$ and $R_r=1$.

Several thermo-mechanical cycles were carried out on freshly prepared hydrogels. In Figure 7.4A we plot (as an example) the strain-fixity and strain-recovery ratio for a 2.4 mM TR4T gel mixed with 8.4 moles of glutaraldehyde per mole of protein and deformed at 20 and 60 % strain. It can be seen that both $R_r$ and $R_f$ are constant for at least 6 cycles. The strain-recovery ratio ($R_r$), did not depend on the applied strain and was approximately 1, even after several thermo-mechanical cycles, showing that our system can fully recover to its programmed shape. Such a complete recovery was found for all tested TR4T hydrogels. The strain-fixity ratio ($R_f$) for a 2.4 mM hydrogel mixed with 8.4 moles of glutaraldehyde per mole of protein was around 0.85, independently of the applied strain (Figure 7.4A). However, contrary to $R_r$, $R_f$ was found to depend on the tested system, varying between 0.92 for the

lowest protein concentration and 0.82 for the highest protein concentration, when mixed with 8.4 moles of glutaraldehyde per mole of protein. When the amount of glutaraldehyde was doubled, $R_r$ was 0.64 (Figure 7.4B).

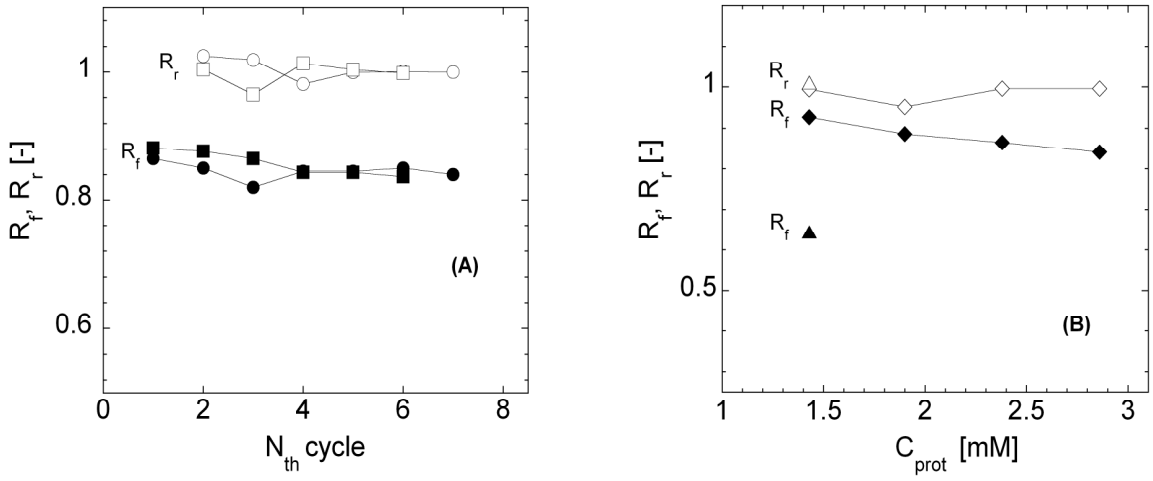


Figure 7.4 (A) Strain-recovery ratio $R_r$ (open symbols) and strain-fixity ratio $R_f$ (filled symbols) for a 2.4 mM TR4T protein solution mixed with 8.4 moles of glutaraldehyde per mole of protein, deformed at 20 % (□■) and 60 % (○●) strain. (B) Strain-fixity ratio ($R_f$) (open symbols) and strain-fixity ratio $R_f$ (filled symbols) as a function of protein concentration for systems crosslinked with 8.4 (◇◆) and 16.8 (△▲) moles of glutaraldehyde per mole protein.

The fixity ratio is determined by the relative strength of the permanent (fixed) and the physical network. The stress in the fixed network after unloading (*i.e.* at a strain $\gamma_u$) equals $G_f \cdot \gamma_u$, while the stress in the physical network (which has its reference state at a strain $\gamma_0$) is $G_f \cdot (\gamma_0 - \gamma_u)$. A simple force balance thus gives:

$$G_f \cdot \gamma_u = G_0 \cdot (\gamma_0 - \gamma_u) \qquad \text{(Eq. 7.3)}$$

from which we obtain the strain fixity ratio ($R_f$) as:

$$R_f = \frac{\gamma_u}{\gamma_0} = \frac{G_0}{G_0 + G_f} \qquad \text{(Eq. 7.4)}$$

where $G_0$ is the storage modulus of the physical network and $G_f$ is the storage modulus of the chemical (fixed) network

It is clear from Equation 7.4 that the strain-fixity should not depend on the applied strain, as long as the deformation is in the linearly elastic regime. This agrees with our findings in Figure 7.4A.

From the measured values for the moduli of the fixed network and the strain-fixity ratios, we can obtain the modulus of the physical network from equation 7.2. The values for $G_0$ obtained in this way are shown in Figure 7.5 as a function of the protein concentration. In the same figure we show the moduli of the physical network at the same concentrations, measured in the absence of the chemical crosslinking (determined in Chapter 3). It is clear that the modulus of the physical network is much higher in the presence than in the absence of the chemical crosslinking. This surprising enhancement shows that the physical crosslinks are not independent of the chemical ones. The effect could be due to changes in the gel topology *i.e.* fewer intramolecular (looped) assemblies between the collagen-like end blocks.

In order to check in a different way, whether there is an enhancement of the physical network in the presence of chemical crosslinking we have measured the elasticity of the "double network" for 2.4 mM TR4T crosslinked with 8.4 moles of glutaraldehyde per mole of protein. At 5 °C the measured storage modulus for the double network was ~6500 Pa. Taking into account that the elastic contribution of the chemical network was around 2000 Pa, we find that the extra contribution of the physical network to the combined modulus is ~4500 Pa, which is roughly 4.5 times higher than the storage modulus of the physical network in the absence of chemical crosslinking. However, this is still about two times lower than the value obtained from the strain-fixity ratio (see Figure 7.5).

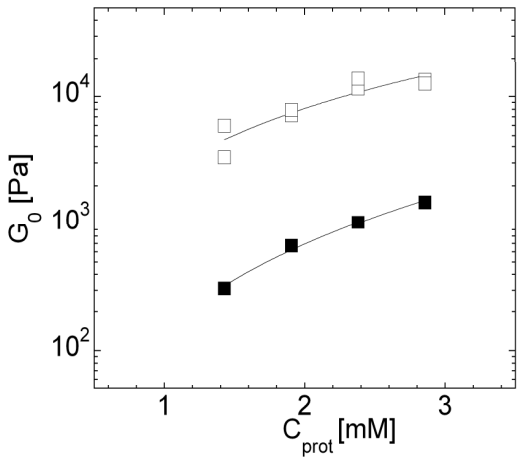


Figure 7.5 Storage modulus of the physical network ($G_0$) formed by TR4T with 8.4 moles of glutaraldehyde per mole of protein at 5 ºC as a function of protein concentration in the presence (□) and absence (■) of the chemical network.

Possibly, chemical bonds that are very close to a helix, act together with that helix as a single elastically effective bond, when testing the double network. By contrast, in the shape

memory experiments, after removal of the load the chemical bonds and helices act against each other, and so become mutually distinguishable.

***Kinetics of permanent shape recovery***

The shape-memory behaviour of our materials arises from the reversible association of the collagen-like end blocks into triple helical nodes. As we have shown in Chapters 3 and 5, the association and dissociation of the triple helical nodes strongly depend on the temperature. Therefore, in Figure 7.6 we present the kinetics of shape recovery at different temperatures. At 5 ºC (278 K), the sample maintains its temporary shape and there is almost no recovery within the observation time, both for 20 % and for 60 % strain. This is as expected, as the relaxation time of a single triple helix at this temperature is very long, around $10^5$ s, as measured previously [15]. At 20 and 25 °C there is some recovery, but, this recovery is much slower than the natural dissociation of triple helices at these temperatures. As shown in Chapter 3, the relaxation time of a single triple helix is on the order of 1400 s at these temperatures. However, the strain did not decreased considerably, even after 10 hours of observations. The recovery speeds up with temperature, and takes only a few minutes above the melting temperature ($T_m$≈42 °C).

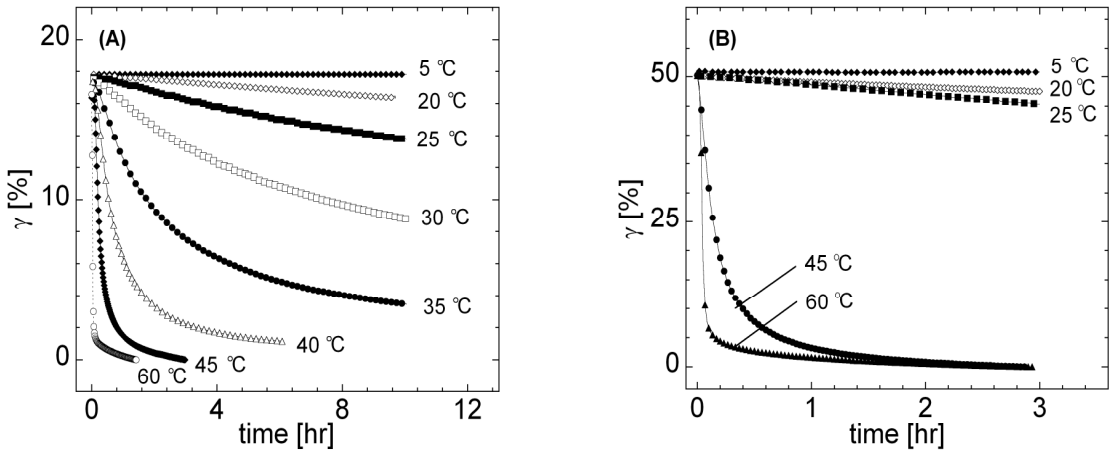


Figure 7.6 Relaxation of the temporary shape at different temperatures (as indicated) for a 2.4 mM TR4T, crosslinked with 8.4 moles of glutaraldehyde per mole of protein, deformed by (A) 20 % and by (B) 60 %.

In order to understand the recovery kinetics of the temporary shape of our materials we describe it by a mechanical model, as illustrated in Figure 7.7A. The fixed network is represented as an elastic spring characterized by a modulus $G_f$ and the physical network is

represented by a Maxwell element (a spring and a dashpot connected in series) characterized by a plateau modulus $G_0$ and a relaxation time $\tau$.

In the beginning of the shape-memory cycle, at high temperature, only the fixed network is present with storage modulus $G_f$ (Figure 7.7A). Applying a deformation $\gamma=\gamma_0$ (Figure 7.7B) leads to a stress in the fixed network $\sigma_f=G_f \cdot \gamma_0$. Cooling then leads to the formation of the physical network (Figure 7.7C). When the load is taken away (Figure 7.7D) the two networks readjust quickly to restore mechanical equilibrium, resulting almost instantaneously in a strain $\gamma_u$ as given by Equation 7.1. After this initial readjustment, the sample then recovers further towards its initial unstrained state at a rate that depends on the temperature. When the temperature is raised above the melting temperature $T_m$, the physical network melts and the recovery is rapid (Figure 7.7F).

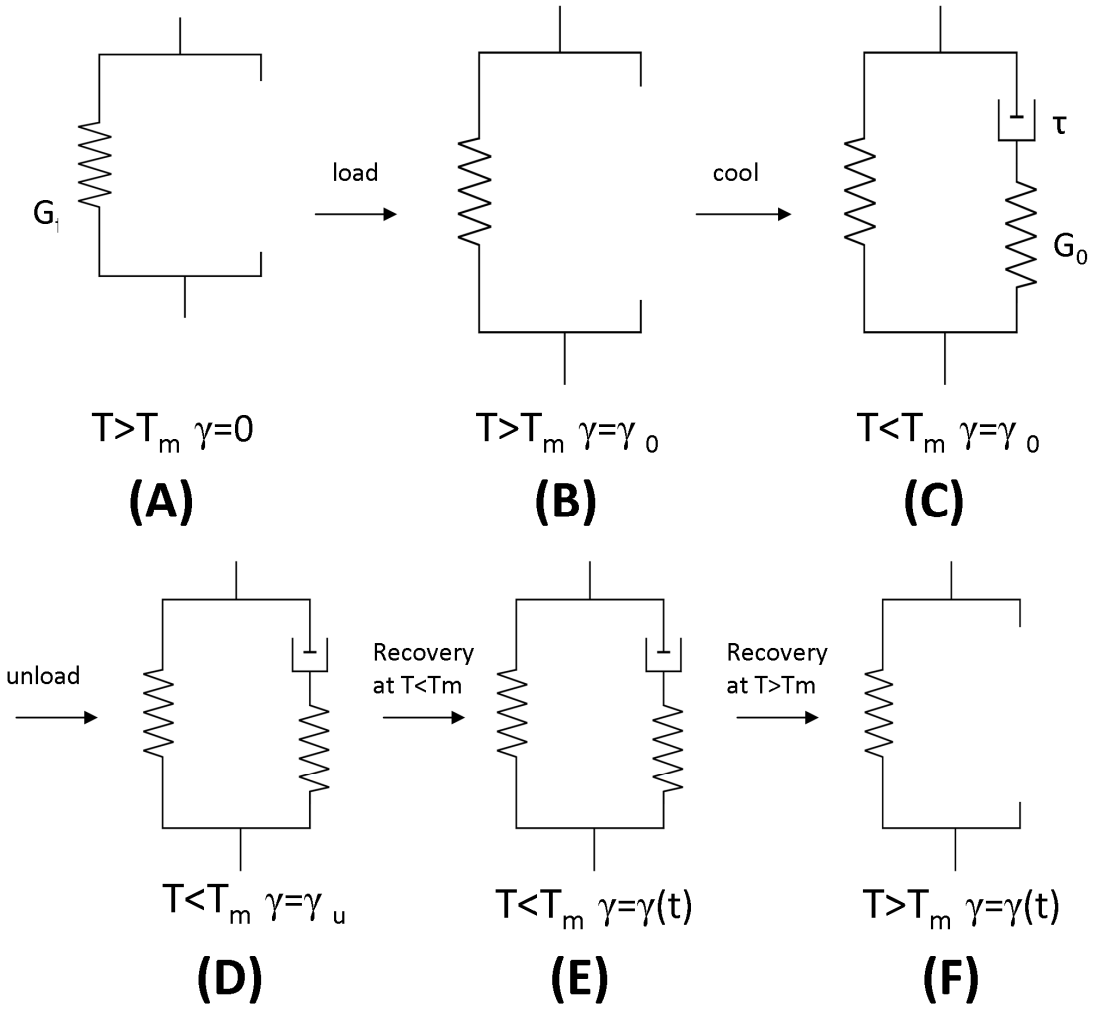


Figure 7.7 Mechanical model with a spring element (a fixed network) in parallel with a Maxwell element *i.e.* a spring and a dashpot in series (a physical network).

The recovery rate is determined by the rate of helix melting in this case. This can be seen in Figure 7.6 for 45, 50 and 60 °C. Note that the melting rate is still relatively low for 45 °C (just above $T_m$), while it is higher for higher temperatures. It can be seen in Figure 7.6 that this fast recovery (on the order of minutes) is followed by a slower recovery (on the order of hours) in all cases. We attribute this slower recovery phase to the presence of some slowly relaxing bonds in the chemical network also above $T_m$.

When the final temperature is below the melting temperature (Figure 7.7E) the sample still recovers, but at a much smaller rate. This recovery is due to the transient character of the triple helices, which can dissociate and reform on timescales of the relaxation time τ. The recovery rate can be obtained from the constitutive equation of the physical network, which relates the strain in the physical network $\gamma_p$ to the stress $\sigma_p$. For a Maxwell model this is:

$$\frac{d\gamma_p}{dt} = \frac{1}{G_0}\frac{d\sigma_p}{dt} + \frac{\sigma_p}{G_0 \cdot \tau} \qquad \text{(Eq.7.5)}$$

Because the reference state of the physical network is at a strain $\gamma_0$, its effective strain equals $\gamma_p=\gamma_0-\gamma$. Moreover, mechanical equilibrium implies that the stress in the physical network must balance that in the fixed network, so that $\sigma_p=\sigma_f=G_f\cdot\gamma$. From this we obtain the following differential equation for the strain recovery:

$$\frac{d\gamma}{dt} = -\frac{G_f}{G_f + G_0}\cdot\frac{\gamma}{\tau} \qquad \text{(Eq. 7.6)}$$

The solution of this equation with the initial condition $\gamma(0)=\gamma_u=R_f\cdot\gamma_0$, gives an exponential recovery process:

$$\gamma(t) = R_f \cdot \gamma_0 \exp\left(-\frac{\left(1-R_f\right)}{\tau}\cdot t\right) \qquad \text{(Eq. 7.7)}$$

where we have used equation 7.2. The recovery time is proportional to the natural helix relaxation time τ, but it is larger by a factor $1/(1-R_f)$. As $R_f$ is typically between 0.8 and 0.9 (Figure 7.4B), the recovery is expected to be 5 to 10 times slower than the natural helix dissociation rate. For the curves in Figure 7.6A at 30-40 ºC, we indeed observe exponential recovery, though only at the start of the experiment. The initial exponential decay is followed by a slow relaxation regime, similar to that observed at temperatures above $T_m$. Such findings indicate that the chemical crosslinking introduced appearance of slowly-relaxing species,

which are present also above $T_m$. It is not very clear at this point, whether the origin of this slowly relaxing species is the physical or the chemical network. At temperatures 25, 20 and 5 ºC the exponential decay is not so clear, because the observation time is still too short compared to the typical recovery time.

***Visualization of shape- memory effect***

In Figure 7.8A we present a piece of gel in its programmed shape (cylinder), formed by a 4.8 mM solution of TR4T, crosslinked with 8.4 moles of glutaraldehyde per mole of protein. The programmed shape of the gel was "pinned" in a temporary shape (7.8B) by deforming the sample at 60 °C, lowering the temperature to 20 °C and waiting 24 hours so that the physical gel can form. After 24 hours of holding the sample in the strained state the deformation was taken away. The sample could recover its original (programmed) shape (Figure 7.8C) either within a few days at room temperature (Figure 7.8D) or within a few minutes upon heating to 60 °C (Figure 7.8E and supplementary movie). The same cycle of deformation and triggered recovery could be repeated many times.

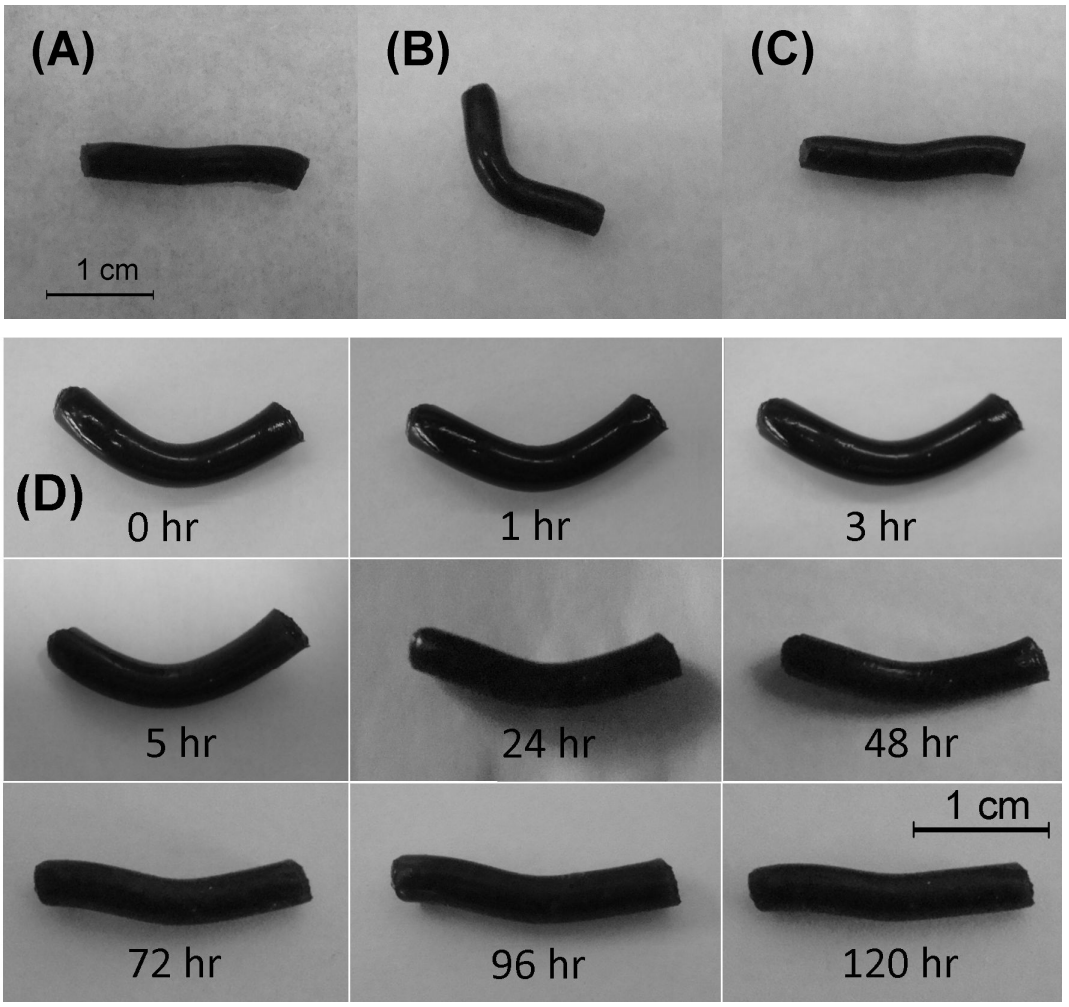

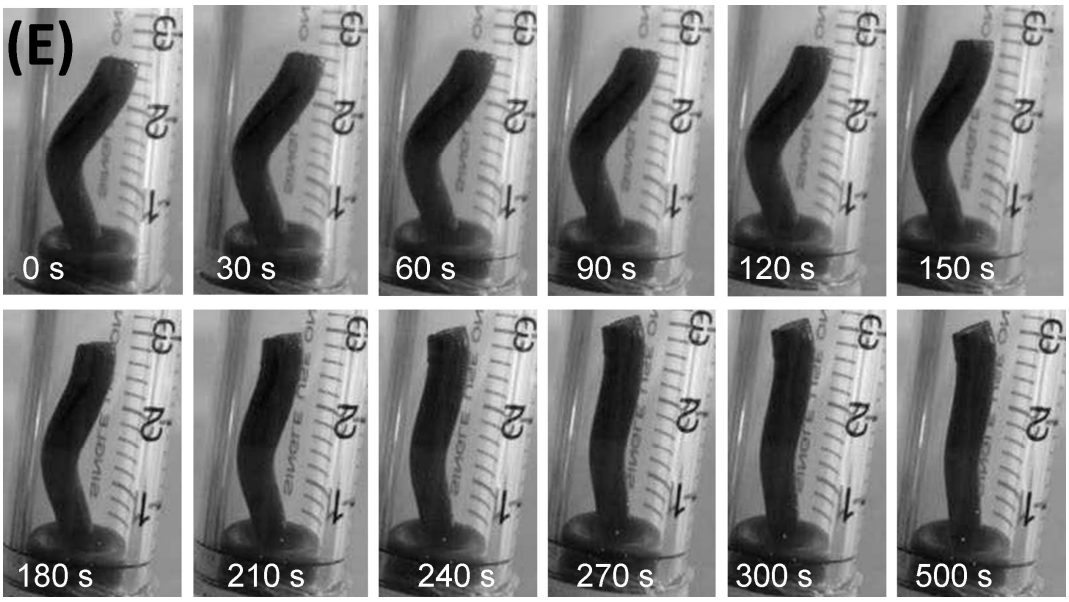


Figure 7.8 4.8 mM TR4T solution crosslinked with 8.4 moles of glutaraldehyde per mole of protein in: (A) its programmed shape before deformation, (B) its temporary shape, and (C) in its programmed shape after recovery. (D) Shape recovery at room temperature. (E) Shape recovery at 60 ºC.

## 7.4 Concluding remarks

In this Chapter we have demonstrated shape-memory behaviour of lightly crosslinked telechelic biopolymers, with a random coil-like middle block and collagen-like end blocks. The shape-memory behaviour of the presented materials arises from the reversible association of the collagen-like end blocks into triple helical nodes. The association and dissociation of the triple helices, and thereby the shape-memory behaviour of our hydrogels, strongly depend on the temperature. At room temperature the relaxation of the temporary shape takes a few days, at 45 ºC around 1-2 hours, and at 50 and 60 ºC only a few minutes. The shape-recovery process at different temperatures was studied in more detail and interpreted using a mechanical model composed of two springs and a dashpot. Using this model, we could explain why the temporary shape was maintained so efficiently, despite the finite lifetime of the triple helices.

In a future the rate of the shape-recovery can be adjusted not only by changing the temperature but also by changing the physicochemical properties of the physical hydrogel, superimposed onto the chemical network. As we have demonstrated previously, the melting behaviour, as well as the elastic properties of the physical gels, formed by the telechelic biopolymers can be easily tuned by changing the molecular design of the polypeptide [16]. An

additional advantage of our shape-memory materials is that they are formed by biopolymers, which are biodegradable and biocompatible [23].

## References


[1] C.M. Yakacki, R. Shandas, D. Safranski, A.M. Ortega, K. Sassaman, K. Gall, Strong, tailored, biocompatible shape-memory polymer networks. Advanced Functional Materials 18(16) (2008) 2428-2435.

[2] A. Lendlein, S. Kelch, Shape-memory polymers as stimuli-sensitive implant materials. Clinical Hemorheology and Microcirculation 32(2) (2005) 105-116.

[3] A. Alteheld, Y.K. Feng, S. Kelch, A. Lendlein, Biodegradable, amorphous copolyester-urethane networks having shape-memory properties. Angewandte Chemie-International Edition 44(8) (2005) 1188-1192.

[4] A. Lendlein, H.Y. Jiang, O. Junger, R. Langer, Light-induced shape-memory polymers. Nature 434(7035) (2005) 879-882.

[5] A. Lendlein, S. Kelch, in: O. VanderBiest, M. Gasik and J. Vleugels (Eds.), Functionally Graded Materials Viii, Vol. 492-493, 2005, pp. 219-223.

[6] A.T. Neffe, B.D. Hanh, S. Steuer, A. Lendlein, Polymer Networks Combining Controlled Drug Release, Biodegradation, and Shape Memory Capability. Advanced Materials 21(32-33) (2009) 3394-3400.

[7] C.M. Yakacki, R. Shandas, C. Lanning, B. Rech, A. Eckstein, K. Gall, Unconstrained recovery characterization of shape-memory polymer networks for cardiovascular applications. Biomaterials 28(14) (2007) 2255-2263.

[8] A. Lendlein, S. Kelch, Shape-memory polymers. Angewandte Chemie-International Edition 41(12) (2002) 2034-2057.

[9] Z.G. Wei, R. Sandstrom, S. Miyazaki, Shape-memory materials and hybrid composites for smart systems - Part I Shape-memory materials. Journal of Materials Science 33(15) (1998) 3743-3762.

[10] X.L. Luo, X.Y. Zhang, M.T. Wang, D.H. Ma, M. Xu, F.K. Li, Thermally stimulated shape-memory behavior of ethylene oxide ethylene terephthalate segmented copolymer. Journal of Applied Polymer Science 64(12) (1997) 2433-2440.

[11] Y. Osada, A. Matsuda, Shape-memory in hydrogels. Nature 376(6537) (1995) 219-219.

[12] T. Hirai, H. Maruyama, T. Suzuki, S. Hayashi, Shape memorizing properties of a hydrogel of poly(viny alcohol). Journal of Applied Polymer Science 45(10) (1992) 1849-1855.

[13] J.H. Li, J.A. Viveros, M.H. Wrue, M. Anthamatten, Shape-memory effects in polymer networks containing reversibly associating side-groups. Advanced Materials 19(19) (2007) 2851-+.

[14] P.J. Skrzeszewska, F.A. de Wolf, M.W.T. Werten, A.P.H.A. Moers, M.A. Cohen Stuart, J. van der Gucht, Physical gels of telechelic triblock copolymers with precisely defined junction multiplicity. Soft Matter 5(10) (2009) 2057-2062.

[15] P.J. Skrzeszewska, F.A. de Wolf, M.A. Cohen Stuart, J. van der Gucht, Kinetics of network formation by telechelic polypeptides with trimeric nodes. Soft Matter 6(2) (2010) 416-422.

[16] H. Teles, P.J. Skrzeszewska, M.W.T. Werten, J. van der Gucht, G. Eggink, F.A. de Wolf, Influence of molecular size on gel-forming properties of telechelic collagen-inspired polymers. Soft Matter 6(19) (2010) 4681-4687.

[17] D. Hopwood, C.R. Allen, M. McCabe, The reactions between glutaraldehyde and various proteins. An investigation of their kinetics. Histochemical Journal 2(2) (1970) 137-150.

[18] M.W.T. Werten, H. Teles, A. Moers, E.J.H. Wolbert, J. Sprakel, G. Eggink, F.A. de Wolf, Precision Gels from Collagen-Inspired Triblock Copolymers. Biomacromolecules 10(5) (2009) 1106-1113.

[19] J.A. Gerrard, P.K. Brown, S.E. Fayle, Maillard crosslinking of food proteins II: the reactions of glutaraldehyde, formaldehyde and glyceraldehyde with wheat proteins in vitro and in situ. Food Chemistry 80(1) (2003) 35-43.

[20] J.H. Tramezzani, S. Chiocchi, G.F. Wassermann, New technique for light and electron microscopic identification of adrenaline- and nonadrenaline storing cells. J Histochem Cytochem 12 (1964) 890-899.

[21] J.D. Ferry, Viscoelastic Properties of Polymers, Wiley, New York, 1980.

[22] J.H. Bowes, C.W. Cater, Interaction of aldehydes with collagen. Biochimica Et Biophysica Acta 168(2) (1968) 341-351.

[23] H. Teles, T. Vermonden, G. Eggink, W.E. Hennink, F.A. de Wolf, Hydrogels of collagen-inspired telechelic triblock copolymers for sustained release of proteins. Journal of Controlled Release 147(2) (2010) 298-303.

# Chapter 8

# Summary and General Discussion

## 8.1 Summary

The rapid increase of the quality of life together with the progress of medical science asks for the development of new, tuneable and controllable materials. For the same reason, materials used for biomedical applications have to be increasingly biocompatible, biodegradable and biofunctional. Most of the available systems, however, lack one property or the other. For example, conventional animal-derived gelatin that is often used in biomedicine, is susceptible to a risk of contamination with prions or viruses and has a risk of bringing out allergic reactions, particularly against the non helix-forming domains of collagen [1]. Furthermore, gelatin is composed of a variety of molecules and structures with different thermal stabilities and molecular sizes. This, in combination with the impossibility to change the molecular structure at will, limits the chances to elucidate the relation between the structure and function. On the other hand, synthetic materials that have a rather well-controlled size distribution often lack biocompatibility, biofunctionality or biodegradability. In addition to that, as their synthesis often requires toxic solvents, their application in the human body is restricted. All the drawbacks of the presently used materials have brought scientists towards a new approach in designing materials *viz.* genetic engineering. Rapid progress in recombinant techniques has led to new ways of producing molecules with well-defined composition and structure and with full control over the length and sequence of the biopolymer and its constituent blocks. These methods thus combine the advantages of natural and synthetic polymers. Using molecular biology tools, unique molecules can be created by merging in a desired manner naturally occurring self-assembling motifs such as elastin, silk or collagen [2-4], or entirely artificial fragments. As we show in this thesis, the precise control over the molecular design of these biotechnologically produced block polypeptides is extremely valuable as it also leads to control over their physicochemical properties.

In this thesis we present a new class of monodisperse, biodegradable and biocompatible network-forming block polymers that are produced by genetically modified strain of yeast, *Pichia pastoris* (**Chapter 2**). Trimer-forming end blocks, abbreviated as T, consisting of nine Pro-Gly-Pro amino acid triplets, are symmetrically flanking a random coil-like middle block composed of four or eight repeats of highly hydrophilic R or P sequences (Figure 8.1). R and P are identical with respect to length (99 amino acids) and composition but have different amino acid sequences. The P block has a glycine in every third position (as in collagen) but does not form any supramolecular structures and maintains a random coil-like conformation at any temperature [5]. The R block is a shuffled version of the P block. Four recombinant

gelatins are reported in this thesis, denoted as TR4T, TR8T, TP4T and TP8T (Figure 8.1). All of these were successfully produced with high yields (1-3 g/l of fermentation broth) by the *Pichia pastoris* GS115 strain transformed with a pPIC9 vector with the gene of interest in its expression cassette.

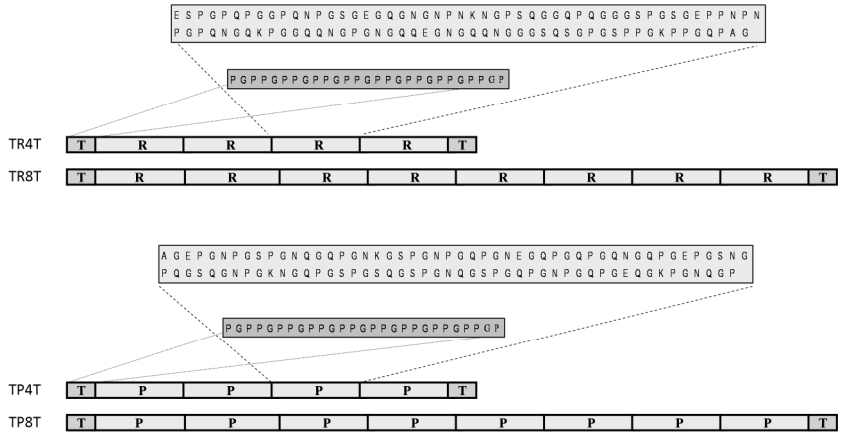


Figure 8.1 Schematic representation of collagen-inspired telechelic polypeptides: TR4T, TR8T, TP4T and TP8T.

In **Chapter 3** we described the linear rheological properties of hydrogels formed by TR4T polypeptides. At a temperature of 50 °C, the solution does not show any viscoelastic response. However, upon cooling, the collagen-like trimer-forming domains (T) start to assemble into triple helical nodes and a well-defined network, with a node multiplicity of three, is formed. In the beginning of the gelation process, viscous properties are predominant, but as the network formation progresses, the elastic properties prevail. A plateau storage modulus is reached within a few hours. At this point the triple helices are in equilibrium with the free T blocks. An equilibrium or near-equilibrium state is reached, contrary to natural gelatin, because the collagen-like (T) assembling domains are relatively short and well-defined. The T blocks are solely responsible for the network formation. We have shown that a solution of the middle blocks only (*i.e.* R4) does not demonstrate any elastic response at any time and temperature. In addition, differential scanning calorimetry (DSC) (Chapter 5) proved that the collagen-like side blocks are near-quantitatively responsible for trimerization, as the observed melting enthalpies are in good agreement with values obtained by Frank *et al*. [6] for free $(Pro\text{-}Gly\text{-}Pro)_{10}$ peptides. The equilibrium fraction of T blocks involved in triple helices shifts with temperature. By lowering the temperature, the fraction of triple helices increases, while the fraction of free ends decreases. There are two possibilities to form a triple

helix. It can be formed either by three T blocks from three different chains, or by three T blocks from two different chains, so that two side blocks come from the same polypeptide. As a consequence, the network is composed of dangling ends, elastically active bridges and inactive loops (Figure 8.2). Because of the precisely-known junction multiplicity of three, we could develop an analytical model that links the internal structure of the gel, with dangling ends, loops, and bridges, to the physicochemical properties. This model uses a limited set of input parameters that can all be measured independently. It describes the experimental data quantitatively without further adjustable parameters. Using this model, we could show that the observed strong dependency of the storage modulus, the relaxation time and the viscosity on concentration and temperature is related to the changes in the number of loops, active bridges, and dangling ends in the gel matrix.

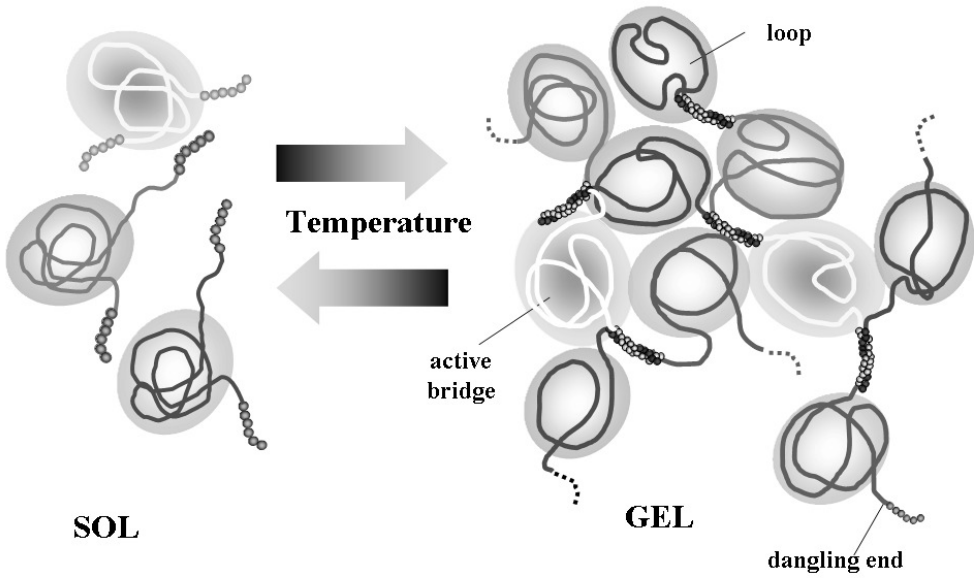


Figure 8.2 Network formation by collagen-inspired telechelic biopolymers.

In **Chapter 4** we show that the number of intermolecular junctions and intramolecular loops depends not only on protein concentration and temperature but also on the length and the stiffness of the middle block. We synthesised new triblock copolymers with middle blocks, of different lengths and amino acid sequences, named TP4T, TR8T and TP8T (Figure 8.1). For all new proteins, there is a strong dependency of the storage modulus, the relaxation time and the viscosity on concentration and temperature (as for TR4T). However at comparable molar concentrations, the longer versions of polypeptides *i.e.* TR8T and TP8T

show a significantly higher storage modulus and relaxation time than their counterparts TR4T and TP4T. This is because a longer middle block leads to a larger radius of gyration ($R_g$), which decreases the probability that two end blocks from the same molecule associate with each other, and form a loop. The consequence of fewer loops in the system is a higher storage modulus and a higher overall relaxation time. Besides the effect of polymer length, we also observed that the R series, *i.e.* TR4T and TR8T, show a higher storage modulus than their P counterparts, *i.e.* TP4T and TP8T, at the same concentration and temperature. This can be explained by differences in coil flexibility. Although the P and R blocks have exactly the same amino acid composition, their amino acid sequence is different. Fitzkee *et al*. [7] have shown that even a polypeptide chain that assumes a random coil conformation still has locally folded conformations that contribute to the overall flexibility of the chain. This apparently leads to a smaller radius of gyration for the P middle block than for the R middle block and thus to a higher probability of loop formation.

Even though the melting behaviour obtained with DSC is the same for all four polypeptides (as the end blocks stay the same), the temperature at which the $G_0$ value approaches zero and the gel completely loses its elastic properties varies with the length of the middle block. Shorter molecules, *i.e.* TP4T and TR4T, melt at lower temperatures. A solution of 1.2 mM TP4T melts at 298 K, while TP8T at a comparable molar concentration melts at a temperature which is 15 degrees higher. Furthermore, the R versions show slightly higher melting temperatures than the P versions. These differences in melting behaviour are related to the gel structure and the relative probabilities of forming intramolecular and intermolecular assemblies. We could account for these findings with the help of the analytical model presented in **Chapter 3**. The only parameter that had to be varied in the model was the coil size of the polymer, since the enthalpy and the melting temperatures of the triple helices did not change with the length of the middle block. The theoretical calculations clearly show that the molecules with smaller $R_g$ form up to 30 % more loops than their bigger counterparts. Loops that act as gel stoppers do not contribute to the network elasticity and significantly lower the melting temperatures detected with rheology.

The network junctions in our gels are solely formed by triple helices. The mechanism of junction formation by the T blocks can be well-described by a two-step kinetic model (**Chapter 5**). Prior to triple helix propagation, a trimeric nucleus has to be formed. For dilute systems, nucleation is the limiting step, giving an apparent reaction order of three. These results indicate that only triple helices are stable. For more concentrated solutions, when nucleation is relatively fast, propagation of triple helices becomes rate-limiting and the

apparent reaction order is close to unity. The propagation of triple helices is probably limited by *cis-trans* isomerization of peptide bonds, in which proline residues are involved.

Above overlap concentration (C*) the measured enthalpy for stable gels (~15 hours) indicates that almost 100 % of the T blocks are involved in triple helices. Values obtained by us are in good agreement with values obtained by Frank *et al.* [6] for single $(Gly\text{-}Pro\text{-}Gly)_{10}$ peptides. Conversely, at concentrations below C*, the enthalpy per mole of protein is becoming less, suggesting that the fraction of free ends or mismatched helices becomes more pronounced. The apparent melting temperature increases slightly with increasing concentration. This can be explained on the basis of the reaction stoichiometry under equilibrium conditions [8, 9]. Except for the highest measured concentration (2.4 mM), the apparent melting temperature revealed a dependence on the scan rate, indicating that it was not possible to maintain equilibrium during the heating step. At a concentration of 2.4 mM concentration there is no scan rate dependence, since the melting occurs at a higher temperature, where the dissociation kinetics is faster [4, 10].

The kinetics of triple helix formation determines the rate of gel formation. The gelation starts when the first triple helical node is formed. At that time viscous properties (loss modulus) predominate, but as the network formation evolves the elastic response (storage modulus) becomes more pronounced. The storage modulus (G') reaches a plateau value within a few hours. Changes in network structure and mechanical properties of the gel in time can be predicted from the kinetics of triple helix formation, using the model presented in **Chapter 3**. By comparing the kinetics obtained with rheology and with DSC we could see that for our system, the helix content is not simply proportional to the network progress and that the relation between the elastic properties (G') and the helix content ($p_H$) depends on the protein concentration. The reason for this concentration dependence is the formation of loops, which is more likely at low concentrations.

The investigated hydrogels undergo time-dependent macroscopic fracturing when a constant shear rate or shear stress is applied (start-up and creep experiments, respectively) **(Chapter 6)**. Observations with particle image velocimetry (PIV) showed that in the beginning of a start-up (or creep) experiment the sample flows homogenously. After some time, the gel fractures, and is separated into two fractions. The inner region moves at the same velocity as the moving bob, while the outer fraction does not move at all. From the rate-dependence of the fracture strength we can conclude that gel fracture is due to stress-activated rupture of the triple helical nodes in the network. When the deformation is taken away, the gel can heal (**Chapter 6**). The capacity of self-healing is due to the transient character of the

network nodes with a finite relaxation time. Such behaviour, impossible for most permanent gels, is highly desired in many applications, as hydrogels are often subjected to deformations, which easily go beyond the linear regime. As we present in Figure 8.3, TR4T gels cut into small pieces (grey and transparent), can heal within 2 hours. As measured with rheology the broken gel can recover up to 100 % of its initial elastic properties, even after several fracturing cycles. Interestingly, the kinetics of healing differs from the kinetics of fresh gel formation (**Chapter 5**). The latter is characterized by a lag-phase before elastic properties start to appear. This lag-phase occurs because at low degrees of crosslinking there is not yet a percolated network, so that the storage modulus is undetectable. By contrast, the recovery of the gel after rupturing is much faster and does not show a lag-phase. The elastic modulus, depending on the rupturing history, comes back to its initial value within 1-5 hours. These findings indicate that outside the fracture zone, the network nodes have not dissociated significantly, so that healing only requires the reformation of junctions that connect the undamaged pieces of the network (gel clusters).

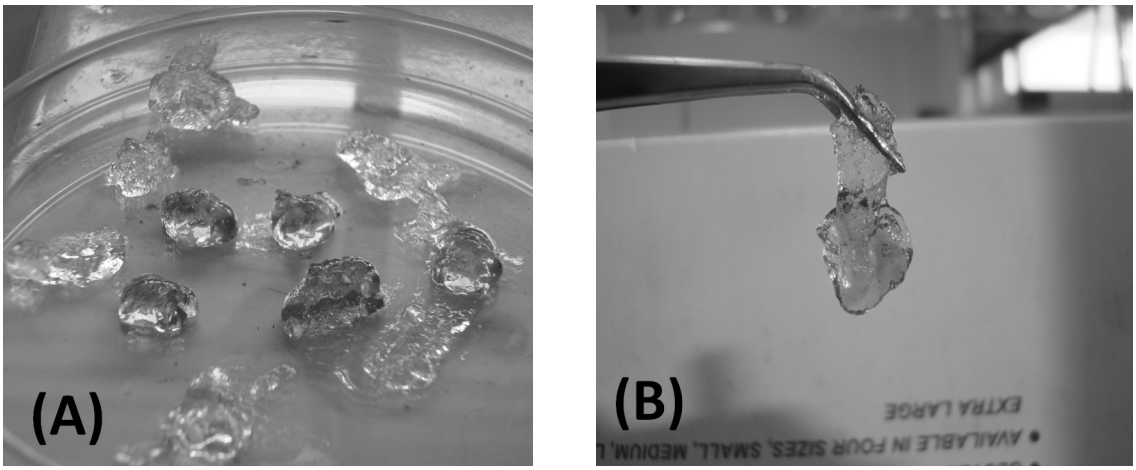


Figure 8.3 Self-healing of TR4T hydrogels. (A) Pieces of broken gel. (B) Two gel pieces healed after 2 hours.

In **Chapter 7** we demonstrated the shape-memory effects in hydrogels formed by permanently crosslinked TR4T molecules. The programmed shape of these hydrogels was achieved by chemical crosslinking of lysine residues present in the random coil. The chemical network could be stretched up to 200 % and "pinned" in a temporary shape by lowering the temperature and allowing the collagen-like end blocks to assemble into the physical nodes. The deformed shape of hydrogel can be maintained, at room temperature, for several days, or relaxed within few minutes upon heating to 50 ºC or higher. The presented hydrogels could return to their programmed shape even after several thermo-mechanical cycles, hence

indicating that they remember the programmed shape. We have studied in more detail the shape recovery process by describing our hydrogels by a mechanical model composed of two springs and a dashpot. With the help of this model we showed that above the melting temperature of the triple helices, the recovery is exponential and that the decay time is roughly ten times slower than the relaxation of the physical network.

## 8.2 Biomedical applications - perspectives and considerations

The class of collagen-inspired self-assembling materials, which we present in this thesis are nice model systems for a systematic study of physical networks, but they also have a lot of potential for biomedical applications. In this section we discuss the possibilities for these self-assembling hydrogels in biomedicine.

***Drug delivery systems***

One of the major goals of modern medicine is to ensure that the required amount of an active substance is available at the desired time at the desired location in the body. Consequently, a lot of effort is put into designing delivery systems with precisely adapted release profiles, sensitive to external stimuli such as temperature or pH. A frequently used group of materials in this field are hydrogels, both chemically and physically crosslinked. In the case of covalently crosslinked networks the release of the drug is mostly via diffusion of the drug out of the gel particle after it swells. The rate of drug release is governed by the resistance of the network to volume increase [11]. Although permanent networks are widely used as drug carriers they have some disadvantages such as incomplete release of active substances and poor biodegradability in the body. The problem can be partially solved by introducing enzymatic cleavage or hydrolysis sites into the main chain, but still the hydrogel erosion cannot be precisely controlled and complete material degradation can not be guaranteed.

These obstacles can be overcome by using physical hydrogels that are formed by weak interactions. These can dissociate in a controlled manner and completely release the active component. In contrast to chemical gels, erosion of physical gels occurs spontaneously. The erosion rate is determined by the life time of the junctions, but it depends also on the relative amount of intramolecular loops and intermolecular junctions, as demonstrated by Shen *et al.* [12]. These authors showed that, by using triblock polymers with dissimilar coiled-coil side

domains rather than identical ones, loop formation could be suppressed, leading to a lower erosion rate [12].

The potential of our gels for drug delivery applications was tested by Teles *et al*. [13]. It was shown that trapped proteins (BSA) can be completely released from TR4T and TR8T gels, both at 37 ºC and 20 ºC. The release at 37 ºC from 20 % gels was completed within 48 hours while at 20 ºC it took about 5 times longer. At body temperature the release was mostly driven by dissociation of trimeric junction and dissolution of the separate polymer chains (gel erosion). At 20 ºC the junction life time was long so that erosion was slower and swelling and diffusion played a more important role. The observations of Teles are in agreement with studies of several groups that demonstrated the importance of hydrogel erosion for controlled release [12, 14].

The erosion rate of physical hydrogels is governed by the junction relaxation time. The mean relaxation time of transient networks can be manipulated either by varying the gel architecture (**Chapter 3 and 4**) or by changing the relaxation time of a single triple helix. The gel architecture (*i.e.* the number of loops and bridges) can be altered either as we show in **Chapter 3** by changing the protein concentration or as we demonstrate in **Chapter 4** by manipulating the design of the middle block. The number of loops becomes lower as the spacer length and stiffness increase (**Chapter 4**). The lifetime of a single node can be changed by enzymatic hydroxylation of proline to hydroxyproline, [15] which leads to more hydrogen bonds among adjacent T blocks, or by changing the length of the collagen-like T domains. Preliminary results showed that average relaxation time of the network is roughly hounded times higher for molecules with collagen-like domains composed of sixteen Pro-Gly-Pro repeats instead of nine (unpublished data).

For these biotechnologically produced collagen-inspired polymers, the length or the composition of the blocks can be changed simply by changing the DNA template. This, in combination with the model elaborated in **Chapter 3** and **4** that links the internal gel architecture with the physicochemical gel behaviour, gives ample possibilities to design materials with custom-desired release profiles of active components.

***Tissue engineering***

Materials for tissue engineering scaffolds have to mimic the in vivo extracellular matrix environment. They provide physical support, but also have to guarantee proper adhesion of cells and controlled release of growth factors. A very important role in scaffolds design is played by the mechanical properties of the matrix [16-18]. As shown by Engler *et al.* [17], the

elasticity of the matrix directs stem cell development to different lineages. Soft networks (0.1-1 kPa), which mimic brain tissue, promote neuron development, stiffer scaffolds (8-17 kPa) are myogenic, while gels with an elastic modulus of 24-40 kPa promote growth of bone cells. The stiffness of the matrix affects focal-adhesions and the organization of the cytoskeleton structure, and thus contractility, motility and spreading [16, 18]. Another significant factor, which plays a role in tissue growth is the degradation rate of the scaffold. The degradation should be synchronized with cellular repair in such a way, that tissue replaces the material within the desired time interval. The scaffold disintegration also controls the release of growth factors. For naturally derived materials such as alginate, the degradation rate could be influenced by partial oxidation of the polymer chain or *via* a bimodal molecular weight distribution [19]. For synthetic polymers different degradation profiles can be realized by incorporating in the polymer backbone groups with different susceptibility to hydrolysis [19].

Presently the most widely used scaffolds for tissue engineering are natural polymers such as collagen, gelatin, and polysaccharides [20] or synthetic, biodegradable polymers such as poly (L-lactic acid) (PLLA), poly(glycolic acid) (PGA), and poly(ethylene glycol) (PEG). [21-23]. Although these materials show promising properties, their use is limited as they suffer from batch to batch variations, polydispersity, viral contamination, allergic reactions or toxic byproducts after degradation. Also their mechanical properties are poorly-controlled and it is difficult to relate the molecular structure to the resulting properties. Furthermore, in the case of synthetic polymers, there is no intrinsic mechanism to interact with cells and to propagate cell adhesion proliferation or migration. This problem can be partially solved by functionalizing synthetic materials with bioactive molecules, such as collagen [24] or short peptides (for example arginine-glycine-aspartic (RGD) or tyrosine-isoleucine-glycine-serine-arginine (YIGSR) [25]). It remains difficult, however, to precisely control the spatial distribution, of these biofunctional domains [25].

A very promising alternative for the currently used scaffolds are hydrogels formed by self-assembling protein polymers [2, 26-28], including the collagen-inspired polypeptides presented in this thesis. Our block polymers form physical gels with precisely controlled elastic properties. As discussed in **Chapter 3** and **4**, the gel structure and the resulting mechanical properties strongly depend on concentration, temperature and on the molecular design of the polymer. Within the investigated range of conditions our gels have an elastic modulus between 0.03 and 5 kPa. Thus they seem most appropriate for neuron cell growth [17]. Moreover, it is also possible to incorporate specific short adhesive peptide sequences (such as RGD) in the middle block to improve attachment and cell propagation.

The presently investigated proteins, with T domains composed of nine Pro-Gly-Pro repeats, still need some enhancement in terms of stability. As shown by Teles *et al.* the currently available molecules erode within 2 days [13]. For tissue engineering applications, this is too fast. We therefore propose some strategies to stabilize our hydrogels. A first possibility alternative is to introduce amino acids which can form chemical bonds such as cysteines that can form disulfide bridges under oxidizing conditions [29], or lysines, which can be functionalized with acrylate and then photo-crosslinked with UV radiation [30-32]. However, one has to be aware that this additional procedure may have negative side effects such as toxic byproducts, incomplete polymer degradation in the body, or loss of responsiveness to external stimuli. Alternatively, the erosion can be moderately slowed down by increasing the relaxation time of the network (as discussed in section on drug delivery systems).

***Wound dressing materials***

Under normal circumstances wound healing is a very long process. In order to speed it up, so that bacterial infections or wound dehydration can be avoided, wound dressing materials are used [33-37]. These materials should fulfil several general requirements such as biocompability, ease of application and removal, proper adherence (to avoid fluid pockets, in which bacteria could proliferate), ease in gas exchange between tissue and environment, and controlled release of active components such as antimicrobial agents or wound repair agents (for example Epidermal Growth Factor (EGF)) [37].

All above-mentioned requirements can be fulfilled by the collagen-inspired hydrogels presented in this thesis. The advantage of our materials is that they can follow the contour of the wound and entirely fill it, thus forming an efficient barrier for microbes, but at the same time being permeable for water vapour and oxygen. Furthermore they can entrap active components and release them in a controlled way during the healing process, as discussed above. Depending on the circumstances, the release profile can be synchronised with the wound healing process. An additional advantage of our genetically engineered molecules is that adhesion domains can be introduced along the middle block, assuring better integration of the gel with the damaged tissue.

## 8.3 Final conclusions and outlook

In this final chapter we have discussed the potential of our collagen-inspired materials in biomedical applications. They are biocompatible and biodegradable, whilst offering numerous

possibilities to change the molecular design in order to meet the desired mechanical or biological properties. Furthermore, the well-defined nature of the triple helical junctions allows us to predict the mechanical properties of the gel from the molecular design of polypeptides. This exclusive feature of our system makes it unique and offers great flexibility to design custom biomedical materials.

Biomedical needs, however, are very variable and often require an individual approach. That is why in our group we have created a family of genetically engineered block copolypeptides. Besides collagen we use other motifs present in nature, such as silk or elastin. We can combine these motifs in various ways in order to create unique stimuli-responsive (often multi-responsive) molecules that can meet individual application needs.

The silk-like domains consist of $(Gly\text{-}Ala\text{-}Gly\text{-}Ala\text{-}Gly\text{-}Ala\text{-}Gly\text{-}Xxx)_n$ repeats. Position Xxx is occupied by charged amino acids such as histidine, lysine or glutamic acid. When the charge is screened, the molecules assemble, forming first β sheet-like secondary structures, and then long fibres. As shown by Martens *et al.* [38], block polymers comprising silk-like domains with glutamic acid or histidine in the Xxx position form fibre-like gels at a pH of 2 or 12, respectively. They also assemble when mixed with oppositely charged (coordination) polymers [3, 38]. Probably, the assembling conditions can be tuned even more precisely by adjusting the isoelectric point of the assembling domain. This will allow the production of hydrogels that are formed after being injected into the body, while they disassemble (releasing the drug) when exposed to the acidic or the alkaline conditions. The nanofibre gels are also stable enough to serve as scaffolds for tissue engineering [39-41].

Another motif that has been used is elastin. It consists of $(Val\text{-}Pro\text{-}Gly\text{-}Xxx\text{-}Gly)_n$ repeats and it self-assembles above a lower critical solution temperature (LCST). The transition temperature can be tuned by introducing more or less polar amino acid residues in position Xxx. By combining elastin-like or collagen-like blocks with silk-like blocks, thermo and pH responsive networks can be obtained. This may allow us to switch from fibre-like gels to associative networks.

Block polypeptides, produced using recombinant techniques, besides biocompability and biodegradability offer many possibilities to adjust the molecular design in will, to realize the desired mechanical or biological properties. Three dimensional structures with different thermal stabilities can be programmed by combining in a precise manner various amino acid sequences. The obtained materials can respond to external stimuli such as pH, ionic strength or temperature. They can also carry peptides fragments that can enhance cells adhesion and proliferation or induce crystallization.

The new approach in material science, which we present in this thesis, opens a new world of polymers, in which the main constraint is imagination.

## References


[1] European Commission, Updated opinion on the safety with regards to TSE risks of gelatine derived from ruminant bones or hides. (2003).

[2] E.R. Wright, V.P. Conticello, Self-assembly of block copolymers derived from elastin-mimetic polypeptide sequences. Advanced Drug Delivery Reviews 54(8) (2002) 1057-1073.

[3] A.A. Martens, J. van der Gucht, G. Eggink, F.A. de Wolf, M.A.C. Stuart, Dilute gels with exceptional rigidity from self-assembling silk-collagen-like block copolymers. Soft Matter 5(21) (2009) 4191-4197.

[4] P.J. Skrzeszewska, F.A. de Wolf, M.W.T. Werten, A.P.H.A. Moers, M.A. Cohen Stuart, J. van der Gucht, Physical gels of telechelic triblock copolymers with precisely defined junction multiplicity. Soft Matter 5(10) (2009) 2057-2062.

[5] M.W.T. Werten, H. Teles, A. Moers, E.J.H. Wolbert, J. Sprakel, G. Eggink, F.A. de Wolf, Precision Gels from Collagen-Inspired Triblock Copolymers. Biomacromolecules 10(5) (2009) 1106-1113.

[6] S. Frank, R.A. Kammerer, D. Mechling, T. Schulthess, R. Landwehr, J. Bann, Y. Guo, A. Lustig, H.P. Bachinger, J. Engel, Stabilization of short collagen-like triple helices by protein engineering. Journal of Molecular Biology 308(5) (2001) 1081-1089.

[7] N.C. Fitzkee, G.D. Rose, Reassessing random-coil statistics in unfolded proteins. Proceedings of the National Academy of Sciences of the United States of America 101(34) (2004) 12497-12502.

[8] J. Engel, H.T. Chen, D.J. Prockop, H. Klump, Triple helix reversible coil conversion of collagen-like polypeptides in aqueous and non aqueous solvents - comparison of thermodynamic parameters and binding of water to (L-Pro-L-Pro-Gly)n and (L-Pro-L-Hyp-Gly)n Biopolymers 16(3) (1977) 601-622.

[9] A.V. Persikov, Y.J. Xu, B. Brodsky, Equilibrium thermal transitions of collagen model peptides. Protein Science 13(4) (2004) 893-902.

[10] S. Boudko, S. Frank, R.A. Kammerer, J. Stetefeld, T. Schulthess, R. Landwehr, A. Lustig, H.P. Bachinger, J. Engel, Nucleation and propagation of the collagen triple helix in single-chain and trimerized peptides: Transition from third to first order kinetics. Journal of Molecular Biology 317(3) (2002) 459-470.

[11] P. Gupta, K. Vermani, S. Garg, Hydrogels: from controlled release to pH-responsive drug delivery. Drug Discovery Today 7(10) (2002) 569-579.

[12] W. Shen, K.C. Zhang, J.A. Kornfield, D.A. Tirrell, Tuning the erosion rate of artificial protein hydrogels through control of network topology. Nature Materials 5(2) (2006) 153-158.

[13] H. Teles, T. Vermonden, G. Eggink, W.E. Hennink, F.A. de Wolf, Hydrogels of collagen-inspired telechelic triblock copolymers for sustained release of proteins. Journal of Controlled Release 147(2) (2010) 298-303.

[14] K.S. Anseth, A.T. Metters, S.J. Bryant, P.J. Martens, J.H. Elisseeff, C.N. Bowman, In situ forming degradable networks and their application in tissue engineering and drug delivery. Journal of Controlled Release 78(1-3) (2002) 199-209.

[15] R.E. Rhoads, Udenfrie.S, Bornstei.P, In vitro enzymatic hydroxylation of prolyl residues in alpha1-CB2 fragment of rat collagen. Journal of Biological Chemistry 246(13) (1971) 4135-&.

[16] D.E. Discher, P. Janmey, Y.L. Wang, Tissue cells feel and respond to the stiffness of their substrate. Science 310(5751) (2005) 1139-1143.

[17] A.J. Engler, S. Sen, H.L. Sweeney, D.E. Discher, Matrix elasticity directs stem cell lineage specification. Cell 126(4) (2006) 677-689.

[18] R.J. Pelham, Y.L. Wang, Cell locomotion and focal adhesions are regulated by substrate flexibility. Proceedings of the National Academy of Sciences of the United States of America 94(25) (1997) 13661-13665.

[19] G. Chan, D.J. Mooney, New materials for tissue engineering: towards greater control over the biological response. Trends in Biotechnology 26(7) (2008) 382-392.

[20] Y.C. Wang, L.B. Wong, H. Mao, Creation of a long-lifespan ciliated epithelial tissue structure using a 3D collagen scaffold. Biomaterials 31(5) 848-853.

[21] M. Martina, D.W. Hutmacher, Biodegradable polymers applied in tissue engineering research: a review. Polymer International 56(2) (2007) 145-157.

[22] B.S. Kim, D.J. Mooney, Engineering smooth muscle tissue with a predefined structure. Journal of Biomedical Materials Research 41(2) (1998) 322-332.

[23] B.S. Kim, D.J. Mooney, Development of biocompatible synthetic extracellular matrices for tissue engineering. Trends in Biotechnology 16(5) (1998) 224-230.

[24] A.J. Engler, M.A. Griffin, S. Sen, C.G. Bonnetnann, H.L. Sweeney, D.E. Discher, Myotubes differentiate optimally on substrates with tissue-like stiffness: pathological implications for soft or stiff microenvironments. Journal of Cell Biology 166(6) (2004) 877-887.

[25] L.Y. Koo, D.J. Irvine, A.M. Mayes, D.A. Lauffenburger, L.G. Griffith, Co-regulation of cell adhesion by nanoscale RGD organization and mechanical stimulus. Journal of Cell Science 115(7) (2002) 1423-1433.

[26] R.E. Sallach, W.X. Cui, F. Balderrama, A.W. Martinez, J. Wen, C.A. Haller, J.V. Taylor, E.R. Wright, R.C. Long, E.L. Chaiko, Long-term biostability of self-assembling protein polymers in the absence of covalent crosslinking. Biomaterials 31(4) (2010) 779-791.

[27] W. Shen, J.A. Kornfield, D.A. Tirrell, Structure and mechanical properties of artificial protein hydrogels assembled through aggregation of leucine zipper peptide domains. Soft Matter 3(1) (2007) 99-107.

[28] J.S. Guo, K.K.G. Leung, H.X. Su, Q.J. Yuan, L. Wang, T.H. Chu, W.M. Zhang, J.K.S. Pu, G.K.P. Ng, W.M. Wong, X. Dai, W.T. Wu, Self-assembling peptide nanofiber scaffold promotes the reconstruction of acutely injured brain. Nanomedicine-Nanotechnology Biology and Medicine 5(3) (2009) 345-351.

[29] W. Shen, R.G.H. Lammertink, J.K. Sakata, J.A. Kornfield, D.A. Tirrell, Assembly of an artificial protein hydrogel through leucine zipper aggregation and disulfide bond formation. Macromolecules 38(9) (2005) 3909-3916.

[30] S.A. Maskarinec, D.A. Tirrell, Protein engineering approaches to biomaterials design. Current Opinion in Biotechnology 16(4) (2005) 422-426.

[31] N. Sanabria-DeLong, A.J. Crosby, G.N. Tew, Photo-Cross-Linked PLA-PEO-PLA Hydrogels from Self-Assembled Physical Networks: Mechanical Properties and Influence of Assumed Constitutive Relationships. Biomacromolecules 9(10) (2008) 2784-2791.

[32] J.A. Benton, C.A. DeForest, V. Vivekanandan, K.S. Anseth, Photocrosslinking of Gelatin Macromers to Synthesize Porous Hydrogels That Promote Valvular Interstitial Cell Function. Tissue Engineering Part A 15(11) (2009) 3221-3230.

[33] K.J. Quinn, J.M. Courtney, J.H. Evans, J.D.S. Gaylor, W.H. Reid, Principles of burn dressing. Biomaterials 6(6) (1985) 369-377.

[34] S.B. Lee, Y.H. Kim, M.S. Chong, S.H. Hong, Y.M. Lee, Study of gelatin-containing artificial skin V: fabrication of gelatin scaffolds using a salt-leaching method. Biomaterials 26(14) (2005) 1961-1968.

[35] S.R. Hong, S.J. Lee, J.W. Shim, Y.S. Choi, Y.M. Lee, K.W. Song, M.H. Park, Y.S. Nam, S.I. Lee, Study on gelatin-containing artificial skin IV: a comparative study on the effect of antibiotic and EGF on cell proliferation during epidermal healing. Biomaterials 22(20) (2001) 2777-2783.

[36] B. Balakrishnan, M. Mohanty, P.R. Umashankar, A. Jayakrishnan, Evaluation of an in situ forming hydrogel wound dressing based on oxidized alginate and gelatin. Biomaterials 26(32) (2005) 6335-6342.

[37] A. Schneider, J.A. Garlick, C. Egles, Self-Assembling Peptide Nanofiber Scaffolds Accelerate Wound Healing. Plos One 3(1) (2008).

[38] A.A. Martens, G. Portale, M.W.T. Werten, R.J. de Vries, G. Eggink, M.A.Cohen Stuart, F.A. de Wolf, Triblock Protein Copolymers Forming Supramolecular Nanotapes and pH-Responsive Gels. Macromolecules 42(4) (2009) 1002-1009.

[39] S.G. Zhang, F. Gelain, X.J. Zhao, Designer self-assembling peptide nanofiber scaffolds for 3D tissue cell cultures. Seminars in Cancer Biology 15(5) (2005) 413-420.

[40] F. Zhang, G.S. Shi, L.F. Ren, F.Q. Hu, S.L. Li, Z.J. Xie, Designer self-assembling peptide scaffold stimulates pre-osteoblast attachment, spreading and proliferation. Journal of Materials Science-Materials in Medicine 20(7) (2009) 1475-1481.

[41] F. Gelain, D. Bottai, A. Vescovi, S.G. Zhang, Designer Self-Assembling Peptide Nanofiber Scaffolds for Adult Mouse Neural Stem Cell 3-Dimensional Cultures. Plos One 1(2) (2006).

| | |
|---|---|
| $C_F$ | concentration of free ends |
| $C_{F,0}$ | total (maximum) concentration of end groups |
| $C_H$ | triple helices concentration |
| $C_{H,max}$ | maximum concentration of triple helices |
| $C_J$ | junction point concentration |
| $C_L$ | junctions which form loops |
| $C_T=C_{prot}$ | total concentration of polypeptide |
| C* | overlap concentration |
| $E_a$ | activation energy |
| F | front factor |
| m | multiplicity |
| G’ | storage modulus |
| G” | loss modulus |
| $G_0$ | plateau storage modulus of physical network |
| $G_f$ | plateau storage modulus of chemical (fixed) network |
| $\Delta H$ | molar enthalpy of helix formation |
| $\Delta H_0$ | plateau enthalpy |
| J(t) | compliance as a function of time |
| $k_{a1}$ | rate constant for triple helix nucleation |
| $k_{a2}$ | rate constant for triple helix propagation |
| $k_d$ | dissociation rate constant of single triple helix |
| $k_D$ | overall dissociation rate constant |
| $k_D$’ | enhanced overall dissociation rate constant by applying force (stress) |
| $k_{d,0}$ | prefactor in Arrhenius correlation |
| $K_H$ | equilibrium constant |
| $K_{H,0}$ | prefactor in Van’t Hoff correlation |
| $M_{prot}$ | molar weight of molecule |
| n | total number of chains involved in junctions |
| N | number of Kuhn segments, cycle number |
| <N> | average length of an active chain |
| $N_A$ | Avogadro number |
| $p_F$ | fraction (probability) of free ends |
| $p_H$ | fraction (probability) of triple helices |

| | |
|---|---|
| $p_J=p$ | fraction of junction points fraction of gel |
| $p_L$ | fraction(probability) of loops |
| $r_H=dC_H/dt$ | rate of triple helix formation |
| $r_{H,0}=(dC_H/dt)_0$ | initial rate of triple helix formation |
| $r_{H^*}=dC_{H^*}/dt$ | rate of triple helix nucleus formation |
| $R_f$ | strain-fixity ratio |
| $R_g$ | radius of gyration |
| $R_r$ | strain-recovery ratio |
| $T_m$ | melting temperature of the triple helical nodes |
| $t_g$ | gel point, gel time, gel threshold |
| $t_b$ | rupture time of bond |
| $V_{coil}$ | volume of the polymer coil |
| $\beta$ | probability that given branch, emanating from a junction point is not connected to the infinite cluster |
| $\gamma$ | strain |
| $\gamma_0$ | strain, just before unloading, in thermo-mechanical cycle |
| $\gamma_e$ | strain at the end of the thermo-mechanical cycle |
| $\gamma_p$ | strain applied to the physical network |
| $\gamma_u$ | strain immediately after unloading in thermo-mechanical cycle |
| $\delta$ | potential length of one junction |
| $\eta$ | viscosity |
| $\nu_{eff}$ | total number of elastically active chains |
| $\sigma$ | stress |
| $\sigma_c$ | critical fracturing stress |
| $\sigma_p$ | tress in the physical network |
| $\tau$ | overall relaxation time |
| $\tau_0$ | relaxation time of single triple helix |
| $\upsilon$ | junction point volume |

## Samenvatting

De snelle toename in de kwaliteit van het leven en de vooruitgang in de medische wetenschappen vraagt om de ontwikkeling van nieuwe flexibele en goed te controleren materialen. Om dezelfde redenen, moeten materialen die gebruikt worden in biomedische toepassingen steeds meer biologisch afbreekbaar, bio-compatibel en functioneel zijn. De meeste van de nu beschikbare systemen missen echter één van deze eigenschappen. Gelatine (gewonnen uit dieren), dat vaak wordt gebruikt in de medische wereld, kan leiden tot besmetting met prionen of virussen en kan mogelijk allergische reacties oproepen. Bovendien bestaat gelatine uit verschillende moleculen met verschillende stabiliteit en grootte. De slecht gedefinieerde moleculaire structuur van gelatine maakt het moeilijk om de relatie tussen structuur en functie te verhelderen. Aan de andere kant ontberen synthetische materialen met goed gecontroleerde grootteverdeling vaak biocompatibilitiet, functionaliteit en afbreekbaarheid. Bovendien wordt de toepassing van deze materialen in het menselijk lichaam bemoeilijkt doordat er vaak toxische oplosmiddelen nodig zijn voor de productie van synthetische materialen.

De nadelen van de op dit moment gebruikte materialen hebben ervoor gezorgd dat wetenschappers onderzoek doen naar nieuwe methodes voor het maken van nieuwe materialen, door gebruikmaking van genetische modificatie. De recente ontwikkelingen op het gebied van genetische modificatie en recombinatie hebben geleid tot nieuwe mogelijkheden om moleculen te maken, met controle over de lengte en samenstelling van het biopolymeer. Met behulp van moleculaire biologie kunnen biopolymeren worden gemaakt die bestaan uit in de natuur voorkomende motieven, zoals bijvoorbeeld in elastine, zijde of collageen, maar ook geheel kunstmatige biopolymeren. Zoals we in dit proefschrift hebben laten zien, zorgt de controle over het ontwerp van de met behulp van biotechnologie geproduceerde biopolymeren of blok-polypeptides ervoor dat we ook controle over de fysisch-chemische eigenschappen van biopolymeren hebben. Dit laatste is zeer waardevol.

In dit proefschrift presenteren we een nieuwe groep van biologisch afbreekbare, netwerk-vormende blok-polymeren die worden geproduceerd met behulp van een genetisch gemodificeerde gist-stam, *Pichia pastoris* **(Hoofdstuk 2)**. Eindblokken die trimeren vormen, afgekort als T, bestaan uit negen Pro-Gly-Pro aminozuur tripletten en flankeren symmetrisch een middenblok dat bestaat uit vier of acht herhalingen van zeer hydrofiele R of P sequenties en dat van zichzelf weining of geen structuur heeft (Figuur S.1). R en P zijn identiek wat betreft ketenlengte (99 aminozuren) en compositie, maar de aminozuren zijn anders geordend.

Het P blok heeft een glycine op elke derde plek (net zoals collageen), maar vormt geen supramoleculaire structuren en gedraagt zich als een structuurloze keten bij elke temperatuur. Het R blok is een meer willekeurige (R=Random=willekeurig) vorm van het P blok. Vier recombinante gelatines zijn beschreven in dit proefschrift; TR4T, TR8T, TP4T and TP8T (Figuur S.1). Deze zijn alle succesvol geproduceerd met hoge opbrengst (1-3 gram per liter fermentatie mengsel) door de *Pichia pastoris* GS115 stam, getransformeerd met een pPIC9 vector met daarin het recombinante gen.

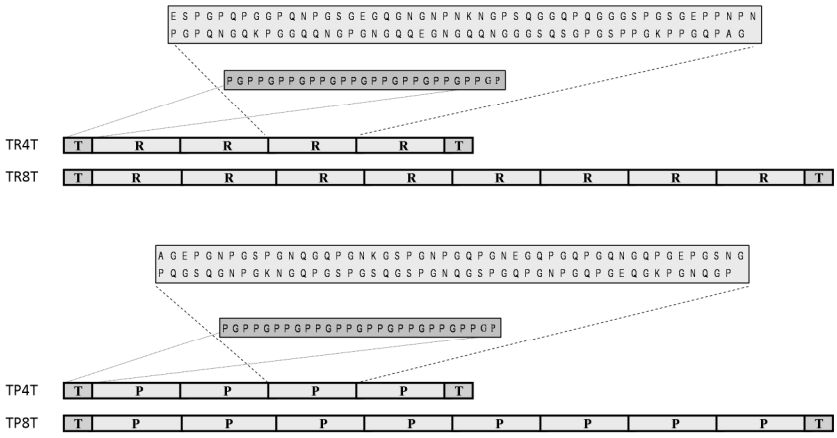


Figuur S.1 Schematische representatie van de op collageen geinspireerde blok-polypeptiden: TR4T, TR8T, TP4T en TP8T.

In **Hoofdstuk 3** hebben we de lineaire reologische eigenschappen beschreven van hydrogels gevormd door TR4T polypeptiden. Bij een temperatuur van 50 °C blijven de polpypeptiden in oplossing zonder een gel te vormen. Echter, bij lagere temperatuur beginnen de collageen-achtige trimeer-vormende domeinen (T) te assembleren in drievoudige knooppunten (trimeren) en wordt een goed gedefinieerd netwerk (gel) gevormd. In het begin van het geleringsproces is het systeem nog vloeibaar, maar naarmate de vorming van het netwerk vordert krijgen de elastische eigenschappen de overhand. Binnen een paar uur is de gelvorming compleet. Het zijn de T blokken die verantwoordelijk zijn voor de netwerkvorming, want we hebben laten zien dat een oplossing van enkel de midden-blokken (R4) geen gel vormt. Bovendien laten calorimetrische metingen zien (Hoofdstuk 5) dat de collageen zijblokken bijna kwanitatief verantwoordelijk zijn voor de trimerizatie, omdat de gevonden smeltenthalpie in goede overeenstemming is met waarden verkregen door Frank *et al*. voor vrije $(Pro\text{-}Gly\text{-}Pro)_{10}$ peptiden. De fractie van de T blokken die in trimeren zitten varieert met de temperatuur. Door de temperatuur te verlagen, neemt het aantal trimeren toe,

terwijl de hoeveelheid vrije einden afneemt. Er zijn twee manieren om een trimeer te vormen: door drie T blokken van drie verschillende polypeptiden, of door drie blokken van twee verschillende polypeptiden. Er zijn daarom drie structuren waaaruit het netwerk bestaat: losse uiteindes (‘dangling ends’), bruggen (‘active bridges’), en lussen (‘loops’) (Figuur S.2). Doordat er een beperkt aantal mogelijkheden is, konden we een model ontwikkelen dat de eigenschappen van het gel voorspelt aan de hand van de aantallen lussen, actieve bruggen en losse einden. Voor dit model zijn verder diverse meetbare eigenschappen van de polypeptiden gebruikt als input. Het model beschrijft de gemeten data kwantitatief. De gemeten eigenschappen van het gel in verschillende omstandigheden konden dankzij het model worden vertaald naar verschillende verhoudingen lussen, actieve bruggen en losse einden.

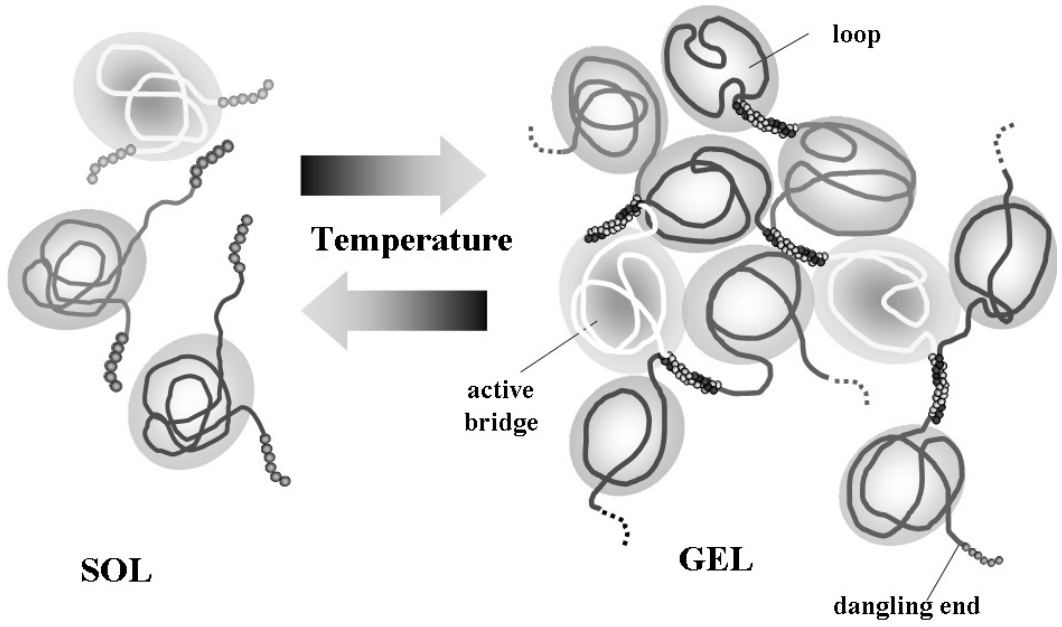


Figuur S.2 Vorming van een gel door op collageen geinspireerde polypeptiden.

In **Hoofdstuk 4** laten we zien dat het aantal actieve bruggen en lussen afhangt van de concentratie polypeptiden, de temperatuur, en de lengte en stijfheid van de middelste blokken. Dit hebben we laten zien door metingen aan nieuwe polypeptiden, waarvan de middelste blokken verschillen in lengte en samenstelling: TP4T, TR8T and TP8T (Figuur S.1). Voor alle nieuwe polypeptiden zijn de eigenschappen sterk afhankelijk van concentratie en temperatuur (net als voor TR4T). Bij vergelijkbare concentraties vormen de langer versies, TR8T en TP8T, aanzienlijk stevigere gelen dan dan hun kortere tegenhangers, TR4T and TP4T. Dit komt omdat bij de langere polypeptiden de kans kleiner is dat de T blokken van

hetzelfde polypeptide elkaar tegenkomen en een lus vormen. Omdat de R ketens minder flexibel zijn dan de P ketens, hebben de gelen van TR4T en TR8T een hogere elasticiteit dan die van hun tegenhangers, TP4T en TP8T.

Ondanks dat calorimetrische metingen laten zien dat de eindblokken bij dezelfde temperatuur uit elkaar vallen voor alle vier de polypeptiden, is de temperatuur waarbij het gel zijn elastische eigenschappen verliest anders. Gelen van de kortere polypeptiden smelten bij lagere temperaturen (TP4T bij 25°C, en TP8T bij 40°C). Gelen van de R-varianten smelten bij net iets hogere temperatuur dan hun P-tegenhangers. De verschillen in smeltgedrag zijn gerelateerd aan de kans dat lussen en actieve bruggen gevormd worden. Met behulp van het analytische model dat is gepresenteerd in **Hoofdstuk 3** konden we dit laten zien. De enige parameter in het model die gevarieerd moest worden was de ketenlengte van het middenblok. Dit omdat de andere eigenschappen niet varieren met de lengte van het middenblok.

In onze gelen bestaan de knooppunten in het netwerk uit driedubbele helixen. Het mechanisme van de vorming van deze knooppunten kan goed worden beschreven met een twee-staps kinetisch model (**Hoofdstuk 5**). Voor verdunde systemen is nucleatie, de vorming van trimeren, de snelheidslimiterende stap, waardoor de reactie schijnbaar derde orde is. Voor meer geconcentreerde systemen is de nucleatie relatief snel, en wordt de voortplanting van trimeren snelheidslimiterend. De reactie is dan ongeveer eerste orde.

De kinetiek van de vorming van trimeren bepaalt de snelheid waarmee het gel zich vormt. De gelvorming begint als de eerste trimeren worden gevormd. Op dat moment is het systeem nog vloeibaar, maar naarmate er een netwerk van trimeren wordt gevormd wordt het systeem steeds elastischer. Veranderingen in de structuur van het netwerk en de mechanische eigenschappen van het gel kunnen worden voorspeld door de kinetiek van de vorming van trimeren te combineren met het model dat is geintroduceerd in **Hoofdstuk 3**. Door verschillende metingen (reologie en calorimetrie) te vergelijken konden we laten zien dat de relatie tussen de eigenschappen van het gel en de hoeveelheid trimeren afhangt van de polypeptide concentratie. Dit komt omdat de vorming van lussen waarschijnlijker is bij lagere concentraties van polypeptiden.

Als de onderzochte gels worden onderworpen aan grote krachten, breken ze op een gegeven moment **(Hoofdstuk 6)**. We onderzoeken de details van dit breken door het gel te vullen met fluorescerende deeltjes en deze deeltjes te volgen met een camera (‘particle image velocimetry’-PIV) terwijl het gel langzaam steeds verder wordt vervormd. Aan het begin van het experiment vervormt het gel overal op dezelfde manier, maar na verloop van tijd breekt het gel en wordt het gescheiden in twee aparte delen. Het breken van het gel komt door de

krachten die worden uitgeoefend op de trimeren leiden tot het ontvouwen van de trimeren. Als de kracht word weggehaald, kunnen de trimetren zich weer opnieuw vormen, waardoor het systeem zich weer volledig herstelt (Hoofdstuk 6). Dit soort gedrag, dat niet mogelijk is voor de meeste gelen met permanente verbindingen, is erg gewenst voor toepassingen omdat hydrogels vaak worden blootgesteld aan grote krachten. Verschillende stukjes TR4T gel (Figuur S.3, verschillende grijstinten), kunnen in twee uur samensmelten tot één gel. Met reologie hebben we gemeten dat het samengesmolten gel (zelfs na meerdere malen breken en samensmelten) dezelfde elastische eigenschappen heeft als het gel voordat deze gebroken is.

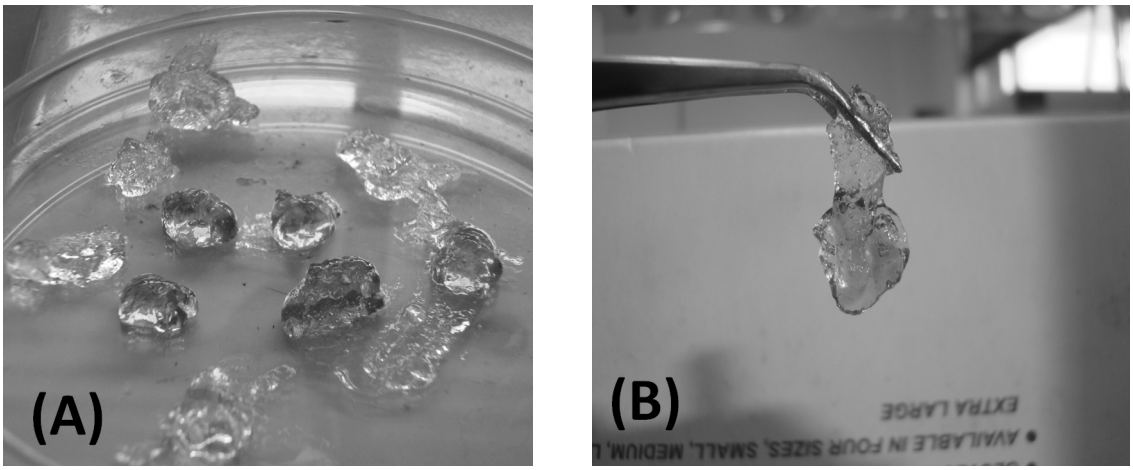


Figuur S.3 Samensmelten van TR4T hydrogels. (A) Stukjes gebroken gel. (B) Twee gel stukjes die na twee uur weer één zijn.

In **Hoofdstuk 7** hebben we laten zien dat gelen van TR4T polypeptiden met permanente dwarsverbanden tussen de polypeptiden kunnen worden gebruikt als materialen met een geheugen. De permanente dwarsverbindingen zijn gemaakt door bepaalde groepen (lysines) in de structuurloze ketens (R) van de polypeptiden chemisch aan elkaar te binden bij hogere temperatuur. Het op deze manier chemisch verbonden netwerk kon tot 200% worden uitgerekt en in een tijdelijke vorm worden gefixeerd bij lagere temperatuur door het laten vormen van trimeren. Bij kamertempertauur duurde het enkele dagen voordat de oorspronkelijke vorm van het chemisch verbonden netwerk weer terug was, maar bij temperaturen boven de 50 ºC keert het materiaal binnen enkele minuten terug naar zijn oude vorm. Zelfs na enkele cycli van vervormen en temperatuurveranderingen blijft dit reversibele gedrag hetzelfde. We hebben dit gedrag in meer detail bestudeerd door de hydrogels te beschrijven met een mechanistisch model dat de balans beschrijft tussen een permanent netwerk en een netwerk met reversibele knooppunten. Met dit model konden we de kinetiek van het herstelproces begrijpen.

# Podsumowanie

Wzrost standartów życiowych oraz szybki rozwój nauk medycznych w wysoko rozwiniętych regionach świata spowodowały gwałtowny rozwój w dziedzinie inżynierii biomateriałowej. Najnowsze materiały, zwłaszcza te stosowane w biomedycynie, powinny być biokompatybilne, biodegradowalne oraz biofunkcjonalne. Ponadto, powinny one posiadać możliwość precyzyjnej kontroli ich właściwości fizyko-chemicznych. Większość z obecnie dostępnych materiałów, charakteryzuje brak którejś z tych pożądanych cech. Przykladem może być popularna żelatyna będąca częściowo zhydrolizowanym kolagenem. Pomimo, iż jest chętnie stosowana w biomedycynie często jest zakażona prionami bądź wirusami pochodzenia zwierzęcego, a tym samym może wywolywac reakcje alergiczne, zwłaszcza przeciw domenom, które nie tworzą potrójnych helis. Ponadto, w zależności od źródła pochodzenia oraz metody ekstrkcji, żelatyna jest mieszaniną cząstek o zróżnicowanej masie molekularnej oraz różnej stabilności termodynamicznej. Wszystkie te wady, w połączeniu z niemożliwością zmiany struktury molekularnej na życzenie, w poważnym stopniu ograniczają możliwość zrozumienia współzależności pomiędzy budową molekularną żelatyny a jej wlaściwościami fizyko-chemicznymi. W przeciwieństwie do materiałów pochodzenia naturalnego materiały syntetyczne posiadają stosunkowo dobrze zdefiniowaną masę molekularną, ale niestety w większości przypadków nie są one biokompatybilne, biofunkcyjne czy biodegradowalne. Ponadto są one często produkowane przy użyciu toksycznych rozpuszczlników co wiąże się z ich ograniczonym zastosowanem w organizmach żywych.

Wymienione powyżej niedoskonałości stosowanych obecnie biomateriałów skłoniły naukowców do poszukiwań nowych metod ich otrzymywania. Narzędziem, które w ostatnich latach zdobywa coraz większą popularność, jest biologia molekularna. Wraz z rozwojem technik inżynierii genetycznej możliwa stała się produkcja czastek o precyzyjnie zdefiniowanej masie molekularnej, składzie oraz sekwencji aminokwasów. Biopolimery produkowane metodami inżynierii genetycznej łączą w sobie zalety polimerów syntetycznych oraz materiałów pochodzenia naturalnego. Przy użyciu biologii molekularnej nowe, unikatowe bloko-biopolimery, mogą być produkowane poprzez łączenie w różny sposób występujących w przyrodzie samoagregujacych się sekwencji białkowych. Używane przez nas samoagregujące sekwencje białkowe to elastyna, jedwab oraz kolagen.

W niniejszej pracy doktorskiej zaprezentowana została nowa klasa monodyspersyjnych, biodegradowalnych i biokompatybilnych bloko-biopolimerów tworzących hydrożele. Badane

molekuły zostały wyprodukowane przez genetycznie zmodyfikowane drożdże *Pichia pastoris*. Łańcuchy otrzymanych biopolimerów zbudowane są z trzech bloków (Rysunek P.1). Bloki boczne, o skróconej nazwie T (*ang.* trimer-forming), składają się z dziewięciu powtórzeń trzech aminokwasów: proliny-glicyny-proliny (GPG). Podobną sekwencją charakteryzuje się kolagen. Dzięki tej specyficznej sekwencji kolagen (oraz w naszym przypadku bloki T) może tworzyc struktury czwartorzędowe tj. potrójne helisy. Blok środkowy prezentowanych bloko-polipeptydów składa się z 4 bądź 8 powtórzen 99 aminokwasów o przypadkowej sekwencji. W badaniach zostały wykorzystane dwa rodzaje tych bloków: blok P i R. Obydwa bloki mają ten sam skład aminokwasów, różnią się natomiast ich sekwencją (patrz Rysunek P.1).

Cztery rodzaje molekuł zostały wykorzystane w badaniach: TR4T, TP4T, TR8T i TP8T (Rysunek P.1). Wszystkie te molekuły zostały wyprodukowane przez zmodyfikowane drożdże *Pichia pastoris,* szczep GS115 z wektorem pPIC9 posiadającym gen odkodowujący dany polipeptyd. Dokładny opis produkcji badanych biopolimerów znajduje się w **Rozdziale 2.**

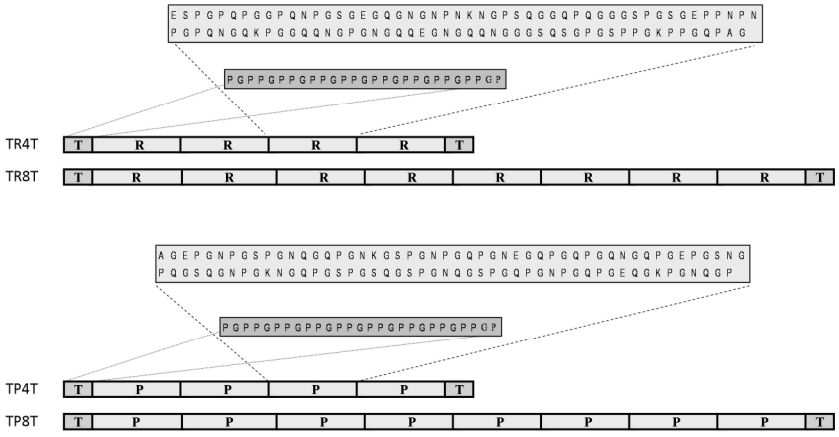


Rysunek P.1 Schemat inspirowanych kolagenem trzybloko-polipeptydów: TR4T, TR8T, TP4T oraz TP8T.

W **rozdziale 3** opisane zostały własności reologiczne hydrożeli formowanych przez molekuły TR4T. W temperaturze 50 °C mieszanina molekuł zachowuje się jak lepki płyn, nie wykazując żadnych własności elastycznych. Po obniżeniu temperatury do 20 °C bloki T (tj. te o sekwencji charakterystycznej dla kolagenu) zaczynają tworzyć potrójne helisy prowadząc do powstania dobrze zdefiniowanej sieci hydrożelowej. Na początku procesu żelowania dominują własności lepkościowe, jednak wraz z postępem tworzenia się sieci hydrożelowej materiał staje się coraz bardziej elastyczny. Po około 6 godzinach hydrożel osiąga tzw. stan

ustalony. Stan ten można scharakteryzować za pomocą wartości modułu elastycznego (G'), innymi słowy potencjału danego ciała do powrotu do kształtu wyjściowego po tym jak zostało zdeformowane. W przeciwieństwie do mieszaniny TR4T, mieszanina R4, czyli mieszanina molekuł zbudowanych wyłącznie z bloku środkowego, nie tworzy sieci hydrożelowej. Takie obserwacje świadczą o tym, że żelowanie występuje dzięki blokom inspirownaym przez kolagen (tj. blokom T).

Równowaga pomiędzy wolnymi a będącymi w potrójnych helisach blokami T, przesuwa się wraz z temperaturą. Po obniżeniu temperatury frakcja potrójnych helis wzrasta, podczas gdy frakcja swobodnych końców maleje. Istnieją dwie możliwości utworzenia potrójnej helisy. Może ona zostać utworzona bądź przez trzy bloki T pochodzące z trzech rożnych molekuł, bądź przez dwa bloki T z tej samej molekuły i jeden blok T z innej molekuły. W konsekwencji sieć hydrożelowa utworzona przez molekuły TR4T składa się z elastycznie aktywnych mostków (*ang.* active bridges), oraz elastycznie nieaktywnych pętli (*ang.* loops) oraz swobodnych końców (*ang.* free ends) (Rysunek P.2).

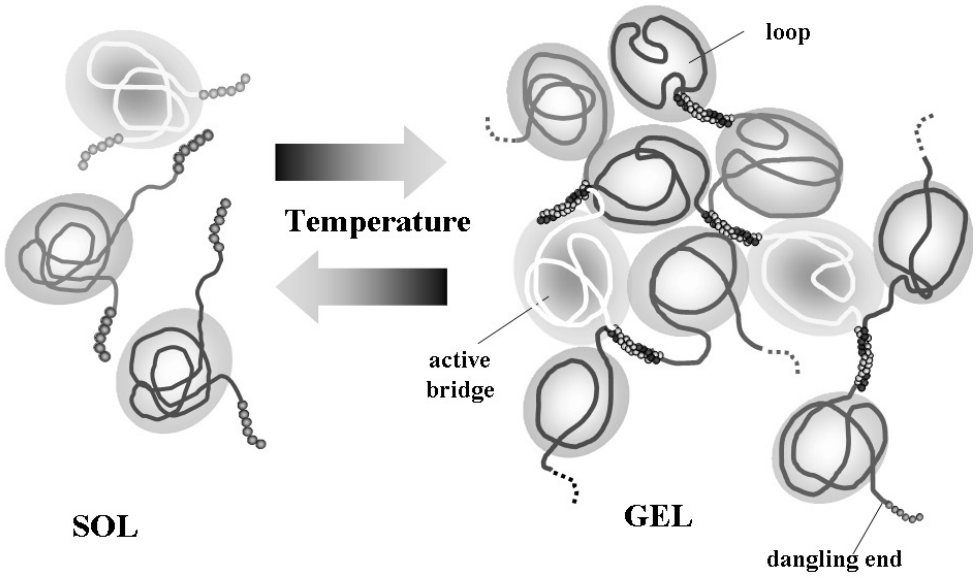


Rysunek P.2 Sieć hydrożelowa uformowana przez molekuły inspirowane kolagenem. 'active bridge'='aktywny mostek', 'dangling end'='swobodny koniec', 'loop'='pętla'

Wiedząc, iż z jednego węzła sieci wychodzą trzy „ramiona" udało nam sie zbudować model matematyczny (z wykorzystaniem rachunku prawdopodobieństwa), dzięki któremu znalezlismy zależność pomiędzy strukturą molekularną sieci hydrożelowej a jej właściowościami fizyko-chemicznymi. Jak już wspomniano wcześniej, sieć hydrożelowa

zbudowana jest z mostków, pętli oraz swobodnych końców. W obliczeniach modelowych wykorzystaliśmy 6 parametrów, które otrzymaliśmy z niezależnych pomiarów, takich jak kalorymetria czy dynamiczne rozpraszanie światła. Obliczenia modelowe przewidują w bardzo dokładny sposób własności fizyko-chemiczne takie jak jak moduł elastyczny czy czas relaksacji. Wyniki modelowania sa zgodne z wynikami eksperymentalnymi. Najważniejszym wnioskiem z badań zaprezentowanych w **Rozdziale 3** jest to, że wraz ze stężeniem białka wzrasta ilość mostków a maleje ilość pętli a im więcej mostków, tym materiał jest bardziej elastyczny.

W **Rozdziale 4** pokazano, iż nano-struktura hydrożelu (tj. ilość mostków, pętli oraz swobodnych końców) zależy nie tylko od stężenia białka oraz temperatury, ale również od długości oraz sztywności bloku o przypadkowej sekwencji tj. bloku środkowego. W celu wyjasnienia wpływu tego bloku na własności fizyko-chemiczne badanych hydrożeli wyprodukowaliśmy trzy dodatkowe molekuły o nazwach TP4T, TR8T oraz TP8T (Rysunek P.1). Na podstawie otrzymanych wyników mogliśmy wywnioskować, iż molekuły z dłuższym blokiem środkowym, tj. TR8T oraz TP8T, mają wyższy moduł elastyczny, aniżeli te z krótszym tj. TR4T oraz TP4T. Jest to spowodowane tym, że molekuły TR8T oraz TP8T mają większy promień bezwładności. Im większy promień bezwładności, tym mniejsze prawdopodobienstwo, iż bloki T z jednej molekuly „spotkają" się w tej samej potrójnej helisie, a tym samym mniejsze prawdopodobieństwo utworzenia pętli. Mniej pętli skutkuje natomiast wzrostem modułu elastycznego.

Sieć hydrożelowa powstaje wyłącznie dzięki tworzeniu potrójnych helis przez bloki inspirowane kolegenem (tj.bloki T). W **Rozdziale 5** badano kinetykę ich tworzenia. Na podstwaie przeprowadzonych badań stwierdzono, iż mechanizm tworzenia potrójnych helis można podzielić na dwa etapy. Pierwszy etap to etap nukleacji. W etapie tym trzy bloki T „zderzają" się ze sobą i zapoczatkowują potrójną helisę. Mechanizm nukleacji przeważa w niskich stężeniach proteiny, gdyż prawdopodobieńswo „zderzenia" się trzech bloków kolagenowych jest znacznie niższe, aniżeli w wyższych stężeniach. Tym samym, przy niskich stężeniach białka tworzenie potrójnych helis jest procesem trzeciorzędowym. Przy wyższych stężeniach, proces nukleacji jest szybszy a mechanizmem limitującym tworzenia potrójnych helis jest ich propagacja. Tym samym proces jest pierwszorzędowy. Propagacja potrójnych helis jest prawdopodobnie limitowana przez izomeryzację *cis-trans* w wiązaniach peptydowych proliny.

Kinetyka tworzenia potrójnych helis ma wpływ (chociaż nie bezpośredni) na tworzenie sieci hydrożelowej. Proces żelowania rozpoczyna się z momentem utworzenia pierwszego

węzła sieci. Aby zaobserwować wzrost elastyczności, musi zostać utworzonych conajmniej 50 % potrójnych helis. Używając modelu matematycznego opracowanego w **Rozdzale 3**, mogliśmy połączyć kinetykę tworzenia potrójnych helis z kinetyką tworzenia sieci hydrożelowej. Ponadto, zaobserwowaliśmy, iż ilość potrójnych helis nie ma bezpośredniego przełożenia na stopień rozwoju sieci hydrożelowej. Wynika to z faktu, iż część potrójnych helis jest zawarta w pętlach, które, jak już wspomniano wcześniej, są elastycznie nieaktywne.

W **Rozdziale 6** badano zachowanie hydrożeli pod wpływem dużych napięć i deformacji (w tzw. reżimie nieliniowym). Pod wpływem dużych sił badane hydrożele ulegają makroskopowej dezintegracji. Krytyczne warunki tego zjawiska zależą od szybkosci deformacji (bądź napięcia) hydrożelu. Naturę dezintegracji żeli badano za pomocą techniki PIV (*ang.* particle image velocimetry). W technice tej zawiesza się w sieci hydrożelowej fluorescencyjne drobiny a następnie śledzi się ich predkość względem ścian reometru, podczas deformacji. Gdy deformacja jest niezbyt duża, prędkość cząsteczek zmienia się liniowo. Wraz ze wzrostem przyłożonych sił część drobin porusza się z predkością ruchomej ściany reometru, część zaś pozostaje nieruchoma. Takie obserwacje świadczą o tym, że żel uległ dezintegracji. Zdezintegrowany żel posiada zdolność samoregeneracji. Jest to możliwe dzięki stosunkowo krótkiemu czasowi relaksacji potrójnych helis. Na Rysunku P.3 prezentujemy zjawisko samoregeneracji (po dwóch godzinach) żelu pociętego na drobne kawałki (szare i przeźroczyste).

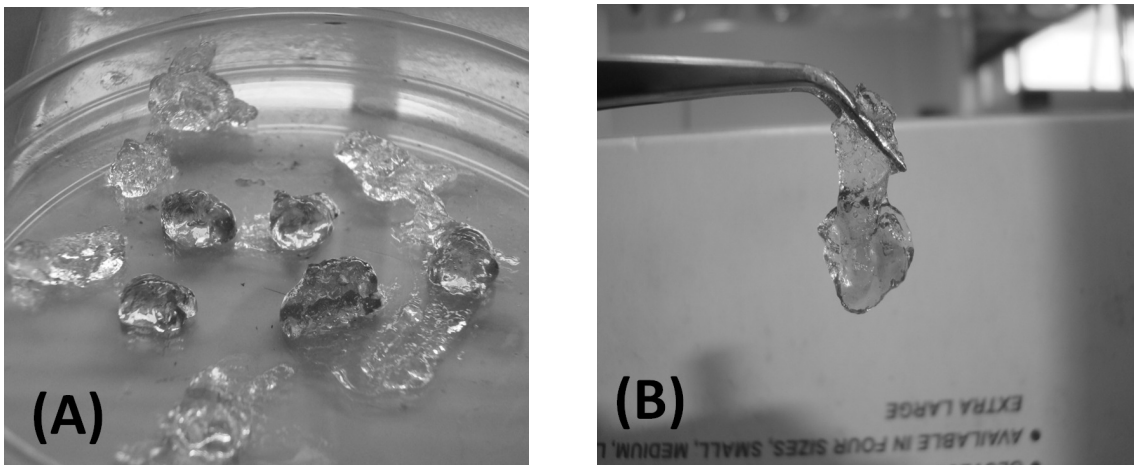


Rysunek P.3 Samoregeneracja hydrożelu utworzonego przez molekuły TR4T. (A) Kawałki zdeintegrowanego hydrożelu. (B) Zregenerowany żel.

W **Rozdziale 7** zaprezentowaliśmy tzw. efekt pamięci kształtu. Najpierw, molekuły TR4T zostały powiązane w permanentną sieć hydrożelową poprzez utworzenie wiązań chemicznych pomiędzy lizyną (przy udziale aldehydu glutarowego). Następnie hydrożel

został zniekształcony o 200 % (w temperaturze 50 °C) i natychmiast „zamrożony” w kształcie wtórnym. „Zamrożenie” kształtu jest możliwe dzięki obniżeniu temperatury podczas deformacji do 20 °C, i utworzeniu potrójnych helis przez kolegenowe bloki T. Po ponownym podwyższeniu temperatury do 50 °C hydrożel powraca do swojego pierwotnego kształtu. W rozdziale 7 skupiliśmy się na procesie powrotu z kształtu wtórnego do kształtu pierwotnego. W tym celu porównujemy nasz system do modelu mechanicznego składającego się z dwóch sprężyn oraz ruchomego tłoka.

## Acknowledgments

The work presented in this thesis would not have been possible without the help and support of several people. That is why in the last pages of this book I would like to acknowledge them.

First of all I would like to thank my parents without whom I would not be here. Mamusiu, tatusiu gdyby nie Wasze zaangażowanie i poświęcenie w moje wychowanie i edukację nigdy bym nie doszła do tego punktu, w którym właśnie sie znajduję. To dzięki Wam posiadłam ciekawość świata i nauki, i to właśnie ten głód wiedzy od Was przejęty doprowadził mnie tutaj (na szczęście nie aż tak daleko od domu ☺). Dziekuję również mojemu „małemu" braciszkowi Marcinkowi (Nioniowi), który już od dzieciństwa zaskakiwał mnie swoimi wynalazkami i miksturami, a który jednak wydoroślał wcześniej niż ja i już wkrótce zostanie szczęśliwym tatą.

I would like to thank, from the bottom of my heart, my co-promoter Dr. Jasper van der Gucht. I thank you for your continuous guidance, support, scientific insight, inspiring discussions and patience with my "a" and "the" ☺. Your knowledge is incredible and I am glad that you shared part of it with me. I am also in debt to my promoter Prof. Martien Cohen Stuart for his guidance, advices, passion and strong believe in designer protein polymers. I would like to express my thanks to Dr. Frits de Wolf for his support, enthusiasm, creativity and new ideas. I also would like to thank Joris Sprakel, who besides being my first office mate, introduced me into the world of hydrogels and rheology. I also thank Marc Werten for his help and guidance in molecular biology and Patrick Van Doeveren for his assistance with 20-L fermentation and trust in my fermentation skills ☺. I thank Remko Fokkink for his help with light scattering and PIV, Anton Korteweg for his help with DSC and Saskia and Ilja for doing some SAXS experiments for me.

I would like to thank all my colleagues from FYSKO. I have enjoyed my life here a lot. I thank my office mates for their great company and the fun we had: Joris, Saskia, Agata, Cecilia, Monika, it was really nice to share the office with you. Agata dzięki za ploteczki i za słowa touchy w chwilach zwątpienia. I thank Marc and Kathelijne for being great PhD trip co-organizers (to Switzerland and France). Yuan, thank you for the funny and nice talks over coffee. I also thank all other Fysko PhD students whom I have met during my time here and whose company I enjoyed a lot: Arnout, Bart, Ilja, Marat, Pascal, Petja, Wiebe, Armando, Dmitry, Evan, Harke, Huanhuan, Lennart, Liyakat, Junyou, Soumi, Thao Yunus. It was nice to meet all of you. Life at Fysko wouldn't run properly without the daily hard work of some

people: Josie, Mara, Anita, Bert, Rhoda, Anneke and Ronald, and that is why I would like to thank them. I also cannot forget about my colleagues from the Biobased Products group. Anais thank you for all talks and words of support and for everything. I hope that now you enjoy your life in Florida and I wish you a lot of luck on the 30th of May. I thank Helena for our fruitful collaboration, which resulted in a nice paper (Chapter 4). I also thank my master student Leon for his work, which I could partially use in the story about shape-memory materials (Chapter 7).

I would like to thank my best friends: Kasia, Justynka and Claudia (the order according to the length of the friendship ☺). Your presence has been making me happy for years. I am so glad that I have you. Thank you for your faith in me and continuous words of support. Thank all of you for all the nice discussions about life and fun moments.

I would like to thank everybody else who came or was willing to come to Wageningen today (20th of May), to celebrate with me this particular day.

Bas(je), I cannot create adequate words, which would express how much I am thankful for your love, words of encouragement and making my life full of sun and full of królików ☺. Thank you…

*Paulina*

## About the author

Paulina Janina Skrzeszewska was born on the 26th of January 1979 in Węgrów, Poland. In 1998 she started her study at Warsaw University of Technology at the Interdisciplinary Department of Biotechnology. During her study she was an active member of IAESTE (International Association for the Exchange of Students for Technical Experience) and rather passive member of BEST (Board of European Students of Technology). Thanks to IAESTE she could make two internships. In 2002 she spent two months at the University of Alicante in Spain at the Faculty of Chemical Engineering at the Department of Physical Chemistry, doing research about the phase equilibrium in tri-components systems. In 2004 she did her internship at Procede BV (Enschede, The Netherlands). The focus of the project in Procede was to optimize the process of cellulose acetate production from raw waste materials. As a member of BEST she participated in summer and spring courses in Kosice, Leuven le Neuve, Paris and Brussels. During her student times her part time job was the sale of her own drawings of Warsaw Old Town. She also won a prize in the fashion drawings contest organized by the polish journal "Gala".

From February 2005 she continued her study as Professional Designer in Engineering at the TU Delft (The Netherlands). As a part of the study, she carried out a one year individual project at DSM Food Specialties (Delft, The Netherlands). The project was about identifying scale-up effects in *A. niger* fermentation. She graduated from the TU Delft in 2007, obtaining the title of PDEng. Since not being "scientifically fulfilled" she continued her education as a PhD student in Wageningen in the group of Physical Chemistry and Colloid Science. The research was focused on a new class of collagen-inspired block polypeptides. The results of this research are presented in this thesis. On the 1st of May 2011 she started her work as a Biopolymer Scientist at Unilever at the department of Process Science, located in Vlaardingen.

## List of publications

**P.J. Skrzeszewska**, F.A. de Wolf, M.W.T. Werten, A.P.H.A. Moers, M.A.Cohen Stuart, J. van der Gucht, Physical gels of telechelic triblock copolymers with precisely defined junction multiplicity. Soft Matter 5(10) (2009) 2057-2062.

**P.J. Skrzeszewska,** F.A. de Wolf, M.A. Cohen Stuart, J. van der Gucht, Kinetics of network formation by telechelic polypeptides with trimeric nodes. Soft Matter 6(2) (2010) 416-422

H. Teles**, P.J. Skrzeszewska**, M.W.T Werten, J. van der Gucht, G. Eggink and F. A. de Wolf, Influence of molecular size on gel-forming properties of telechelic collagen-inspired polymers. Soft Matter 6(19) (2010) 4681-4687

**P. J. Skrzeszewska,** J. Sprakel, F. A. de Wolf, R Fokkink, M. A. Cohen Stuart and J. van der Gucht, Fracture and self-healing in a well-defined self-assembled polymer network. Macromolecules 43 (7) (2010) 3542–3548.

**P.J. Skrzeszewska**, L. N. Jong, F.A. de Wolf, M.A. Cohen Stuart and J. van der Gucht, Shape-memory effects in biopolymer networks with collagen-like transient nodes. Submitted

**P.J. Skrzeszewska,** Marc W. T. Werten, Frits A. de Wolf, Martien A. Cohen Stuart and Jasper van der Gucht, Molecular structure of hydrogels formed by collagen-inspired biopolymers. In preparation

## Overview of completed training activities

### *Courses*

Thermodynamics in Biochemical Eng, Murren (Switzerland)

Advanced Course in Applied Genomics, Wageningen (The Netherlands)

RPK-B Polymer Physics, Utrecht (The Netherlands), 2007

Biopolymers, Wageningen (The Netherlands), 2007

Summer School: scattering methods, Bombannes (France), 2008

Winter school, Han-sur-Lesse (Belgium), 2008

Summer School: rheology, Leuven (Belgium), 2009

### *Conferences and Symposia*

International conference, Ven (Sweden), 2007

Soft Matter Days, Bonn (Germany), 2008

International conference ECIS, Antalya (Turkey), 2009

Soft Matter Meeting, Delft (The Netherlands), 2010

Soft Matter Days, Wageningen (The Netherlands), 2010

ICNP Kottayam (India), 2010

Dutch Polymer Days, Luntren and Veldhoven (The Netherlands), 2007-2010

DPI cluster meetings (The Netherlands) 2007-2011

## Other meetings and activities

Project Management, Delft (The Netherlands)

Scientific writing, Wageningen (The Netherlands), 2008

PhD week, Bilthoven (The Netherlands), 2007

Group meetings 2007-2010

PhD trip 2007, Sweden and Denmark

PhD trip 2009, Switzerland and France

Cover Image:  Inspired by Escher, designed and made by Paulina Skrzeszewska
Printing: Ponsen en Looijen b.v., Ede